UNIVERSITY OF SAAD DAHLAB BLIDA 1
INSTITUTE OF AERONAUTICS AND SPATIAL STUDIES
AERONAUTICAL SCIENCES LABORATORY

THESIS

To obtain the degree of: **Doctor of Philosophy -DLMD-**

Field of research: Aeronautics, Avionics

Active Control of Flutter and LCOs for a Nonlinear Aeroelastic Underactuated Wing

By:

Zahra RAGOUB

Defended in front of the respected dissertation-committee composed of:

President:

Salah BOUKRAA	Professor	University of Blida 1

Examiners:

Laghrouche Mourad	Professor	University of Tizi-Ouzou
Ardjal Aghiles	MCA	University of Tizi-Ouzou

Thesis directors:

Mohand LAGHA	Professor	University of Blida 1
Smain DILMI	MCA	University of Blida 1

Blida, November the 23rd, 2023

ABSTRACT

This dissertation proposes a robust solution for the design and stability of nonlinear aeroelastic airfoils of fixed-wing drones, dealing with the different aeroelastic instabilities that may take place during flight, such as flutter and limit cycle oscillations (LCOs).

Therefore, a two-dimensional nonlinear aeroelastic airfoil is firstly modeled. Where the aerodynamic lift and moment are expressed based on the Wagner's function for unsteady aerodynamics. The dynamic model describes plunge and pitch motions of the aircraft wing section with trailing- and leading-edge control surfaces.

After that, some robust control plants are designed and applied on the built model, in order to eliminate flutter and LCOs. These plants are based essentially on the use of sliding mode control (SMC) which is characterized by the design of a switching function to bring the system's state-trajectory to a sliding surface, and force it to stay in vicinity of this surface, converging then towards stability position. SMC is combined with a fuzzy logic controller to suppress any eventual appearance of chattering phenomenon that may occur because of the switching feature of the SMC. Finally, a high gain observer is added of the combination to estimate some system's states using some other known ones, allowing to minimize the sensors' number and to deal with the system's complexity due to unsteady aerodynamics and the system's structural and aerodynamic nonlinearities.

The obtained simulation results has been exposed and discussed, proving the controllers' efficiency in stabilizing the system, limiting vibrations and delaying flutter appearance, giving then a powerful and economic tool to have well-stabilized chattering-free wings with high performances despite nonlinearities and unsteady aerodynamic loads.

RESUME

Cette thèse propose une solution robuste pour la conception et la stabilité des profils d'ailes aéroélastiques non linéaires des drones à voilure fixe, traitant des différentes instabilités aéroélastiques pouvant survenir pendant le vol, telles que le flottement et les oscillations à cycle limite (LCOs).

Pour cela, un profil d'aile aéroélastique non linéaire bidimensionnel est d'abord modélisé, tel que la portance et le moment aérodynamiques sont exprimés à base de la fonction de Wagner pour l'aérodynamique instationnaire. Le modèle dynamique décrit les mouvements de déplacement vertical et le mouvement de tangage d'une section d'aile à deux surfaces de contrôle en bord de fuite et en bord d'attaque.

Ensuite, des lois de commande robustes sont conçues et appliquées sur le modèle établi, afin d'éliminer le flottement et les LCOs. Ces contrôleurs reposent essentiellement sur l'utilisation de la commande par mode glissant (SMC) qui se caractérise par la conception d'une fonction de commutation pour amener la trajectoire d'état du système vers une surface de glissement, et l'obliger à rester au voisinage de cette surface, convergeant alors vers la position de stabilité. La SMC est combinée à un contrôleur à logique floue pour supprimer toute éventuelle apparition du phénomène de chattering (Broutement) qui peut survenir sous l'effet de la fonction de commutation de la SMC. Enfin, un observateur à grand gain est ajouté à la combinaison pour estimer les états du système en utilisant quelques états connus, permettant donc de minimiser le nombre de capteurs utilisés et de rattraper la complexité du système due à l'introduction de l'aérodynamique instationnaire et aux nonlinéarités structurelles et aérodynamiques du système.

Les résultats de simulation obtenus ont été exposés et discutés, et ont montré l'efficacité des contrôleurs à stabiliser le système, à limiter les vibrations et à retarder l'apparition du flottement, présentant ainsi un outil puissant et économique pour la conception d'ailes bien stabilisées, sans chattering, et avec des performances élevées même sous l'effet des nonlinéarités et des charges aérodynamiques instationnaires.

ملخص

تَقتَرح هذه الأطروحة حلاً مَتِينًا لتصميم و استقرار الأجنحة المرنة غير الخطية الخاصة بالطائرات دون طيار ثابتة الجناح، و التعامل مع مختلف مشاكل عدم استقرار الأنظمة الهوائية المرنة التي قد تحدث أثناء الطيران، كمشكلة الرفرفة و الذبذبات ذات الدورة المحدودة.

من أجل ذلك، تم في البداية تصميم نموذج جناح غير خطي مرن ثنائي الأبعاد، حيث تم استخلاص عبارتَي قوة الرفع و قوة العزم الديناميكي الهوائي باستعمال دالة فاغنر للديناميكية الهوائية المتغيرة. يصف النموذج الديناميكي للنظام مسارَي الحركة العمودية و زاوية الميل (السقوط) لمقطع الجناح ذي القسمين المتحركين المتواجدَين على حافتي الجناح الأمامية و الخلفية.

بعد ذلك، تم تصميم قوانين متينة للتحكم بالنموذج المُصمَّم، بهدف إزالة مشاكل الرفرفة. هذه القوانين مبنية أساسا على قانون التحكم بوضع الانزلاق، الذي يرتكِز على اختيار دالة تبديلية من أجل جذب مسار حركة النظام نحو مساحة أو سطح الانزلاق، و إرغامه على البقاء بجوار هذا السطح إلى غاية الوصول إلى وضعية التوازن المطلوبة. بعدها تم الجمع بين هذا القانون و بين نظام التحكم بالمنطق الغامض من أجل محو كل ظهور محتمَل للذبذبات العالية التي غالبا ما تظهر بسبب الطبيعة التبديلية لقانون التحكم بوضع الانزلاق. في الأخير، تمت إضافة مراقِب عالي المكسب لقانون التحكم الناتج، و ذلك لغرض تقدير مسار حركة النظام اعتمادا على بعض حالات النظام المُعطاة، ما يسمح بتقليل عدد الحساسات اللازمة، و تَدارُك الطبيعة المعقدة للنظام بسبب الديناميكية الهوائية المتغيرة و عدم الخطية الهيكلية و الديناميكية للنظام.

في النهاية، تم عرض و مناقشة نتائج المحاكاة المُحصَّل عليها، و التي أثبتت كفاءة قوانين التحكم المَبْنِيَّة سواء في استقرار النظام، الحد مِن الذبذبات، و تأخير ظهور الرفرفة، و عليه، توفير أداة قوية و اقتصادية لتصميم جناح طائرة جد مستقر، خال من الذبذبات العالية غير المرغوبة، و بأداء عالي حتى تحت تأثير الطبيعة غير الخطية للنظام، و الأعباء الديناميكية الهوائية المتغيرة.

ACKNOWLEDGEMENT

First of all, I; always and forever; thank Allah for all of his uncountable blessings, and for giving me faith and strength to carry on my research from the all beginning and till now. All praise is due to Allah.

I would like to express my sincere gratitude to my parents, without whom I would never have accomplished this work, and to whom I owe every success I have achieved in my life.

Special and genuine thanks to my supervisors: To Pr. Mohand Lagha for his continued advice, patience and support, and for being there for me along all of these years of research, especially in times when it was difficult for me to continue. And to Dr. Smain Dilmi for the insightful ideas I could extract from the multiple and fruitful discussions that we've had.

This work has been carried out in the aeronautical sciences laboratory (LSA), I would like then to thank every member of the lab headed by Pr. Tahar Rezoug, and every member of the institute of aeronautics and spatial studies headed by Pr. Amina Benkhedda, for helping me from near or far.

I would like also to thank the dissertation committee, headed by Pr. Salah Boukraa, for accepting to evaluate this work, and to enrich it through their remarks and comments.

Warm thanks to my dear friend and colleague Nour El Imane Hamda, for standing with me and helping me in the academic and the personal sides, and for sharing with me this path of scientific research with all of its ups and downs.

Last but not least, I would like to dedicate my sincere appreciation to my brother, my sisters, and to all of my friends, for their patience, encouragement and help from near or far. For all those who believed in me, thank you very much, nothing could have been possible without your support.

CONTENTS

List of figures

List of tables

List of symbols

b	Mid-chord distance
c	Chord distance
C_h	Dumping coefficients for plunge displacement
C_α	Dumping coefficients for pitch motion
$C_{l\alpha}$	Lift coefficient derivative per α
$C_{l\beta}$	Lift coefficient derivative per β
$C_{l\gamma}$	Lift coefficient derivative per γ
$C_{m\alpha}$	Moment coefficient derivative per α
$C_{m\beta}$	Moment coefficient derivative per β
$C_{m\gamma}$	Moment coefficient derivative per γ
$\boldsymbol{d}$	Dissipation function of Rayleigh
h	Plunge displacement
I_{gc}	Moment of inertia around the gravity center
I_{ec}	Moment of inertia around the elastic center
k_α	Pitch-motion stiffness coefficient
k_h	Plunge-displacement stiffness coefficient
L	Aerodynamic lift
M	Aerodynamic moment
m_T	Total mass of the wing and its supporting structure
m_w	Wing mass
Q_h	Generalized force of vertical displacement
Q_α	Generalized force of pitch motion
s	Wing section surface
S	Sliding surface
t	Time
T	Kinetic energy
U	Potential energy
U_{eq}	Equivalent control
ΔU	Switching control
V	Freestream velocity

V_{ac}	Aerodynamic center velocity
V_{ec}	Elastic center velocity
$\mathrm{V_F}$	Flutter velocity
V_{gc}	Gravity center velocity
x_α	Distance between gravity center and elastic center
α	Pitch angle
β	Trailing edge control surface deflection
$\boldsymbol{\gamma}$	Leading edge control surface deflection
ρ	Air density
φ	Wagner's function
δw_L	Virtual work due to lift
δw_m	Virtual work due to moment
δh	Virtual plunge displacement
$\delta\alpha$	Virtual pitch motion

ACRONYMS

AE	Aeroelasticity
AFS	Active Flutter Suppression
ASE	Aeroservoelasticity
CFD	Computational-Fluid-Dynamics
CM	Convergence Mode
CSD	Computational-Structural-Dynamics
CSMC	Classical Sliding Mode Control
DOF	Degree Of Freedom
FLC	Fuzzy Logic Controller
FSMC	Fuzzy Sliding Mode Control
FSMHGOC	Fuzzy Sliding Mode with High Gain Observer Controller
FT	Fourier Transform
HGO	High Gain Observer
HOSMC	High Order Sliding Mode Control
LCO	Limit Cycle Oscillation
LECS	Leading Edge Control Surface
LQG	Linear Quadratic Gaussian
LQR	Linear Quadratic Regulator
NLAE	Nonlinear Aeroelasticity
OL	Open Loop
PFS	Passive Flutter Suppression
PID	Proportional Integral Derivative
SMC	Sliding Mode Control
SMHGOC	Sliding Mode Control with High Gain Observer Controller
SSM	Steady State Mode

TAMU	Texas Agricultural and Mechanical University
TECS	Trailing Edge Control Surface
UAV	Unmanned Aerial Vehicle
VSS	Variable Structure System
2D	Two Dimensional

GENERAL INTRODUCTION

Context and motivation of the research:

Air transport safety and aircraft reliability are major concerns for aircraft manufacturers. The challenge is to prevent all accidental situations that may occur during a flight. Modern aircraft may have very flexible structures, this flexibility makes aeroelastic investigation an important subject of aircraft design and verification procedures. One of the main challenges facing aircraft designers today is then the one of aeroelasticity. The complex interactions between dynamics, solid mechanics, and aerodynamic forces can create some issues of aircraft structural fatigue, passenger discomfort, degraded performance, and even catastrophic failure.

Early in aviation history, this problem was minimized at low flight speeds, moderate safety factors, and performance requirements. But, recent aircraft are expected to push the physical limits in terms of speed, altitude, maneuverability, endurance, range and cost. Designers have turned to lightweight materials to use with high-power engines to reduce weight in order to carry more fuel and payloads. These lightweight materials induce more flexibility than conventional aircraft materials that present significant aeroelastic concerns when operated at high speeds and altitudes. One of the most well-known and dangerous phenomena in which aerodynamic surfaces become unstable under certain flight conditions is the flutter phenomenon. This instability can lead to the destruction of the structure, hence the need for preventive procedures.

Flutter suppression is so a very important subject, and each manufacturer has to take all necessary precautions in order to avoid it while maintaining the performance of the aircraft. Several passive techniques have been proposed. However, some methods remain ineffective due to their negative impacts on aircraft performance (weight increase), but with the development of the concept of aeroservoelasticity, it has now become possible to delay and even eliminate this phenomenon while keeping the aircraft performance. With the advance in control technology, active control has become a solution to many aerospace design problems, including flutter. First, classic controllers were used. Then, control methods were improved and more robust controllers began to be used.

While the principles of proportionality and superposition lead, for linear systems, to very general formulations and methods of analysis and synthesis, the situation is quite different for

nonlinear systems. Indeed, by definition, nonlinear systems are of so varied natures, and require different approaches. In the beginning, nonlinearities were considered essentially as imperfections, but very quickly, engineers became aware of the advantages that they could derive from nonlinearities for the design of more efficient systems, a well-designed controller is one of these advantages.

The study presented here is within the framework of exploiting a robust control plant, and applying it on a nonlinear model in an unsteady aerodynamic regime, in the aim of limiting vibrations and delaying the flutter phenomenon.

Objective of the research:

The main objectives of this work are:

- To introduce unsteady aerodynamics in the nonlinear aeroelastic system model using the Wagner's function ;
- To design robust controllers in order to suppress flutter with improved system's performances and increased critical flutter-speed, and to remove the chattering phenomenon completely ;
- To confirm the controllers' effectiveness by exposing and discussing the obtained simulation results ; and
- To provide a rich bibliography to assist the future studies in the domain.

Outline of the thesis:

This thesis is composed of four chapters.

The first chapter provides a general overview of aeroelasticity and its resulting phenomena (Essentially flutter), as well as the proposed solutions for these instabilities from passive techniques to active ones (aeroservoelasticity).

The second chapter begins with establishing the equations that govern the behavior of the aeroelastic system using Lagrange equations. After, the two-degree-of-freedom equations, obtained by the development of the Wagner's function in an unsteady flow will be written in form of a state space representation for the system. Then, a numerical application is made for the TAMU II wing model to simulate its dynamic behavior.

The third chapter presents the utilized controller definitions, the control laws establishment, and the application of these controllers on the studied nonlinear aeroelastic system.

The fourth chapter is devoted to the presentation of simulation results and their interpretations.

Published research papers:

International journals:

Zahra Ragoub, Mohand Lagha, Smain Dilmi. Classical and fuzzy sliding mode control for a nonlinear aeroelastic system with unsteady aerodynamic model. International Journal of Computing and Digital Systems (IJCDS). 2020. https://dx.doi.org/10.12785/ijcds/090608

International communications:

Zahra Ragoub, Mohand Lagha, Smain Dilmi. Observer-Based Fuzzy Sliding Mode Control for Nonlinear Aeroelastic Models via Unsteady Aerodynamic. International Conference on Industrial Instrumentation and Control (ICI2C-2021), Kolkata, India, August 20th- 22nd, 2021. https://doi.org/10.1007/978-981-16-7011-4_28

This paper was awarded as the best paper in robotics in the ICI2C conference.

CHAPTER I:

State of art: Aeroservoelasticity

Contents

I.1. Introduction

This chapter presents brief explanations of the core terms and topics directly related to aeroservoelasticity (ASE) and its phenomena. It shows also the evolution of aeroelasticity (AE) and ASE through time by exposing and synthesizing so many studies that have been done previously and till nowadays. And it finally gives the approach adopted in the current research.

I.2. General Concepts

I.2.1. Aeroservoelasticity

Aeroservoelasticity (ASE) is a multidisciplinary topic that studies the interactions within the triangle of aerodynamics, structural dynamics and control systems of aircraft, as illustrated in figure (I.1) below. In other words, it is the investigation of dynamic interactions between air loads, structural deformations, and automatic flight control systems widely used in modern aircraft [1- 5].

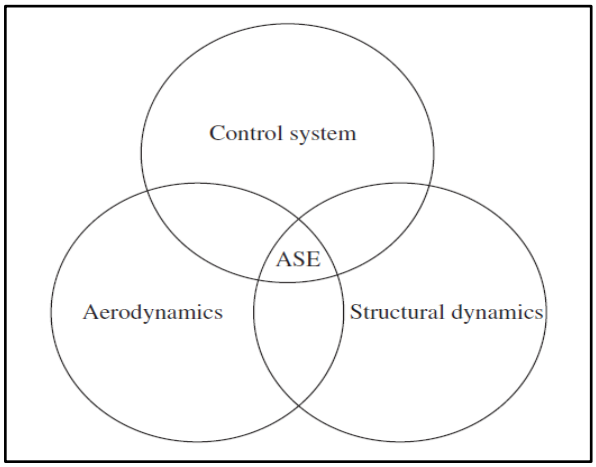

Figure I.1. Aeroservoelasticity interactions

ASE is the meeting point of many sciences and techniques of mechanical and electrical engineering [4, 5]. In recent aircraft, the structures are becoming lighter and more flexible with high air-velocities. And the flight tasks that were carried out by slow human interface are performed by automatic flight control systems with large bandwidth, which means an increased encroachment into the aeroelastic frequency [2], and gives birth to many ASE interactions that may lead to undesired phenomena such as flutter and limit cycle oscillations (LCOs) [2, 3]. Then, it is challenging but also crucial to properly analyze and understand the ASE interactions in order to extend the structures' stability margins [2].

I.2.2. Aeroelasticity

In 1946, A. R. Collar [6] proposed that the three disciplines of dynamics, solid mechanics, and aerodynamics may be effectively viewed as forming a triangle to illustrate aeroelasticity (Figure I.2). AE is then defined as the branch of physics that investigates the interactions among the elastic, aerodynamic, and inertial forces applied on a flexible body in a fluid flow-field, and the influence of the resulting aeroelastic phenomena (Such as flutter and LCOs) on the airplane design [5- 12].

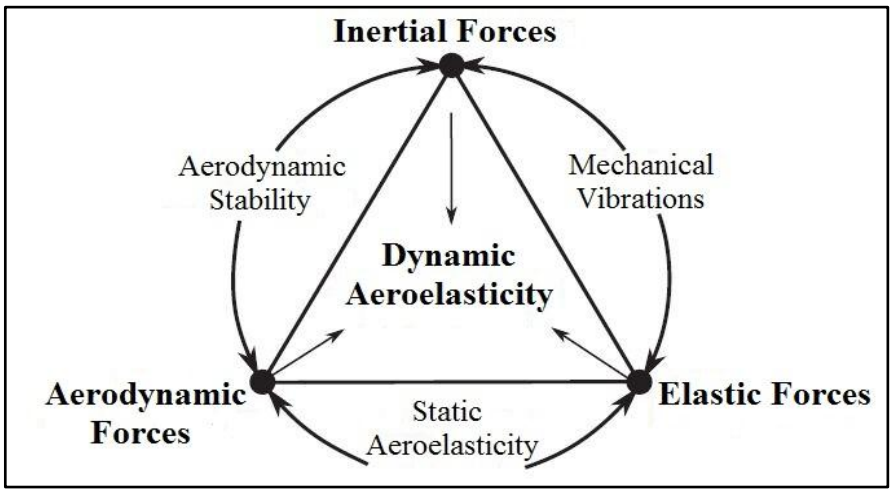

Figure I.2. Collar's Triangle, reproduced from [6]

It can be deduced from figure I.2 that coupling the points of the Collar's triangle leads to have many other technical domains and aeroelastic phenomena [5]. For example,

- Aerodynamic stability = dynamics (Inertial forces) + aerodynamics.
- Mechanical vibrations = dynamics + solid mechanics (Elastic forces).
- Static aeroelasticity = steady-flow aerodynamics + solid mechanics.

When an aeroelastic structure vibrates at a certain frequency, the surrounding flow is disturbed and adapts to this movement. The structure's deformation, as well as its vibration frequency, depends on the aerodynamic loads. During vibration, unsteady aerodynamic forces are applied to the moving structure, inducing an exchange of energy between the fluid and the structure. If the fluid extracts energy from the structure, the vibration amplitude decreases until it returns to equilibrium (Aeroelastic stability). On the other side, an aeroelastic instability corresponds to the excitation of the structure by the fluid, the system can reach then a limit cycle for which the oscillation amplitude is constant or increasing beyond this limit (Flutter) [10- 12]. The aeroelastic phenomena will be discussed later in this chapter.

I.2.3. Aerodynamics

Aerodynamics is a fluid mechanics branch that is interested in the airflow characteristics and behavior (Steady, quasi-steady, or unsteady) around an obstacle (An aeroelastic system for example) [13]. Aerodynamic modeling has a significant importance in the design of aeroelastic structures [13, 14]. In the case of steady aerodynamics, the air flow surrounding the aeroelastic body has aerodynamic forces and moments that are constant with time. When the aerodynamic forces and moments change slightly with time, a simple approach for the determination of these forces and moments is to consider that at any given instant of time, the aerodynamic parameters are constant and equal to the instantaneous values. This is referred to as the quasi-steady assumption, used to simplify the different calculations [15].

While seductive with its ease, the quasi-steady hypothesis is not always sufficiently precise for the aerodynamic calculations, and a more advanced unsteady aerodynamic analysis is required, in which the time variations of aerodynamic forces and moments are took into consideration [15].

I.3. Aeroelastic phenomena

The fluid/structure interactions result-in various phenomena most of which are of an unfavorable effect and need to be considered in different domains, like stability analysis of airplane (wings, wing sections), bridges design, etc. [5, 16].

Two categories of AE can be distinguished [17]: Static AE, resulting from the interaction of elastic and aerodynamic forces, and dynamic AE resulting from the interaction of all of the three forces of the previously exposed Collar's triangle [17].

I.3.1. Static aeroelasticity

Static AE or structures' steady-state response [7] encompasses the study of the deformations of elastic aircraft structures under aerodynamic charges, i.e. when the forces and moments are invariable with time [7, 9, 15]. This study allows controlling the static stability-and-control properties, the loads in steady flights, the distribution of the lift forces, and the control surfaces effectiveness [7]. Two essential static aeroelastic instabilities can be confronted: Divergence and control reversal.

Divergence:

Divergence is a static instability that takes place when an aeroelastic lifting surface deflections intensify the already-applied aerodynamic loads, and then these loads increase in turn the structure's deflections more, until the point of structure's failure is reached [7, 9, 15].

The first encountered case of aircraft divergence was during the Langley's trial to fly few days before the Wright Brothers' successful flights in 1903 (More details are in history section later on), where divergence led to the flight attempt's failure [9, 15, 18].

Control reversal:

The effectiveness of control surfaces (Elevators, ailerons, etc.) is also modified by aeroelastic effects, and there may even be a speed (Reversal velocity) beyond which their effect is reversed [3]. Control reversal is so the loss (Ineffectiveness or reversal) of the desired behavior of a control surface, because of the main lifting surface's deflections [7, 15]. This phenomenon may not be catastrophic, but the fact that the control surface shows decelerated or no responses, or even opposite responses to control systems' applications is also intolerable [15].

I.3.2. Dynamic aeroelasticity

Dynamic AE is about the interactions between elastic, inertial, and unsteady aerodynamic forces, it is then a more complicated issue than the static case since it considers the dynamic (Vibrational) response of the structure [7, 9]. Here are some phenomena.

Buffeting:

Buffeting is an arbitrary high frequency oscillation. It occurs when an unsteady airflow hits the aircraft wing and/or tail, or because of an unexpected pulse of aerodynamic load. It is not that disastrous, but still undesired [7, 9].

Dynamic response:

It is the fact that the aircraft elasticity may significantly change its response to atmospheric disturbances (Gusts, turbulence) or to high-speed maneuvers [3].

Limit Cycle Oscillations (LCO):

LCOs are harmonic Self-Sustaining vibrations, i.e. a stationary state of large amplitude oscillation. This situation can accelerate material fatigue and can cause discomfort for crew and passengers [3, 19]. These oscillations can be caused by structural or aerodynamic nonlinearities (Or by nonlinear control systems in some cases of ASE) [19].

Flutter:

Flutter is a self-excited dynamic instability, coupling the structure's vibration modes with the unsteady airflow that transfers energy to the oscillating body (Or with the control systems' operation frequencies in the case of ASE), resulting in oscillations of exponentially growing amplitude (Negative damping), which can lead to structural failure, a loss of control and even the aircraft destruction [20, 21].

In modern aircraft, flutter comes in the first place as the most disastrous of all the aeroelastic phenomena [7]. Most of time, the flutter velocity is attained way before the divergence speed for example [15], and even though LCO are harmful, they don't present negative damping like does flutter [3]. Consequently, a big interest is accorded to the study, deep analyses, and the prediction and suppression techniques of this phenomenon [9, 18]. The following diagram (Figure I.3) recapitulates aeroelastic and aeroservoelastic phenomena. As noticed in the figure, flutter (And LCOs, that are considered as the direct step before flutter occurrence) can happen as a consequence of fluid/structure interactions and/or of AE/control systems interactions.

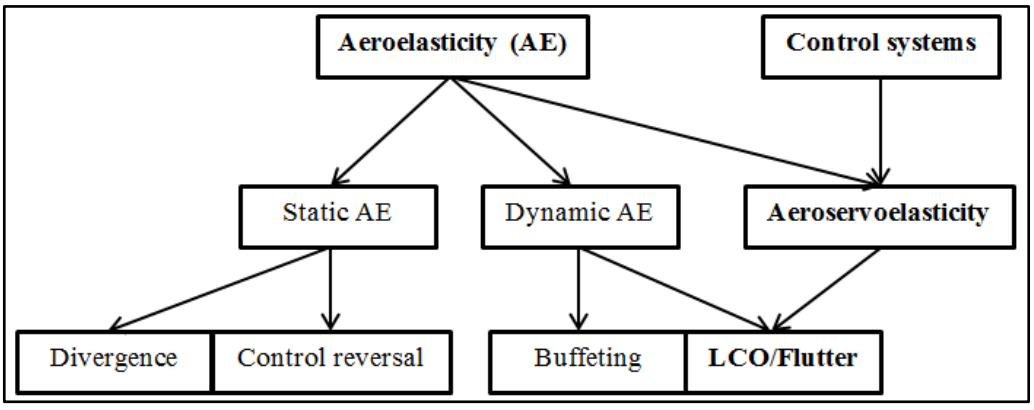

Figure I.3. Aeroelastic/Aeroservoelastic phenomena

I.4. Previous works

History:

The history of AE is not related only to aircraft or manmade structures. In fact, AE and its phenomena exist in nature way before, in plants, in birds' wings, etc. Akmeşe [22] gathered the works of Fung [4], Bisplinghoff et al. [12, 23], Garrick [18, 24], and Felt et al. [25] to give a detailed history for AE and ASE. The coming section presents important points of the AE and ASE history for aircraft, based on the above-mentioned studies and many others, notably those of Singh [7], Nithin and Vijayalakshmi [9], Collar [26], Friedmann [27], Livne [28], and Čečrdle [29].

The aeroelastic effects were present even before the ever first successful flight attempt of the Wright Brothers in December the 17th, 1903. Not long ago, Samuel Langley's airplanes (Aerodromes) failed in the two flight trials that he carried out, even when his half-scaled aerodromes could fly up to 300 meters, and the reason behind the nonsuccess of the second and last flight attempt in December the 8th, 1903 was a wing torsional divergence, where the Wright Brothers' biplane had more wings rigidity than the Langley's airplane, both airplanes are shown in Figure I.4. In 1914, Curtis has provided some changes to the Langley's aerodrome, and the latter flew this time successfully.

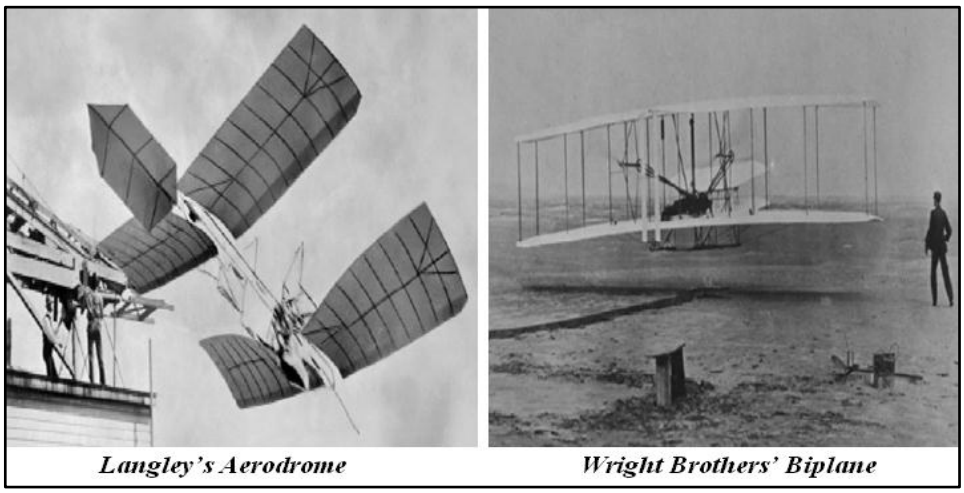

Figure I.4. The Langley's aerodrome and the Wright Brothers' biplane aircraft

The first recorded case of flutter (Documented by F. W. Lanchester) was the Handley Page's 0/400 bomber in 1916 in the United Kingdom (UK), in a form of violent vibrations of the fuselage and the tail due to their low rigidity, and to a coupling between the fuselage torsional vibration mode and the antisymmetric elevators oscillation mode (The two elevators were actuated independently). This problem was resolved by stiffly coupling the elevators by

a torque tube. Since then, flutter became a frequent phenomenon during the World War I (WWI), like the case of the British DH-9 biplane fighter. The adopted solution for this phenomenon then was mass balancing (Placing a mass balance around the structure's hinge line). Many other airplanes suffered from aeroelastic problems, such as:

- Several crashes of the German Fokker's high- wing monoplane D-8 (Despite its great performance), due to torsional divergence;
- Wing aileron flutter in the Van Berkel seaplane in 1923, the Gloster Grebe in 1924, and the Gloster Gamecock in 1925;
- Aileron reversal remarked for the first time in the Bristol Bagshot tests in 1927;
- Crash of a fluttered Junkers JU 90 in 1938 during flight tests;
- Transonic aileron buzz (An aeroelastic phenomenon that occurs for transonic and supersonic airspeeds due to shock waves and pressure vibrations over the airfoil) for the Lockheed P-80, the F-14, and the F-100 between 1944 and 1956;
- LCO experienced by the F-16, F-18, and F-111 between 1947 and 1956.

With every incident due to aeroelastic phenomena, the efforts to understand this field and cure these problems kept growing. The 1920s knew so much interest in the aeroelastic problems analyses (Notably flutter) that it has been named by A. R. Collar [26] the "flutter decade", where the fundamental theories of flutter were drawn up by Küssner in Germany and by Frazer and Duncan in the UK at the end of this decennary. Numerous studies about unsteady aerodynamics were published by Brimbaum, Glauert, Wagner (The Wagner's function in 1925), Frazer, Duncan, and Küssner between 1923 and 1929, and the theory of the distribution of unsteady forces acting on a harmonically oscillating airfoil with one control surface was developed by Theodorsen in the early 1930s, and has been used later in a lot of studies in the unsteady aerodynamic field. This decennary was also called (By Collar) the "theoretical advance decade", in which was the first use of the word "aeroelasticity" by H. Roxbee Cox and A. Pugsley at the Royal Aircraft Establishment, and it knew a big turn in the aircraft design from biplane to monoplane, with a variety of aeroelastic investigations in different directions. Also, some flight test techniques have been developed and used in this period. In 1946, A. R. Collar established the known AE definition through his triangle of forces (Discussed in section I.1.2).

Generally, by the 1950s and 1960s, most of aeroelastic phenomena were well understood and formulated in high-speed aircraft conception and wind tunnel tests utilized to confirm the analytical models, and the number of incidents caused by aeroelastic phenomena fell off from 146 between 1933 and 1945 to seven between 1960 and 1972. The 1970s were considered more special because it knew some important technological advance in the field of AE, like the introduction of the structural dynamics finite elements technique that permitted the analysis of complex aeroelastic systems, the apparition of aeroelastic tailoring thanks to composite materials, and the apparition of the active control technology (Aeroservoelasticity) with analytic and computational methods leveled-up. This advance seemed to be satisfying to researchers since then and till 1999, where Friedmann [27] gave a different vision, affirming that considering AE as full-grown is not completely the right idea, and that many challenges are facing it and will face it in the coming years, like the recent ASE that he predicted it will get more interest and needed enhancements, aeroelastic nonlinearities, computational AE, and the effects of new technologies on the aeroelastic systems modeling, analyses, and control. All of these points became interesting research topics for the subsequent studies.

Aeroelastic analysis, modeling, and flutter prediction:

Since they are multidisciplinary research subjects, AE and ASE are complex domains that require to deal with multiple challenges in different directions like aeroelastic systems' modeling (Taking in account aerodynamic and structural nonlinearities [4]), the analyses and prediction methods of aeroelastic phenomena (Especially flutter), and their suppression techniques [27]. A remarkable number of reviews on AE have been elaborated by researchers, in order to get it clarified and understood [28- 30]. An example of these works is the one of Nithin and Vijayalakshmi [9] who gave a general overview about AE, presenting its definition with some historical development, and explained static and dynamic AE with the most encountered aeroelastic phenomena for every case, such as divergence and flutter. The study affirmed that AE is a vibrating aerospace engineering issue that has an unignorable effect on the design of the recent civil and fighter aircraft.

A special attention is afforded to the aeroelastic systems' modeling and flutter analysis and prediction in multiple relatively-old and recent studies. These studies covered the aeroelastic design of full aircraft (Civil and military airplanes and UAVs), wings, and wing sections, operating in subsonic, transonic, and supersonic flows, under steady, quasi-steady, and unsteady aerodynamics, considering (In the case of nonlinear aeroelasticity NLAE [31]) the

different nonlinearities that can be in the aeroelastic structure (For example a nonlinear stiffness coefficient or a geometric nonlinearity due to large deflections) or in the aerodynamic flow's nature (For example a nonlinearity caused by shock waves movement in a transonic flow) [32- 45]. It can be seen from examining the different investigations in this field that the established models vary from linear single-degree-of-freedom structural models under linear aerodynamic loads, to fully nonlinear models with completely unsteady aerodynamics.

Lee et al. [33] explained in some detail the structural and aerodynamic nonlinearities that can be confronted in aeronautical engineering, and introduced them in the design of a two-degree-of-freedom (2-DOF) two-dimensional airfoil in a subsonic unsteady flow in order to analyze the LCOs, bifurcation and chaos behavior. This investigation has been used as a reference by many succeeding studies in the aeroelastic analyses and modeling field. Nonlinear aeroelastic wing stability was analyzed in [35, 36]. The aeroelastic model was established by combining the structural model and the aerodynamic one in which the unsteady incompressible aerodynamic charges were represented via the Wagner's function. In [38], Iannelli et al. discussed a general approach for modeling an aeroelastic typical section with unsteady aerodynamic loading, exposing and comparing the benefits and cons with some illustrative applications of the two problem formulation approaches which are the frequency and the state-space methods. Then, the advantages of both modeling paths were included in a proposed unified plan of robust modeling. Xiang et al. [39] presented a review of some recent advance and challenges in aircraft nonlinear aeroelasticity for two-dimensional (2-D) airfoils, high-aspect-ratio wings, and full aircraft, including strip theory and vortex-lattice aerodynamic modeling methods.

Flutter analysis and prediction are necessary in the aim of defining the flutter-free flight envelope and fixing safety margins. This includes the aeroelastic system's design where the interactions between the structural vibrations and unsteady aerodynamics are involved, and several tests are run (Numerically, in wind tunnels, ground vibration testing, etc.) for high air velocities, because of the flutter dependence on the air loads which provide energy that feeds the self-excitation of the aeroelastic structure corresponding to flutter occurrence [46- 52]. Flutter calculations need the availability of the airplane's mass, stiffness, and aerodynamic model, which means that to perform these calculations, the aircraft initial model is required [46]. Therefore, if the current design does not fulfill the flutter analyses needs, a redesign is recommended, causing a time and money losses. That's why flutter analyses should be done

in parallel with the airplane's modeling [47]. Lokatt [48] suggested a method to analyze flutter features for a delta wing model which includes structural and aerodynamic modeling uncertainties. This method showed efficiency in analyzing the combined effect of structural and aerodynamic uncertainties, and it has been concluded that these introduced uncertainties are essential in order to have accurate flutter analyses and predictions. Latif et al. [49] presented a new method of flutter examination using a computer-aided design approach for high-aspect-ratio-wing UAVs' modeling where structural and aerodynamic nonlinearities have not been taken into account.

Flutter suppression:

As stated earlier, flutter is the most harmful of all the aeroelastic undesired phenomena. It may cause crew and passengers' discomfort, aircraft performance deterioration and loss of control, it affects also the weapons' targeting in the military aircraft case, and can go generally from structural damages till aircraft destruction [31, 47].

Even though flutter incidents are infrequent at the present moment, this doesn't mean that flutter problems have been completely overcome [31]. Thus, numerous investigations have been carried out, aiming to find efficient techniques to eliminate this disastrous instability and to avoid its catastrophic effects [53- 57]. The flutter elimination methods keep progressing from long time ago and till nowadays, and are classified in two categories which are Passive Flutter Suppression (PFS) and Active Flutter Suppression (AFS) techniques.

Historically, PFS was adopted by researchers in the first flutter suppression investigations [58], where aircraft designers were obliged to make aeroelastic structures heavier by increasing their stiffness and changing the mass and flexural axes, in order to cope with aeroelastic instabilities and maintain the structural integrity, this operation was known as the aeroelastic penalty [31]. In general, PFS techniques involves mass balancing and stiffness or shape changing [56- 62]. In spite of the fact that these methods have a robust performance, they provide additional structure's weight which results in many problems like extra costs (A jump in the fuel consumption, etc.), and may impose constrains that would dangerously affect the airplane performance [56, 59]. Consequently, the research has been redirected at present towards AFS as an alternative to PFS techniques whose usage in aircraft has become very limited to some applications of airplanes' components where active control approach can't be performed with ease, like in the study of Cunha-Filho et al. [60], where surface viscoelastic damping treatments applied on flat panels under supersonic flow were adopted in order to

deal with panel flutter problems. It has been found that the utilized passive strategy has improved the flutter velocity, but, it has been noticed that flutter boundaries depend highly on the viscoelastic treatment's temperature and geometrical features. Also, it has been affirmed that this technique induces additional weight that should not be neglected, and an optimization of the structural and aerodynamic properties has to be introduced in the aim of having maximized damping with minimized mass addition.

Alternatively, active control systems removes the need for extra-weight by providing artificial stiffness and damping to the aircraft structure in order to enhance flutter limits, using aerodynamic control surfaces that are activated by actuators via a feedback system control law which gets the input information from the different sensors. AFS is a main part of active control technology (In the field of ASE) whose objectives are the aeroelastic systems' stabilization and performance enhancement, the aeroelastic instabilities elimination, the passengers' comfort, and the mitigation of gusts' dynamic loads [59, 63, 64]. Livne [63] gave an important contribution in AFS field and in active control theory in general, by presenting a profound review of more than 50 years of investigation in this area, with some history, a state-of-art of the AFS key disciplines, inclosing classical control, modern control, adaptive control, and control of parameter-varying systems. The study offers also a very rich bibliography that contains more than 700 references in the ASE domain, in the aim of helping and leading the current and future works in this field.

Many active controllers have been designed for full aircraft [65, 66] or a flexible part like aeroelastic wings [67, 68], aeroelastic wing sections with only one control surface (Trailing Edge Control Surface TECS) [69- 74], or with both Trailing-and-Leading Edge Control Surfaces [74- 79]. These controllers are classified in two main categories: Classical controllers, like PID (Proportional Integral Derivative), LQG (Linear Quadratic Gaussian), and LQR (Linear Quadratic Regulator) controllers. And modern controllers, like H_∞, μ-analysis, Sliding Mode Control (SMC), and backstepping. A brief comparison between some classical and modern controllers has been made by Malik and Sehgal [80].

Bruce and Jinu [56] reviewed many researchers' investigations in the AFS field to present the development of the solutions to AE and ASE problems through time from passive methods to active ones, arriving to AFS classical and recent techniques (Using Computational-Structural-Dynamics/Computational-Fluid-Dynamics CSD/CFD analysis). The effectiveness of these methods has been shown using LQG and LQR controllers applied

on a nonlinear aeroelastic wing-flap section of a typical airfoil. Stability analysis for a thin triangular wing with a TECS in unsteady flow was studied by Borglund and Kuttenkeuler [69]. This study showed that the use of only one TECS leads to stabilization problems that have been fixed by numerical optimization, and the numerical stability analysis was verified by Experimental flutter tests. Two control strategies based on LQG and H_∞ have been used in [73] for an aeroelastic triangular wing with a control surface in order to analyze and actively suppress flutter. It has been shown that the established controllers have increased the flutter velocity with good system's performance. But, it has been stated that the model is considered linear at every speed value, and then it cannot be effective for large displacements and disturbances.

It is important to know that the majority of the studied systems in AE and ASE domains are under-actuated, i.e. having a lower number of independent actuators than the number of degrees of freedom (DOF) to control (In the opposite case, if the number of actuators is higher than the DOF then the systems are called over-actuated) [81]. The wide use of under-actuation in aeroelastic systems' control design is justified by the need to rely on few actuators to minimize the impact of an eventual actuator's failure, and by the fact that fewer actuators means less weight and costs [82]. A survey about under-actuated mechanical systems has been produced by Liu and Yu in [81], including history, state-of-art, and control design. And a global robust control is derived in [83] for an under-actuated nonlinear wing section.

Robust control:

The main challenges for many studies in active control field are about the controllers' robustness (Insensitivity to uncertainties and disturbances) with the improvement of systems' performances. The common robust control techniques use a nominal model which is subject to uncertainties that are taken into account as a design constraint of the controller so that it can guarantee robust stability and even robust performance. For this reason, robust control approach is attractive and suitable for aircraft control problems [3]. However, the introduction of uncertainties makes the system more complex with important controller's dimensions, which may lead to degradation in term of performance [3]. Then, a trade-off between performance and robustness needs to be managed while designing robust active controllers. This section provides a brief presentation of robust control and some robust controllers with examples from corresponding research. More details about the robust controllers adopted in this work are given in chapter III.

Wang et al. [76] detailed the recent advance in adaptive and robust control used in lifting nonlinear aeroelastic wings having only one TECS and with TLECS, for quasi-steady and unsteady aerodynamic models in subsonic and supersonic flows. They examined the aeroelastic system response to ephemeral and to time-varying disturbances using state estimation and stability analysis methods. Structural nonlinearities with unknown system parameters for a prototypical wing with TLECS were investigated in [77] to design an adaptive and neural controller. Teng [78] and Fatehi et al. [79] used the μ-method for flutter analysis, robust stability prediction, and control of nonlinear aeroservoelastic wings with TLECS for quasi-steady aerodynamic models. This method is based on introducing uncertainties parameters to dynamic pressure, structural stiffness and damping, and analyzing their influence on flutter and stability margins. These studies [78, 79] showed an agreement between predicted and experimental results, but, it is noticed in both investigations that used quasi-steady aerodynamic models, that the μ-analyses did not increase the critical flutter velocity in a significant way. Also, this method generates high order controllers [3].

An efficient solution to the complex control problem of nonlinear uncertain systems is the Sliding Mode Control (SMC) approach [84], which is a special class of variable-structure systems control [85]. SMC is extensively studied and widely used [84- 90] thanks to its advantages. Indeed, SMC has a low sensitivity to perturbations and uncertainties, a finite-time convergence, high accuracy, and relatively simple application [84, 85]. The SMC idea is to drive the system's trajectories to reach a domain (Called sliding surface) in limited time, and to slide around this sliding surface towards the desired equilibrium position, by designing a specific controller that contains a discontinuous control law (A sign function) [84]. In the other hand, the discontinuous nature of SMC law and the neglected or unmodeled dynamics lead often to the appearance of the famous side effect of SMC which is an oscillation phenomenon known as chattering [91- 93]. The chattering phenomenon is the most encountered obstacle in the SMC implementation and the most discussed problem in the literature of SMC [92] because it affects the controller accuracy and causes mechanical parts (Actuators) usury [84, 95].

To reduce or suppress the chattering phenomenon and its negative influence, many solutions have been suggested by researchers, like replacing the switching part of the SMC law by an approximate continuous function (Saturation, hyperbolic tangent, or arc tangent functions), designing a high order SMC law (HOSMC) [91, 92], or combining SMC with other control approaches in a way that allows to take advantage of the properties of these

control laws to deal with chattering and enhance the systems performances [94- 100]. Second-order SMC was coupled with backstepping technique in [95] by adding a disturbance and uncertainty compensator term in the controller's expression, and a modified high order SMC containing a time continuous function to describe nonlinearities was proposed in [96]. Both studies were effective in removing LCOs and stabilizing the system in finite time with no chattering. Liu and Wang [97] exposed (With designs, simple examples, and some Matlab/Simulink implementations) plenty of possible Conventional Sliding Mode Control (CSMC) combinations, from which Fuzzy Sliding Mode Control (FSMC) is proposed as a solution for chattering problems. They gave also various examples of FSMC such as FSMC based on equivalent control, and SMC based on fuzzy switching-gain.

Fuzzy Logic Controller (FLC) relies on linguistic data and rule-based algorithms, his structure is simple to design and does not demand a complete knowledge of the system's model [101], that's why it is commonly used in several domains and for different purposes [101- 106]. However, the FLC approach depends on the human knowledge and expertise about the studied case when selecting membership functions and fuzzy rules [107]. Therefore, FSMC is designed for its ability to fulfill the needed systems' fast convergence ensured by the robust SMC, and to remove the chattering phenomenon thanks to the FLC introduction.

To sum up, one can notice from the examination of the exposed previous works in the areas covered by ASE and the evolution of these works through time; that the investigation in this multidisciplinary domain requires to take into consideration many factors in several fields, for example:

- The choice of the aeroelastic system to study: Full aircraft, wings, wing section(s);
- The aeroelastic systems' modeling: The consideration (Or not) of systems' nonlinearities, the aerodynamic loads nature (Steady, quasi-steady, unsteady), the airflow type (subsonic, transonic, supersonic);
- The control design: Classical/modern, linear/nonlinear, control robustness, etc.

Many strategies and compromises have been adopted by researchers in order to have stabilized systems with improved performances and removed aeroelastic instabilities. One of these strategies is to design a relatively simple model using linearization and simplification hypotheses or neglecting some dynamics (For example the design of a linear aeroelastic wing section under steady or quasi-steady aerodynamic loads), and apply nonlinear complex control laws that considers uncertainties and disturbances (For example the nonlinear μ-

analysis). The reversed strategy is to design a complex model (For example the design of a nonlinear aeroelastic wing with unsteady aerodynamics), and to apply a simple controller (Like the classical PID controller). But, every method has a bill to pay in terms of performance and aeroelastic stability margins. Besides, some linear simple controllers are ineffective for nonlinear uncertain models. Thus, the need to introduce the systems' nonlinearities and to consider the unsteady aerodynamic charges with robust controllers lead to have aeroelastic models and control laws that are becoming more complex with an increased number of systems' states from which some may be unmeasurable [108], which means more sensors and higher costs. To deal with these complexities, the robust established controllers (Such as SMC) can be associated with a state estimator [109]. The literature concerning observer-based SMC is relatively few [110], however, this research topic is getting more investigated and used nowadays [111] thanks to its ability to ensure robust and stable models with few known systems' states.

I.5. Approach

In the present thesis, robust control laws are designed and applied on a nonlinear aeroelastic UAV's wing section (Fixed-wing UAV category) with TLECS undergoing unsteady aerodynamic loads, in order to have a well-stabilized aeroelastic system, to suppress flutter and LCO, to enhance the system's performance and the stability boundaries notably the flutter velocity. This new direction in the ASE research field passes by fulfilling the following tasks:

- The introduction of unsteady aerodynamics in the nonlinear aeroelastic system model (Structural nonlinearity) using the Wagner's function;
- Designing a SMC law, a FSMC, and a FSMC based on a High Gain Observer (HGO) where:

✓ SMC is used to ensure fast flutter/LCO elimination and system's stabilization in a finite time, with high performances and increased flutter speed margins;

✓ FLC ensures the suppression of the chattering phenomenon; and

✓ HGO used to estimate the system's states that are numerous due to the unsteady aerodynamics and the structural nonlinearities introduction and that are also hard to measure.

- Discussing and comparing the controllers' effectiveness in suppressing instabilities and improving performances, by visualizing the obtained simulation results, and proposing some future directions in ASE.
- Provide a rich bibliography which contains several documents dealing with the essential disciplines that are enclosed in ASE, and that can be useful as a starting point for future investigations in the ASE field.

CHAPTER II:

The aeroelastic system’s modeling

Contents

II.1. Introduction

The first step in the control and performances' improvement of an aeroelastic system is to establish its mathematical model. This allows also analyzing, understanding, and predicting the aeroelastic phenomena that can take place, and the dynamic behavior of the system when the latter is subject to external influences and contains structural or aerodynamic nonlinearities, and consequently, being able to define and to push the aeroelastic system's stability margins.

In classical theory, structures and aerodynamics are assumed to be linear when modeling the aeroelastic interactions. Though, it has been shown through many wind-tunnels' experiments and flight tests that this theory could not predict some undesired aeroelastic phenomena such as LCOs and unexpected control surfaces' responses [33], hence, it is necessary to consider the different structural and aerodynamic nonlinearities in the system's model.

It is also important for modeling accuracy, to take unsteady aerodynamic loads into account. The theories in unsteady-aerodynamics modeling started from the 1920s with some researcher's studies, notably with the Theodorsen's function established in the frequency domain, and the Wagner's function in the time domain (Figure II.1). A relation between the two functions is explained by leishman and Nguyen [112] who affirmed that these functions are related by Fourier Transform (FT) methods (Figure II.1), explaining that the Wagner's function can reproduce the frequency response with accuracy using FT techniques and Jones's approximation [112- 115]. Although, the introduction of unsteady aerodynamics in AFS field is a new concept, where most of the studies in modeling and in control were made separately, and the AFS research was performed for quasi-steady or even steady aerodynamic flows [3].

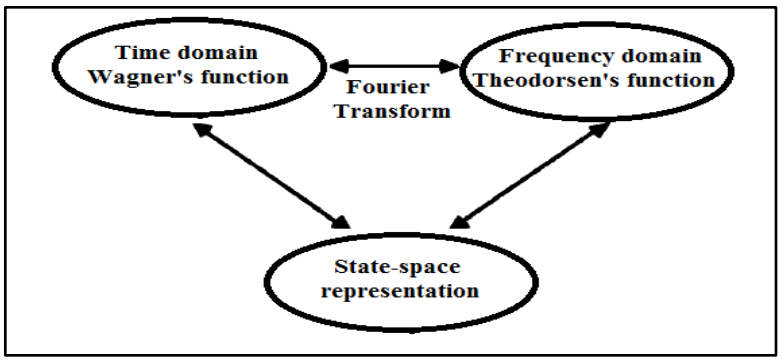

Figure II.1. Relation between Theodorsen's and Wagner's functions for unsteady aerodynamic modeling

The present chapter details the followed steps for modeling a two-dimensional (2D) 2-DOF nonlinear aeroelastic airfoil with TLECS, operating in a subsonic incompressible airflow with an airspeed V, starting with structural modeling via the Lagrange formalism used to obtain the governing equations of motion for the aeroelastic system. After that, the aerodynamic lift (L) and moment (M) are expressed based on the Wagner's function for unsteady aerodynamics [24]. Structural and aerodynamic models are finally combined in order to have the adopted nonlinear aeroelastic system's model under its state-space representation, where the flight dynamic model describes the plunge and pitch motions for the studied system. For the numerical application of the established model, the TAMU II wing model parameters are used, this wing model has been exploited in several studies, like in [33, 75, 114, 116].

II.2. Mathematical model establishment

The system's mathematical model is built by combining structural and aerodynamic models as will be detailed in the coming sections, taking into consideration some assumptions that aim to facilitate the system's modeling and study by eliminating the physical effects of low importance, such as neglecting the gravity effect and assuming the pitch angle to have small values [3].

II.2.1. Structural modeling

In order to obtain this model, some formalism like the one of Newton or that of Lagrange can be applied. The latter is a powerful tool particularly suitable for putting complex systems under equations [117]. It is a procedure to establish the equations of motion, by calculating the kinetic and potential energies of the studied system (See appendix A). The considered 2D typical section's geometry is presented in figure II.2 bellow [30].

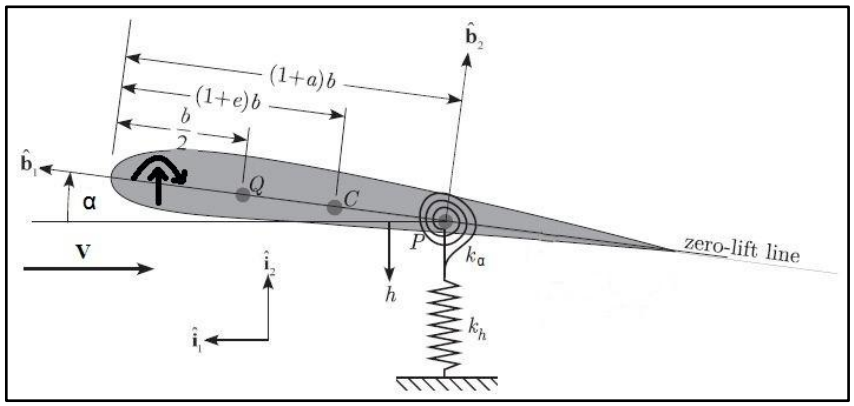

Figure II.2. The geometry of the studied 2D wing section [30]

Two movements are considered: The pitching motion α (Torsion) around the elastic axis (The axis which is perpendicular to the shear axis [3]), and the vertical motion h (Plunge displacement, bending or flexure), where the structural stiffness for the two motions is modeled by two springs of stiffness coefficients k_α and k_h respectively, where k_h is assumed to be constant and k_α has the following general expression:

$$K_\alpha = \sum_{i=1}^{n} C_i \alpha^{i-1} \quad \text{with} \quad C_i \in R \tag{II.1}$$

As shown in figure II.2, three remarkable points can be distinguished: The center of gravity C, the elastic center P, and the aerodynamic center Q, where the dimensionless parameters a and e ($-1 < a < 1$ and $-1 < e < 1$) determine the position of the points C and P.

Knowing that c is the chord and b is the mid-chord ($c = 2b$), the position of the aerodynamic center Q is found starting from the quarter-chord position ($c/4$) [30]. The aerodynamic lift L and moment M are measured at the aerodynamic center.

The $\vec{\imath}$ frame represents the inertial frame, and the $\vec{b}$ frame is fixed to the wing, its origin is the center of elasticity P and its direction is shown in figure II.2, where the axis ($\overrightarrow{b_1}$) is oriented towards the leading edge direction.

The Lagrange equations used to define the plunge and pitch motions' equations are obtained by calculating the potential and kinetic energies of the studied system.

Potential energy

The studied system's potential energy consists entirely of elastic energy knowing that the effect of gravity is neglected. It represents then the elastic energy stored in the two springs.

The total potential energy U is given by this equation:

$$U = \frac{1}{2} K_h \, h^2 + \frac{1}{2} k_\alpha(\alpha) \, \alpha^2 \tag{II.2}$$

All the equation parameters are defined in the section above.

Kinetic energy

The total kinetic energy of the system T is given by:

$$T = \frac{1}{2} m \overrightarrow{V_{gc}} . \overrightarrow{V_{gc}} + \frac{1}{2} I_{gc} \dot{\alpha}^2 \tag{II.3}$$

Where:

I_{gc} is the moment of inertia around the gravity center.

m is the wing mass.

V_{gc} is the gravity center velocity, it is calculated using the following formula [30].

$$\overrightarrow{V_{gc}} = \overrightarrow{V_{ec}} + \dot{\alpha}\overrightarrow{b_3} \times b[(1+a)-(1+e)]\overrightarrow{b_1} \quad \text{(II.4)}$$

With:

$\overrightarrow{V_{ec}}$ is the elastic center velocity, it has the following expression.

$$\overrightarrow{V_{ec}} = -\dot{h}\overrightarrow{\imath_2} \quad \text{(II.5)}$$

h is the plunge displacement.

Knowing that $\overrightarrow{b_2} = \overrightarrow{b_3} \times \overrightarrow{b_1}$ then, the expression of $\overrightarrow{V_{gc}}$ becomes as follows:

$$\overrightarrow{V_{gc}} = -\dot{h}\overrightarrow{\imath_2} + \dot{\alpha}b(a-e)\overrightarrow{b_2} \quad \text{(II.6)}$$

The link between the $\vec{\imath}$ and the $\vec{b}$ frames is given by the following matrix relation:

$$\begin{bmatrix}\overrightarrow{b_1}\\ \overrightarrow{b_2}\end{bmatrix} = \begin{bmatrix}\cos(\alpha) & \sin(\alpha)\\ -\sin(\alpha) & \cos(\alpha)\end{bmatrix}\begin{bmatrix}\overrightarrow{\imath_1}\\ \overrightarrow{\imath_2}\end{bmatrix} \quad \text{(II.7)}$$

Assuming the pitch angle is small, i.e. $\cos(\alpha) \approx 1$ and $\sin(\alpha) \approx \alpha$, and using equation (II.7), the following expression is obtained.

$$\overrightarrow{V_{gc}}.\overrightarrow{V_{gc}} = \dot{h}^2 + b^2{x_\alpha}^2\dot{\alpha}^2 + 2\mathrm{b}x_\alpha\dot{\mathrm{h}}\dot{\alpha} \quad \text{(II.8)}$$

x_α represents the distance between gravity center and elastic center, where: $x_\alpha = (a-e)$.

The following expression of T is obtained by substituting equation (II.8) in equation (II.3).

$$T = \frac{1}{2}m\left(\dot{h}^2 + b^2{x_\alpha}^2\dot{\alpha}^2 + 2\mathrm{b}x_\alpha\dot{\mathrm{h}}\dot{\alpha}\right) + \frac{1}{2}I_{gc}\dot{\alpha}^2 \quad \text{(II.9)}$$

The relationship between the moment of inertia around the elastic center I_{ec} (Or in another word around the elastic axis) and the moment of inertia around the gravity center I_{gc} is [118]:

$$I_{ec} = I_{gc} + mb^2x_\alpha^2\,[\cos(\alpha)]^2 \cong I_{gc} + mb^2x_\alpha^2 \quad \text{(II.10)}$$

The expression of I_{gc} is replaced in equation (II.9), the kinetic energy is written as follows.

$$T = \frac{1}{2}m\left(\dot{h}^2 + 2x_\alpha b\dot{h}\dot{\alpha}\right) + \frac{1}{2}I_{ec}\dot{\alpha}^2 \quad \text{(II.11)}$$

Generalized forces

Generalized forces are calculated using the method of virtual work, i.e. the work given by a virtual displacement due to external forces [30] which are in this case the aerodynamic lift and moment.

The total virtual work exerted by the lift L and the moment M is given by:

$$\delta w = Q_h \delta h + Q_\alpha \delta\alpha \quad \text{(II.12)}$$

δh : is the virtual plunge displacement.

$\delta\alpha$: is the virtual pitch motion.

In order to calculate the virtual displacement due to lift, the velocity of the aerodynamic center $\overrightarrow{V_{ac}}$ is needed.

$$\overrightarrow{V_{ac}} = -\dot{h}\overrightarrow{\imath_2} + \dot{\alpha}b\left(\frac{1}{2} + a\right)\overrightarrow{b_2} \quad \text{(II.13)}$$

Then, the virtual displacement due to lift $\overrightarrow{\delta P_{ca}}$ can be obtained by replacing the point above each variable in equation (II.13) by δ [30]. Then:

$$\overrightarrow{\delta P_{ca}} = -\delta h\overrightarrow{\imath_2} + b\delta\alpha\left(\frac{1}{2} + a\right)\overrightarrow{b_2} \quad \text{(II.14)}$$

So, the virtual work due to lift δw_L is given by:

$$\delta w_L = L\left[-\delta h + b\left(\frac{1}{2} + a\right)\delta\alpha\right] \quad \text{(II.15)}$$

The angular velocity of the wing is $\dot{\alpha}\overrightarrow{b_3}$ then, the virtual rotation due to aerodynamic moment δR_{ac} has the following expression:

$$\delta R_{ac} = -\delta\alpha\overrightarrow{b_3} \quad \text{(II.16)}$$

So, the virtual work due to moment δw_m is:

$$\delta w_m = M\delta\alpha \quad \text{(II.17)}$$

The total virtual work done by the lift L and the moment M is then:

$$\delta w = \delta w_L + \delta w_m = L\left[-\delta h + b\left(\frac{1}{2} + a\right)\delta\alpha\right] + M\delta\alpha \quad \text{(II.18)}$$

By correspondence between equations (II.12) and (II.18), the generalized forces become:

$$Q_h = -L \tag{II.19}$$

$$Q_\alpha = M + x_\beta L \tag{II.20}$$

With : $x_\beta = \mathrm{b}\left(\frac{1}{2} + a\right)$

The equations of motion can now be obtained by combining all the pieces, using Lagrange's equations, where:

$$\begin{aligned} &\frac{d}{dt}\left(\frac{\partial(T-U)}{\partial \dot{h}}\right) - \frac{\partial(T-U)}{\partial h} = Q_h \\ &\frac{d}{dt}\left(\frac{\partial(T-U)}{\partial \dot{\alpha}}\right) - \frac{\partial(T-U)}{\partial \alpha} = Q_\alpha \end{aligned} \tag{II.21}$$

After derivation, the equations of motion become:

$$\begin{aligned} &m\,\ddot{h} + m\,b\,x_\alpha\,\ddot{\alpha} + k_h\,\mathrm{h} = -L \\ &m\,b\,x_\alpha\,\ddot{h} + I_{ec}\,\ddot{\alpha} + k_\alpha\,\alpha = M \end{aligned} \tag{II.22}$$

In order to model the viscous dumping, the following dissipation function of Rayleigh is used:

$$d = \frac{1}{2}C_h\dot{h}^2 + \frac{1}{2}C_\alpha\dot{\alpha}^2 \tag{II.23}$$

Where: C_h and C_α are the dumping coefficients for plunge displacement and for pitch motion respectively.

The relation (II.23) is included in Lagrange equations as follows:

$$\begin{aligned} &\frac{d}{dt}\left(\frac{\partial(T-U)}{\partial \dot{h}}\right) + \frac{\partial d}{\partial \dot{h}} - \frac{\partial(T-U)}{\partial h} = Q_h \\ &\frac{d}{dt}\left(\frac{\partial(T-U)}{\partial \dot{\alpha}}\right) + \frac{\partial d}{\partial \dot{\alpha}} - \frac{\partial(T-U)}{\partial \alpha} = Q_\alpha \end{aligned} \tag{II.24}$$

Substituting the equations (II.2), (II.11), (II.20), and (II.23) in equation (II.24), the 2-DOF aeroelastic system's governing equations are finally obtained.

$$m\,\ddot{h} + m\,x_\alpha\,b\,\ddot{\alpha} + C_h\dot{h} + k_h h = -L \tag{II.25}$$

$$mx_\alpha b\ddot{h} + I_{ec}\ddot{\alpha} + C_\alpha\dot{\alpha} + k_\alpha(\alpha)\alpha = M \tag{II.26}$$

These equations can be written in the following matrix form.

$$I\begin{bmatrix}\ddot{h}\\ \ddot{\alpha}\end{bmatrix} + F\begin{bmatrix}\dot{h}\\ \dot{\alpha}\end{bmatrix} + E\begin{bmatrix}h\\ \alpha\end{bmatrix} = \begin{bmatrix}-L\\ M\end{bmatrix} \quad \text{(II.27)}$$

With:

$$\mathrm{I} = \begin{bmatrix} m & m\,x_\alpha \mathrm{b} \\ m\,x_\alpha \mathrm{b} & I_{ec}\end{bmatrix} \qquad F = \begin{bmatrix} C_h & 0 \\ 0 & C_\alpha\end{bmatrix} \qquad \mathrm{E} = \begin{bmatrix} k_h & 0 \\ 0 & k_\alpha(\alpha)\end{bmatrix}$$

I is the matrix of inertia ; **F** is the matrix of dumping ; and **E** is the matrix of stiffness.

II.2.2. Aerodynamic modeling

The aerodynamic lift and moment acting on a 2D airfoil in an incompressible subsonic flow are modeled using the Wagner's function $\varphi(t)$ and the Jones' approximation for unsteady aerodynamics theory [5, 76, 112, 113 114]. This approximation agrees with the accurate response within a precision of 1%, which is sufficient for most practical aims according to the Leishman's study [119]. The expressions of *L* and *M* are as follows.

$$L(t) = \pi\rho b^2 s\left[\ddot{h} - ab\ddot{\alpha} + V\dot{\alpha}\right] + 2\pi\rho Vbs\left[\dot{h}(0) + V\alpha(0) + b\left(\frac{1}{2} - a\right)\dot{\alpha}(0)\right]\varphi(t) +$$

$$2\pi\rho Vbs\int_0^t \varphi(t-\sigma)\left[\ddot{h} + b\left(\tfrac{1}{2} - a\right)\ddot{\alpha} + V\dot{\alpha}\right]d\sigma + \rho V^2 bsC_{l\beta}\beta + \rho V^2 bsC_{l\gamma}\gamma \quad \text{(II.28)}$$

And:

$$M(t) = \pi\rho b^3 s\left[a\ddot{h} - b\left(\frac{1}{8} + a^2\right)\ddot{\alpha} - V\left(\frac{1}{2} - a\right)\dot{\alpha}\right] +$$

$$2\pi\rho Vb^2 s\left(\frac{1}{2} + a\right)\left[\dot{h}(0) + V\alpha(0) + b\left(\frac{1}{2} - a\right)\dot{\alpha}(0)\right]\varphi(t) +$$

$$2\pi\rho Vb^2 s\left(\frac{1}{2} + a\right)\int_0^t \varphi(t-\sigma)\left[\ddot{h} + b\left(\frac{1}{2} - a\right)\ddot{\alpha} + V\dot{\alpha}\right]d\sigma +$$

$$\rho V^2 b^2 sC_{m\beta}\beta + \rho V^2 b^2 sC_{m\gamma}\gamma \quad \text{(II.29)}$$

ρ is the air density. V is the freestream velocity. s is the wing section surface. β and γ are respectively the trailing-edge and leading-edge control surfaces deflections. $C_{l\alpha}$, $C_{l\beta}$, $C_{l\gamma}$ and $C_{m\alpha}$, $C_{m\beta}$, $C_{m\gamma}$ are the lift and the moment coefficients derivatives per α, β and γ respectively. φ(t) and φ̇(t) are respectively, the Wagner's function and its derivative [113], where:

$$\varphi(t) = 1 - C_1 e^{-\varepsilon_1(V/b)t} - C_2 e^{-\varepsilon_2(V/b)t} \quad \text{(II.30)}$$

With: $C_1 = 0.165$; $C_2 = 0.335$; $\varepsilon_1 = 0.0455$ and $\varepsilon_2 = 0.3$

$$\dot{\varphi}(t) = C_1\varepsilon_1(V/b)e^{-\varepsilon_1(V/b)t} + C_2\,\varepsilon_2(V/b)e^{-\varepsilon_2(V/b)t} \quad \text{(II.31)}$$

Using the integration by parts and the Wagner's function definition, the equations (II.28) and (II.29) become as follows.

$$L(t) = \pi\rho b^2 s\left[\ddot{h} - ab\ddot{\alpha}\right] - 2\pi\rho Vbs\left[h(0) + b\left(\frac{1}{2} - a\right)\alpha(0)\right]\dot{\varphi}(t) +$$
$$2\pi\rho Vbs\left\{\varphi(0)\dot{h} + b\left(\frac{1}{2} - a\right)\left[\varphi(0) + \frac{1}{1-2a}\right]\dot{\alpha} + \dot{\varphi}(0)h + \left[V\varphi(0) + b\left(\frac{1}{2} - a\right)\dot{\varphi}(0)\right]\alpha\right\}$$
$$- 2\pi\rho Vbs\left[\lambda_{h_1}e^{-\varepsilon_1 t}\int_0^t h(\sigma)e^{\varepsilon_1\sigma}d\sigma + \lambda_{h_2}e^{-\varepsilon_2 t}\int_0^t h(\sigma)e^{\varepsilon_2\sigma}d\sigma\right] +$$
$$2\pi\rho Vbs\left[\lambda_{\alpha_1}e^{-\varepsilon_1 t}\int_0^t \alpha(\sigma)e^{\varepsilon_1\sigma}d\sigma + \lambda_{\alpha_2}e^{-\varepsilon_2 t}\int_0^t \alpha(\sigma)e^{\varepsilon_2\sigma}d\sigma\right] +$$
$$\rho V^2 bsC_{l\beta}\beta + \rho V^2 bsC_{l\gamma}\gamma \quad \text{(II.32)}$$

And:

$$M(t) = \pi\rho b^3 s\left[a\ddot{h} - b\left(\frac{1}{8} + a^2\right)\ddot{\alpha}\right] - 2\pi\rho Vb^2 s\left(\frac{1}{2} + a\right)\left[h(0) + b\left(\frac{1}{2} - a\right)\alpha(0)\right]\dot{\varphi}(t) +$$
$$2\pi\rho Vb^2 s\left(\frac{1}{2} + a\right)\left\{\varphi(0)\dot{h} + b\left(\frac{1}{2} - a\right)\left[\varphi(0) - \frac{1}{1+2a}\right]\dot{\alpha} + \dot{\varphi}(0)h\right\} +$$
$$2\pi\rho Vb^2 s\left(\frac{1}{2} + a\right)\left[V\varphi(0) + b\left(\frac{1}{2} - a\right)\dot{\varphi}(0)\right]\alpha -$$
$$2\pi\rho Vb^2 s\left(\frac{1}{2} + a\right)\left[\lambda_{h_1}e^{-\varepsilon_1 t}\int_0^t h(\sigma)e^{\varepsilon_1\sigma}d\sigma + \lambda_{h_2}e^{-\varepsilon_2 t}\int_0^t h(\sigma)e^{\varepsilon_2\sigma}d\sigma\right] +$$
$$2\pi\rho Vb^2 s\left(\frac{1}{2} + a\right)\left[\lambda_{\alpha_1}e^{-\varepsilon_1 t}\int_0^t \alpha(\sigma)e^{\varepsilon_1\sigma}d\sigma + \lambda_{\alpha_2}e^{-\varepsilon_2 t}\int_0^t \alpha(\sigma)e^{\varepsilon_2\sigma}d\sigma\right] +$$
$$\rho V^2 b^2 sC_{m\beta}\beta + \rho V^2 b^2 sC_{m\gamma}\gamma \quad \text{(II.33)}$$

Where: $\lambda_{h_i} = C_i{\varepsilon^2}_i$ and $\lambda_{\alpha_i} = C_i\varepsilon_i\left[V - \varepsilon_i b\left(\frac{1}{2} - a\right)\right]$

In the aim of simplifying the numerical integration of the integral-differential equations (II.32) and (II.33), Lee et al. [33] have derived another form for equations these equations, where they have introduced some new variables.

The final forms of L and M are then as follows [33].

$$L(t) = \pi\rho b^2 s\left[\ddot{h} - ab\ddot{\alpha}\right] - 2\pi\rho Vbs\left[h(0) + b\left(\frac{1}{2} - a\right)\alpha(0)\right]\dot{\varphi}(t) +$$
$$2\pi\rho Vbs\left\{\varphi(0)\dot{h} + b\left(\frac{1}{2} - a\right)\left[\varphi(0) + \frac{1}{1-2a}\right]\dot{\alpha} + \dot{\varphi}(0)h + \left[V\varphi(0) + b\left(\frac{1}{2} - a\right)\dot{\varphi}(0)\right]\alpha\right\} -$$
$$2\pi\rho Vbs\left[\lambda_{h_1} w_1 + \lambda_{h_2} w_2 - \lambda_{\alpha_1} w_3 - \lambda_{\alpha_2} w_4\right] + \rho V^2 bsC_{l\beta}\beta + \rho V^2 bsC_{l\gamma}\gamma \quad \text{(II.34)}$$

And:

$$M(t) = \pi\rho b^3 s\left[a\ddot{h} - b\left(\frac{1}{8} + a^2\right)\ddot{\alpha}\right] - 2\pi\rho Vb^2 s\left(\frac{1}{2} + a\right)\left[h(0) + b\left(\frac{1}{2} - a\right)\alpha(0)\right]\dot{\varphi}(t) +$$
$$2\pi\rho Vb^2 s\left(\frac{1}{2} + a\right)\left\{\varphi(0)\dot{h} + b\left(\frac{1}{2} - a\right)\left[\varphi(0) - \frac{1}{1-2a}\right]\dot{\alpha} + \dot{\varphi}(0)h\right\} +$$
$$2\pi\rho Vb^2 s\left(\frac{1}{2} + a\right)\left\{\left[V\varphi(0) + b\left(\frac{1}{2} - a\right)\dot{\varphi}(0)\right]\alpha\right\} -$$
$$2\pi\rho Vb^2 s\left(\frac{1}{2} + a\right)\left[\lambda_{h_1} w_1 + \lambda_{h_2} w_2 - \lambda_{\alpha_1} w_3 - \lambda_{\alpha_2} w_4\right] +$$
$$\rho V^2 b^2 sC_{m\beta}\beta + \rho V^2 b^2 sC_{m\gamma}\gamma \quad \text{(II.35)}$$

With:

$$w_1 = \int_0^t e^{-\varepsilon_1(t-\sigma)} h(\sigma)\, d\sigma \quad ; \quad w_2 = \int_0^t e^{-\varepsilon_2(t-\sigma)} h(\sigma)\, d\sigma$$
$$w_3 = \int_0^t e^{-\varepsilon_1(t-\sigma)} \alpha(\sigma)\, d\sigma \quad ; \quad w_4 = \int_0^t e^{-\varepsilon_2(t-\sigma)} \alpha(\sigma)\, d\sigma$$
$$\lambda_{h_1} = C_1(V/b)\varepsilon^2{}_1 \quad ; \quad \lambda_{\alpha_1} = C_1(V/b)\varepsilon_1\left[V - \varepsilon_1 b\left(\tfrac{1}{2} - a\right)\right]$$
$$\lambda_{h_2} = C_2(V/b)\varepsilon^2{}_2 \quad ; \quad \lambda_{\alpha_2} = C_2(V/b)\varepsilon_2\left[V - \varepsilon_2 b\left(\tfrac{1}{2} - a\right)\right]$$

II.3. State space representation of the TAMU II wing model

II.3.1. The TAMU II wing model

II.3.1.1. Description

The wing model used in this work and modeled by the equations built above is known as the TAMU II wing model. It is a 2-DOF model with two control surfaces, one in the trailing edge and another in the leading edge (As shown in figure II.3 below). It has been adopted after the low efficiency of the single trailing-edge control surface model (TAMU I wing model) in suppressing aeroelastic instabilities [78].

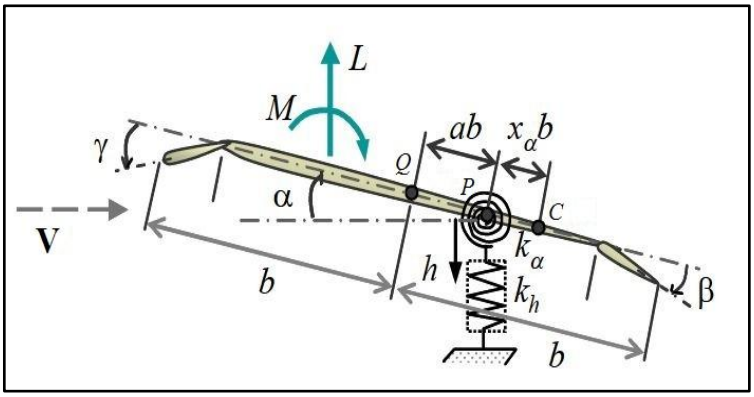

Figure II.3. Aeroelastic model for a flexible wing with TLECS – TAMU II wing model

The TAMU II model is developed in Texas Agricultural and Mechanical University (TAMU) for experiments on nonlinear aeroelastic test devices in wind tunnels, in the purpose of studying the effectiveness of the LCOs elimination techniques for nonlinear aeroelastic systems [75, 78, 114, 116]. A detailed description of the TAMU II wing model is given by Platanitis and Strganac in [75]. Figure II.4 is a photograph that presents a top view with transparent skin of the adopted model, where two FUTABA S9402 servomotors are distinguished. These motors actuate the control surfaces and each one of them can generate 0.654 N.m of torque at a tension of 05 V. Two E2-1024-375-H optical encoders are also mounted in order to permit the control surface deflections' measurements that are then compared to the commanded inputs. It can be also remarked in the same figure that the sizes of the trailing-edge and leading-edge control surfaces are respectively about 20% and 15% from the length of the chord.

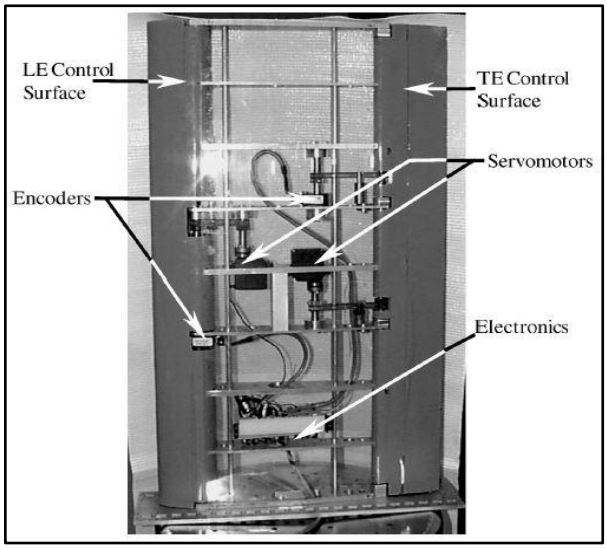

Figure II.4. Top view with transparent skin of TAMU II wing model [75]

II.3.1.2. TAMU II wing model parameters

The equations of motion for this wing model are given as follows [75, 78, 116].

$$m_T\ddot{h} + m_w\, x_\alpha\, b\, \ddot{\alpha} + C_h\dot{h} + k_h\, h = -L \quad \text{(II.36)}$$

$$m_w\, b\, x_\alpha\ddot{h} + I_{ea}\ddot{\alpha} + k_\alpha(\alpha)\alpha + C_\alpha\dot{\alpha} = M \quad \text{(II.37)}$$

m_T is the total mass of the wing and its supporting structure.

m_w is the wing mass.

The stiffness coefficient in pitch motion $k_\alpha(\alpha)$ has the following expression **[3, 96]**.

$$k_\alpha(\alpha) = 12.77 + 53.47\,\alpha + 1003\,\alpha^2 \quad \text{(II.38)}$$

For numerical applications on the equations of motion, the TAMU II wing model parameters are given in table II.1 that follows [3, 75, 96, 116].

Table II.1. TAMU II wing model parameters

Parameter	Value	Unit
ρ	1.225	$Kg\ /m^3$
a	-0.6719	dimensionless
b	0.1905	m
x_α	$-(0.0998 + a)$	dimensionless
s	0.5945	m^2
k_h	2844.4	N/m
k_α	$12.77 + 53.47\,\alpha + 1003\,\alpha^2$	$N.m/rad$
C_h	27.43	Kg/s
C_α	0.0360	$Kg.m^2/s$
m_w	5.230	Kg
m_T	15.57	Kg
I_{ea}	0,14193	$Kg.m^2$
C_{l_α}	6.757	dimensionless
C_{m_α}	$(0.5 + a)\ C_{l_\alpha}$	dimensionless
C_{l_β}	3.774	dimensionless
C_{m_β}	-0.6719	dimensionless
C_{l_γ}	-0.1566	dimensionless
C_{m_γ}	-0.1005	dimensionless

II.3.2. The state space representation

To establish the state space representation (See appendix B) of the studied system, the expressions of the aerodynamic lift L and moment M given by (II.34) and (II.35) successively are substituted in (II.36) and (II.37), so that the following expressions are obtained.

$$m_T\,\ddot{h} + m_w\,x_\alpha\,b\,\ddot{\alpha} + C_h\,\dot{h} + k_h\,h =$$
$$-\pi\rho b^2 s\left[\ddot{h} - ab\ddot{\alpha}\right] + 2\pi\rho Vbs\left[h(0) + b\left(\frac{1}{2} - a\right)\alpha(0)\right]\dot{\varphi}(t) -$$
$$2\pi\rho Vbs\left\{\varphi(0)\dot{h} + b\left(\frac{1}{2} - a\right)\left[\varphi(0) + \frac{1}{1-2a}\right]\dot{\alpha} + \dot{\varphi}(0)h + \left[V\varphi(0) + b\left(\frac{1}{2} - a\right)\dot{\varphi}(0)\right]\alpha\right\} +$$
$$2\pi\rho Vbs\left[\lambda_{h_1} w_1 + \lambda_{h_2} w_2 - \lambda_{\alpha_1} w_3 - \lambda_{\alpha_2} w_4\right] - \rho V^2 bsC_{l\beta}\beta - \rho V^2 bsC_{l\gamma}\gamma \qquad \text{(II.39)}$$

And:

$$m_w\,b\,x_\alpha\,\ddot{h} + I_{ea}\,\ddot{\alpha} + k_\alpha(\alpha)\,\alpha + C_\alpha(\dot{\alpha})\,\dot{\alpha} =$$
$$\pi\rho b^3 s\left[a\ddot{h} - b\left(\frac{1}{8} + a^2\right)\ddot{\alpha}\right] - 2\pi\rho Vb^2 s\left(\frac{1}{2} + a\right)\left[h(0) + b\left(\frac{1}{2} - a\right)\alpha(0)\right]\dot{\varphi}(t) +$$
$$2\pi\rho Vb^2 s\left(\frac{1}{2} + a\right)\left\{\varphi(0)\dot{h} + b\left(\frac{1}{2} - a\right)\left[\varphi(0) - \frac{1}{1-2a}\right]\dot{\alpha} + \dot{\varphi}(0)h\right\} +$$
$$2\pi\rho Vb^2 s\left(\frac{1}{2} + a\right)\left[V\varphi(0) + b\left(\frac{1}{2} - a\right)\dot{\varphi}(0)\right]\alpha - 2\pi\rho Vb^2 s\left(\frac{1}{2} + a\right)\left[\lambda_{h_1} w_1 + \lambda_{h_2} w_2 -\right.$$
$$\left.\lambda_{\alpha_1} w_3 - \lambda_{\alpha_2} w_4\right] + \rho V^2 b^2 sC_{m\beta}\beta + \rho V^2 b^2 sC_{m\gamma}\gamma \qquad \text{(II.40)}$$

Equations (II.39) and (II.40) can be rewritten in the following form in order to adapt them to the desired representation.

$$\ddot{h}\,[m_T + \pi\rho b^2 s] + \ddot{\alpha}\,[m_w x_\alpha b - \pi\rho b^3 sa] + \dot{h}\,[C_h + 2\pi\rho Vbs\varphi(0)] +$$
$$\dot{\alpha}\left[2\pi\rho Vb^2 s\left(\frac{1}{2} - a\right)\varphi(0) + \pi\rho Vb^2 s\right] +$$
$$h\,[k_h + 2\pi\rho Vbs\dot{\varphi}(0)] + \alpha\left[2\pi\rho V^2 bs\varphi(0) + 2\pi\rho Vb^2 s\left(\tfrac{1}{2} - a\right)\dot{\varphi}\,(0)\right] +$$
$$\dot{\varphi}(t)\left[-2\pi\rho Vbsh(0) - 2\pi\rho Vb^2 s\left(\frac{1}{2} - a\right)\alpha(0)\right] +$$
$$2\pi\rho Vbs\left\{w_1[-\lambda_{h_1}] + w_2[-\lambda_{h_2}] + w_3[\lambda_{\alpha_1}] + w_4[\lambda_{\alpha_2}]\right\} +$$
$$\beta\left[\rho V^2 bsC_{l\beta}\right] + \gamma\left[\rho V^2 bsC_{l\gamma}\right] = 0 \qquad \text{(II.41)}$$

And:

$$\ddot{h}[m_w x_\alpha b - \pi\rho b^3 sa] + \ddot{\alpha}\left[I_{ea} + \pi\rho b^4 s\left(\frac{1}{8} + a^2\right)\right] +$$
$$\dot{h}\left[-2\pi\rho V b^2 s\left(\frac{1}{2} + a\right)\varphi(0)\right] + \dot{\alpha}\left[C_\alpha - 2\pi\rho V b^3 s\left(\frac{1}{4} - a^2\right)\varphi(0) + 2\pi\rho V b^3 s\left(\frac{1}{4} - \frac{a}{2}\right)\right] +$$
$$+h\left[-2\pi\rho V b^2 s\left(\frac{1}{2} + a\right)\dot{\varphi}(0)\right] +$$
$$\alpha\left[k_\alpha(\alpha) - 2\pi\rho V^2 b^2 s\left(\frac{1}{2} + a\right)\varphi(0) - 2\pi\rho V b^3 s\left(\frac{1}{4} - a^2\right)\dot{\varphi}(0)\right] +$$
$$\dot{\varphi}(t)\left[2\pi\rho V b^2 s\left(\frac{1}{2} + a\right)h(0) + 2\pi\rho V b^3 s\left(\frac{1}{4} - a^2\right)\alpha(0)\right] +$$
$$2\pi\rho V b^2 s\left(\frac{1}{2} + a\right)\{w_1[\lambda_{h_1}] + w_2[\lambda_{h_2}] + w_3[-\lambda_{\alpha_1}] + w_4[-\lambda_{\alpha_2}]\} +$$
$$\beta[-\rho V^2 b^2 s C_{m\beta}] + \gamma[-\rho V^2 b^2 s C_{m\gamma}] = 0 \qquad \text{(II.42)}$$

After that, equations (II.41) and (II.42) are combined in a way to eliminate the second derivative of the pitch angle $\ddot{\alpha}$ which leads to have the following expression of $\ddot{h}$ (The second derivative of the plunge displacement per time).

$$\ddot{h} = \dot{h}\left[\frac{\left[-2\pi\rho V b^2 s\left(\frac{1}{2}+a\right)\varphi(0)\right]B - [C_h + 2\pi\rho V b s\varphi(0)]C}{D}\right] +$$
$$\dot{\alpha}\left[\frac{\left[C_\alpha - 2\pi\rho V b^3 s\left(\frac{1}{4}-a^2\right)\varphi(0) + 2\pi\rho V b^3 s\left(\frac{1}{4}-\frac{a}{2}\right)\right]B}{D}\right] - \dot{\alpha}\left[\frac{\left[2\pi\rho V b^2 s\left(\frac{1}{2}-a\right)\varphi(0) + \pi\rho V b^2 s\right]C}{D}\right] +$$
$$h\left[\frac{\left[-2\pi\rho V b^2 s\left(\frac{1}{2}+a\right)\dot{\varphi}(0)\right]B - [k_h + 2\pi\rho V b s\dot{\varphi}(0)]C}{D}\right] +$$
$$\alpha\left[\frac{\left[k_\alpha(\alpha) - 2\pi\rho V^2 b^2 s\left(\frac{1}{2}+a\right)\varphi(0) - 2\pi\rho V b^3 s\left(\frac{1}{4}-a^2\right)\dot{\varphi}(0)\right]B}{D}\right] - \alpha\left[\frac{\left[2\pi\rho V^2 b s\varphi(0) + 2\pi\rho V b^2 s\left(\frac{1}{2}-a\right)\dot{\varphi}\,(0)\right]C}{D}\right] +$$
$$\dot{\varphi}(t)\left[\frac{\left[2\pi\rho V b^2 s\left(\frac{1}{2}+a\right)h(0) + 2\pi\rho V b^3 s\left(\frac{1}{4}-a^2\right)\alpha(0)\right]B}{D}\right] + \dot{\varphi}(t)\left[\frac{\left[2\pi\rho V b s h(0) + 2\pi\rho V b^2 s\left(\frac{1}{2}-a\right)\alpha(0)\right]C}{D}\right]$$
$$w_1\left[\frac{\left[2\pi\rho V b^2 s\left(\frac{1}{2}+a\right)\lambda_{h_1}\right]B + [2\pi\rho V b s\lambda_{h_1}]C}{D}\right] + w_2\left[\frac{\left[2\pi\rho V b^2 s\left(\frac{1}{2}+a\right)\lambda_{h_2}\right]B + [2\pi\rho V b s\lambda_{h_2}]C}{D}\right] +$$
$$w_3\left[\frac{\left[-2\pi\rho V b^2 s\left(\frac{1}{2}+a\right)\lambda_{\alpha_1}\right]B - [2\pi\rho V b s\lambda_{\alpha_1}]C}{D}\right] + w_4\left[\frac{\left[-2\pi\rho V b^2 s\left(\frac{1}{2}+a\right)\lambda_{\alpha_2}\right]B - [2\pi\rho V b s\lambda_{\alpha_2}]C}{D}\right] +$$
$$\beta\left[\frac{[-\rho V^2 b^2 s C_{m\beta}]B - [\rho V^2 b s c_{l\beta}]C}{D}\right] + \gamma\left[\frac{[-\rho V^2 b^2 s C_{m\gamma}]B - [\rho V^2 b s c_{l\gamma}]C}{D}\right] \qquad \text{(II.43)}$$

Now, the same equations are combined in a way to eliminate $\ddot{h}$, leading to have the following expression of $\ddot{\alpha}$.

$$\ddot{\alpha} = \dot{h}\left[\frac{[C_h+2\pi\rho Vbs\varphi(0)]B+\left[2\pi\rho Vb^2s\left(\frac{1}{2}+a\right)\varphi(0)\right]A}{D}\right]+$$
$$\dot{\alpha}\left[\frac{\left[2\pi\rho Vb^2s\left(\frac{1}{2}-a\right)\varphi(0)+\pi\rho Vb^2s\right]B}{D}\right]-\dot{\alpha}\left[\frac{\left[C_\alpha-2\pi\rho Vb^3s\left(\frac{1}{4}-a^2\right)\varphi(0)+2\pi\rho Vb^3s\left(\frac{1}{4}-\frac{a}{2}\right)\right]A}{D}\right]-$$
$$h\left[\frac{[k_h+2\pi\rho Vbs\dot{\varphi}(0)]B+\left[2\pi\rho Vb^2s\left(\frac{1}{2}+a\right)\dot{\varphi}(0)\right]A}{D}\right]+\alpha\left[\frac{\left[2\pi\rho V^2bs\varphi(0)+2\pi\rho Vb^2s\left(\frac{1}{2}-a\right)\dot{\varphi}(0)\right]B}{D}\right]-$$
$$\alpha\left[\frac{\left[k_\alpha(\alpha)-2\pi\rho V^2b^2s\left(\frac{1}{2}+a\right)\varphi(0)-2\pi\rho Vb^3s\left(\frac{1}{4}-a^2\right)\dot{\varphi}(0)\right]A}{D}\right]+\dot{\varphi}(t)\left[\frac{\left[-2\pi\rho Vbsh(0)-2\pi\rho Vb^2s\left(\frac{1}{2}-a\right)\alpha(0)\right]B}{D}\right]-$$
$$\dot{\varphi}(t)\left[\frac{\left[2\pi\rho Vb^2s\left(\frac{1}{2}+a\right)h(0)+2\pi\rho Vb^3s\left(\frac{1}{4}-a^2\right)\alpha(0)\right]A}{D}\right]+w_1\left[\frac{[-2\pi\rho Vbs\lambda_{h_1}]B-\left[2\pi\rho Vb^2s\left(\frac{1}{2}+a\right)\lambda_{h_1}\right]A}{D}\right]+$$
$$w_2\left[\frac{[-2\pi\rho Vbs\lambda_{h_2}]B-\left[2\pi\rho Vb^2s\left(\frac{1}{2}+a\right)\lambda_{h_2}\right]A}{D}\right]+w_3\left[\frac{[2\pi\rho Vbs\lambda_{\alpha_1}]B+\left[2\pi\rho Vb^2s\left(\frac{1}{2}+a\right)\lambda_{\alpha_1}\right]A}{D}\right]+$$
$$w_4\left[\frac{[2\pi\rho Vbs\lambda_{\alpha_2}]B+\left[2\pi\rho Vb^2s\left(\frac{1}{2}+a\right)\lambda_{\alpha_2}\right]A}{D}\right]+$$
$$\beta\left[\frac{[\rho V^2bsC_{l\beta}]B+[\rho V^2b^2sC_{m\beta}]A}{D}\right]+\gamma\left[\frac{[\rho V^2bsC_{l\gamma}]B+[\rho V^2b^2sC_{m\gamma}]A}{D}\right] \quad \text{(II.44)}$$

The equations (II.43) and (II.44) can be written as follows.

$$\ddot{h} = a_{31}h + a_{32}\alpha + a_{33}\dot{h} + a_{34}\dot{\alpha} + a_{35}w_1 + a_{36}w_2 + a_{37}w_3 + a_{38}w_4 + d_1\dot{\varphi}(t) + b_{31}\beta + b_{32}\gamma \quad \text{(II.45)}$$

And:

$$\ddot{\alpha} = a_{41}h + a_{42}\alpha + a_{43}\dot{h} + a_{44}\dot{\alpha} + a_{45}w_1 + a_{46}w_2 + a_{47}w_3 + a_{48}w_4 + d_2\dot{\varphi}(t) + b_{41}\beta + b_{42}\gamma \quad \text{(II.46)}$$

Where:

The terms $d_1\dot{\varphi}(t)$ and $d_2\dot{\varphi}(t)$ are negligible compared to the other terms **[30]**.

$$A = m_T + \pi\rho b^2 s\ ;\ B = m_w x_\alpha b - \pi\rho b^3 sa\ ;\ C = I_{ea} + \pi\rho b^4 s\left(\frac{1}{8}+a^2\right)\ ;\ D = AC - B^2\ ;$$

$$a_{31} = \frac{\left[-2\pi\rho Vb^2s\left(\frac{1}{2}+a\right)\dot{\varphi}(0)\right]B-[k_h+2\pi\rho Vbs\dot{\varphi}(0)]C}{D}\ ;\ a_{32} = \frac{B\,k_\alpha}{D} + G_1 - G_2\ ;$$

$$G_1 = \frac{\left[-2\pi\rho V^2b^2s\left(\frac{1}{2}+a\right)\varphi(0)-2\pi\rho Vb^3s\left(\frac{1}{4}-a^2\right)\dot{\varphi}(0)\right]B}{D}\ ;\ G_2 = \frac{\left[2\pi\rho V^2bs\varphi(0)+2\pi\rho Vb^2s\left(\frac{1}{2}-a\right)\dot{\varphi}\,(0)\right]C}{D}\ ;$$

$$a_{33} = \frac{\left[-2\pi\rho Vb^2s\left(\frac{1}{2}+a\right)\varphi(0)\right]B-[C_h+2\pi\rho Vbs\varphi(0)]C}{D}\ ;$$

$$a_{34} = \frac{\left[C_\alpha-2\pi\rho Vb^3s\left(\frac{1}{4}-a^2\right)\varphi(0)+2\pi\rho Vb^3s\left(\frac{1}{4}-\frac{a}{2}\right)\right]B-\left[2\pi\rho Vb^2s\left(\frac{1}{2}-a\right)\varphi(0)+\pi\rho Vb^2s\right]C}{D}\ ;$$

$$a_{35} = \frac{\left[2\pi\rho Vb^2s\left(\frac{1}{2}+a\right)\lambda_{h_1}\right]B+[2\pi\rho Vbs\lambda_{h_1}]C}{D}\ ;\ a_{36} = \frac{\left[2\pi\rho Vb^2s\left(\frac{1}{2}+a\right)\lambda_{h_2}\right]B+[2\pi\rho Vbs\lambda_{h_2}]C}{D}\ ;$$

$$a_{37} = \frac{\left[-2\pi\rho Vb^2s\left(\frac{1}{2}+a\right)\lambda_{\alpha_1}\right]B-[2\pi\rho Vbs\lambda_{\alpha_1}]C}{D}\ ;\ a_{38} = \frac{\left[-2\pi\rho vb^2S\left(\frac{1}{2}+a\right)\lambda_{\alpha_2}\right]B-[2\pi\rho Vbs\lambda_{\alpha_2}]C}{D}\ ;$$

$$b_{31} = \frac{[-\rho V^2 b^2 s C_{m\beta}]B - [\rho V^2 b s c_{l\beta}]C}{D}\ ;\ b_{32} = \frac{[-\rho V^2 b^2 s C_{m\gamma}]B - [\rho V^2 b s c_{l\gamma}]C}{D}\ ;$$

$$a_{41} = \frac{[k_h + 2\pi\rho V b s\dot{\varphi}(0)]B + \left[2\pi\rho V b^2 s\left(\frac{1}{2}+a\right)\varphi(0)\right]A}{D}\ ;\ a_{42} = G_3 - \frac{A\,k_\alpha}{D} - G_4\ ;$$

$$G_3 = \frac{\left[2\pi\rho V^2 b s\varphi(0) + 2\pi\rho V b^2 s\left(\frac{1}{2}-a\right)\dot{\varphi}(0)\right]B}{D}\ ;\ G_4 = \frac{\left[-2\pi\rho V^2 b^2 s\left(\frac{1}{2}+a\right)\varphi(0) - 2\pi\rho V b^3 s\left(\frac{1}{4}-a^2\right)\dot{\varphi}(0)\right]A}{D}\ ;$$

$$a_{43} = \frac{[C_h + 2\pi\rho V b s\varphi(0)]B + \left[2\pi\rho V b^2 s\left(\frac{1}{2}+a\right)\varphi(0)\right]A}{D}\ ;$$

$$a_{44} = \frac{\left[2\pi\rho V b^2 s\left(\frac{1}{2}-a\right)\varphi(0) + \pi\rho V b^2 s\right]B - \left[C_\alpha - 2\pi\rho V b^3 s\left(\frac{1}{4}-a^2\right)\varphi(0) + 2\pi\rho V b^3 s\left(\frac{1}{4}-\frac{a}{2}\right)\right]A}{D}\ ;$$

$$a_{45} = \frac{[-2\pi\rho V b s\lambda_{h_1}]B - \left[2\pi\rho V b^2 s\left(\frac{1}{2}+a\right)\lambda_{h_1}\right]A}{D}\ ;\ a_{46} = \frac{[-2\pi\rho V b s\lambda_{h_2}]B - \left[2\pi\rho V b^2 s\left(\frac{1}{2}+a\right)\lambda_{h_2}\right]A}{D}\ ;$$

$$a_{47} = \frac{[2\pi\rho V b s\lambda_{\alpha_1}]B + \left[2\pi\rho V b^2 s\left(\frac{1}{2}+a\right)\lambda_{\alpha_1}\right]A}{D}\ ;\ a_{48} = \frac{[2\pi\rho V b s\lambda_{\alpha_2}]B + \left[2\pi\rho V b^2 s\left(\frac{1}{2}+a\right)\lambda_{\alpha_2}\right]A}{D}\ ;$$

$$b_{41} = \frac{[\rho\, V^2 b s C_{l\beta}]\,B + [\,\rho\, V^2 b^2 s C_{m\beta}]A}{D};\qquad b_{42} = \frac{[\rho\, V^2 b s C_{l\gamma}]\,B + [\,\rho\, V^2 b^2 s C_{m\gamma}]A}{D};$$

Considering the state vector x and the control vector u, where:

$$x = [x_1\ x_2\ x_3\ x_4\ x_5\ x_6\ x_7\ x_8]^T = [\mathrm{h}\ \dot{\mathrm{h}}\ \alpha\ \dot{\alpha}\ \mathrm{w}_1\ \mathrm{w}_2\ \mathrm{w}_3\ \mathrm{w}_4]^T \tag{II.47}$$

$$u = \begin{bmatrix} b_{31}\beta + b_{32}\gamma \\ b_{41}\beta + b_{42}\gamma \end{bmatrix} \tag{II.48}$$

Then, the following expression is obtained.

$$\dot{x}(t) = [\dot{x_1}\ \dot{x_2}\ \dot{x_3}\ \dot{x_4}\ \dot{x_5}\ \dot{x_6}\ \dot{x_7}\ \dot{x_8}]^T = [\dot{h}\ \ddot{h}\ \dot{\alpha}\ \ddot{\alpha}\ \dot{w_1}\ \dot{w_2}\ \dot{w_3}\ \dot{w_4}]^T \tag{II.49}$$

The state space expression of the nonlinear studied system is written as follows.

$$\begin{aligned}
\dot{x_1} &= \dot{h} = x_2 \\
\dot{x_2} &= \ddot{h} = a_{31}x_1 + a_{32}x_3 + a_{33}x_2 + a_{34}x_4 + a_{35}x_5 + a_{36}x_6 + a_{37}x_7 + a_{38}x_8 + b_{31}\beta + b_{32}\gamma \\
\dot{x_3} &= \dot{\alpha} = x_4 \\
\dot{x_4} &= \ddot{\alpha} = a_{41}x_1 + a_{42}x_3 + a_{43}x_2 + a_{44}x_4 + a_{45}x_5 + a_{46}x_6 + a_{47}x_7 + a_{48}x_8 + b_{41} + b_{42}\gamma \\
\dot{x_5} &= \dot{w_1} = h - \varepsilon_1 w_1 = x_1 - \varepsilon_1 x_5 \\
\dot{x_6} &= \dot{w_2} = h - \varepsilon_2 w_2 = x_1 - \varepsilon_2 x_6 \\
\dot{x_7} &= \dot{w_3} = \alpha - \varepsilon_1 w_3 = x_3 - \varepsilon_1 x_7 \\
\dot{x_8} &= \dot{w_4} = \alpha - \varepsilon_2 w_4 = x_3 - \varepsilon_2 x_8
\end{aligned} \tag{II.50}$$

This system of nonlinear equations is written under the following form:

$$\dot{x}(t) = f\big(x(t), u(t)\big) \tag{II.51}$$

f is a nonlinear function.

One can notice that the studied aeroelastic system described by the obtained model is nonlinear due to the variations of the stiffness coefficient k_α with the pitch angle α following the expression (II.38). The model has also variable parameters that change with the freestream velocity (V) variation.

II.4. Conclusion

In this chapter, the dynamic model of a nonlinear flexible wing section with TLECS (TAMU II wing model) has been developed. Structural modeling based on Lagrange formalism has been combined with the unsteady aerodynamic model introduced via the Wagner's function in order to make the aeroelastic system under equations. Then, these equations have been put in the suitable state space form, which allows the establishment and synthesis of the control laws considered to be better adequate to the specific problem of aeroelastic systems' control, which will be the subject of the next chapter.

CHAPTER III:

Design of the robust control laws

Contents

III.1. Introduction

Automatics is the art of analyzing, modeling and then controlling dynamic systems. It is also that of processing information and making decisions. Its application fields are various: Mechanics, electronics, space industry, etc. [120]. For many years, developers have given particular interest to the aircraft safety and stability in flight, this is one of the most active research topics in aeronautics aiming to ensure stable flight, to avoid any harmful action on the airplane's structure, and for the users comfort [121]. Therefore, the control systems must provide the stability and performance of a given model, this challenging objective needs an understanding of the system's dynamics and a control techniques' improvement, in order to have controlled systems that are faster, more efficient, robust, and operating in large flight intervals [120, 122]. For that, the designed control laws have to be robust in a way that ensures low sensitivity to the parameters' uncertainties and variations, and to external disturbances.

In order to have efficient control systems, it is necessary to have all the information and specific conditions to the followed design process. Nevertheless, in a lot of cases, the only accessible data of the system is the input and output variables from which the states of the chosen model need to be reconstructed. The idea here is based on the use of observers [120].

This chapter details a synthesis of the adopted control laws deemed to be better suitable to the specific problem of flexible aircraft explained and modeled in the previous chapters, and the steps followed to establish and apply these controllers on the studied second order nonlinear system.

The designed control laws in this work are:

- Classical Sliding Mode Control (CSMC) ;
- Fuzzy Sliding Mode Control (FSMC) ;
- Sliding Mode Control with High Gain Observer (SMHGO) ; and
- Fuzzy Sliding Mode Control with High Gain Observer (FSMHGO).

III.2. Sliding mode control

SMC is a particular case of the theory of Variable Structure Systems (VSS) [123- 125], which has been the subject of numerous studies for nearly sixty years. The first works on VSS were initiated by Filippov in 1960 with his work on the differential equations with discontinuous second member [126]. This research area knew a new boom at the end of the

1970s when Emelyanov [127] and Utkin [128] introduced the theory of sliding modes based on the study of Filippov. After that, the research has been resumed in the United States by Slotine [129]. Currently, this control technique has a wide range of applications in a wide variety of fields such as mechanics, robotics, and electrical engineering [100, 110, 123, 130], thanks to its main advantages:

- Its high accuracy and efficiency for linear and nonlinear systems ;
- Its robustness (Perturbations' rejection and insensitivity towards parameters variations) ;
- Its design which is relatively simple.

SMC is mainly characterized by a choice of a switching function. In variable structure systems with sliding mode, the state trajectory is brought to a surface (hyperplane), and then with the help of the switching law, it is forced to remain in the vicinity of this surface. The latter is called the sliding surface around which the movement known by the sliding regime occurs. The trajectory in the phase plane consists of the following three modes, as represented in figure (III.1) [128].

- *The convergence mode (CM)*: During which the variable to be regulated moves from any initial point in the phase plane towards the switching surface S(x) = 0. This mode is characterized by the control law and the convergence criterion.

- *The sliding mode (SM)*: In which the state variable reaches the sliding surface and slides towardsthe origin of the phase plane. The dynamics in this mode is characterized by the choice of the sliding surface S(x).

- *The steady state mode (SSM)*: It concerns the study of the system's response around its equilibrium position (Origin of the phase plane). It is characterized by the quality and the controller's performance.

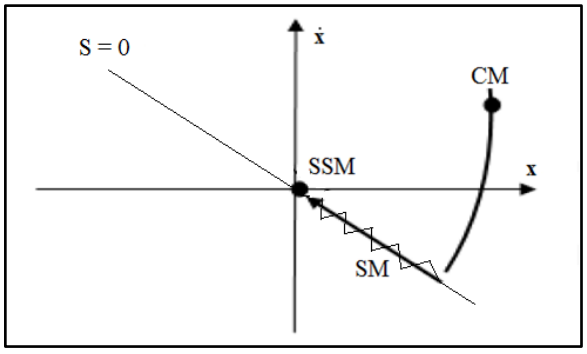

Figure III.1. Different modes for the state trajectory in the phase plane

III.2.1. Definition of the sliding mode control law

The design of the SMC law can be divided into three dependent steps, as follows.

- The choice of the sliding surface ;
- The establishment of the convergence conditions; and
- The control law determination.

The sliding surface (S)

The function S is usually called surface in literature, it can be in form of a line or a hyper surface according to the controlled system's order. The linear function $S(x)$ has to satisfy the conditions of convergence and stability of the system [122].

Slotine has proposed a general form for the definition of sliding surfaces in the phase plane as shown in figure (III.2) [128]. Its purpose is to ensure the convergence of a state variable x towards its desired value x_d , this function is given by the following equation [128, 131].

$$S(x) = \left[\frac{d}{dt} + k\right]^{r-1} e_x(x) \qquad \text{(III.1)}$$

$e_x(x)$ is the difference between the regulated variable and the desired one, $e_x(x) = x - x_d$

k : A positive coefficient that represents the slope of the sliding surface.

r : The relative degree of the system, it represents the number of times the surface should be derived to have the controller's expression.

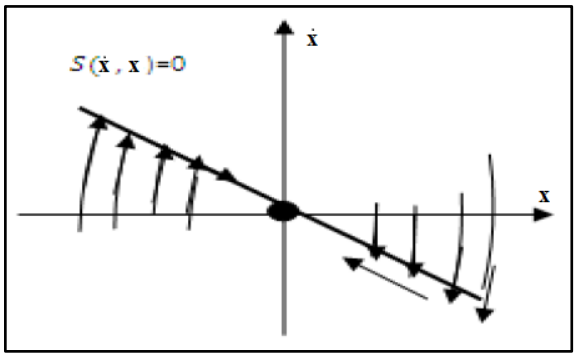

Figure III.2. The sliding surface

The convergence conditions

The convergence-existence conditions are the criteria that allow the system's dynamic to converge towards the sliding surface and to remain there independently of disturbances. There are two considerations corresponding to the convergence of the system's state.

a) Direct switching function: It is the first convergence condition (Attractivity). It is proposed and studied by Emilyanov [127] and Utkin [128]. It gives a dynamic convergence to the sliding surface towards zero. It is formulated by:

$\dot{S}(x) > 0$ when S(x) < 0
$\dot{S}(x) < 0$ when S(x) > 0 (III.2)

In other words:

$$\dot{S}(x)S(x) < 0 \quad \text{(III.3)}$$

b) Lyapunov function: The determination of the sliding domain can be reduced to the study of the system's stability in the sliding regime [131]. This study is based on the use of Lyapunov function $V(x)$. It is a positive scalar function ($V(x) > 0$) for the system state variables, where the control law have to decrease this function ($\dot{V}(x) < 0$).

The basic idea is to choose a scalar function S(x) that guarantees the attractivity of the controlled variable towards its desired value and to construct a control law such that the square of the surface corresponds to a Lyapunov function which is defined by:

$$V(x) = \frac{1}{2} S^2(x) \quad \text{(III.4)}$$

Then:

$$\dot{V}(x) = \dot{S}(x)S(x) \quad \text{(III.5)}$$

In order for this Lyapunov function to decrease, it is sufficient to ensure that:

$$\dot{V}(x) < 0 \quad \text{(III.6)}$$

The control law determination

SMC is generally composed of two terms [131]:

$$U = U_{eq} + \Delta U \quad \text{(III.7)}$$

$\boldsymbol{U_{eq}}$: A continuous term, called the equivalent controller. It has been proposed by Utkin [128], and it corresponds to the so-called ideal sliding regime, for which the operating point remains on the surface, and the derivative of the sliding surface function remains equal to zero i.e. $\dot{S}(x) = 0$.

$\boldsymbol{\Delta U}$ **:** A discontinuous term, called the switching (Commutation) controller. It makes the operating point remain close to the surface. Its main purpose is to verify the attractivity conditions. It has the following expression [131].

$$\Delta U = -l\, Sign(S) \tag{III.8}$$

l is a positive scalar.

The function $Sign(S(x,t))$ is presented in figure (III.3), and defined as follows.

$$Sign(S) = \begin{cases} +1 & Si \quad S > 0 \\ -1 & Si \quad S < 0 \end{cases} \tag{III.9}$$

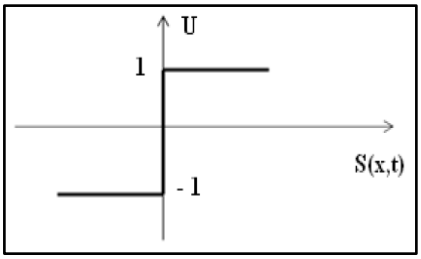

Figure III.3. Representation of the Sign(S) function

To sum up, the SMC law's general structure is shown in the figure III.4 right below.

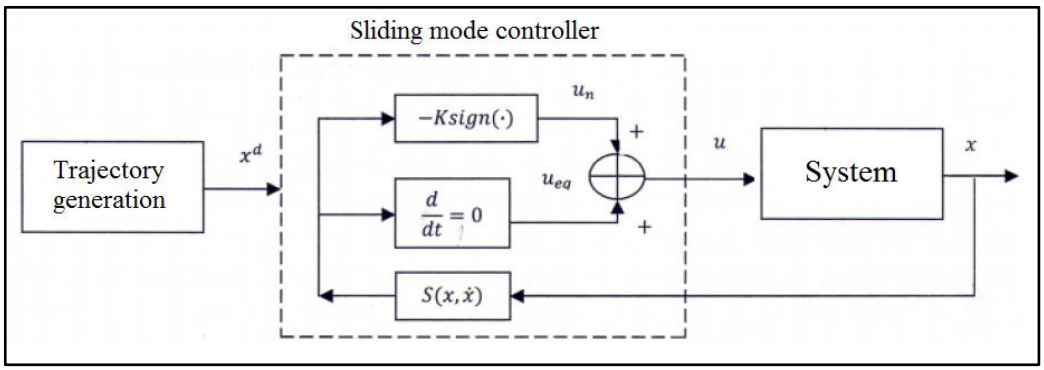

Figure III.4. SMC general structure

III.2.2. The chattering phenomenon

In an ideal sliding regime, the use of the discontinuous Sign function means that the commutation controller ΔU switches between the two values $\pm l$ with an infinite frequency, which cannot exist in practical cases. Thus, during the sliding regime, the discontinuities in the SMC law can lead to strong oscillations of the state trajectory around the sliding surface, this phenomenon is called "chattering" and illustrated in figure (III.5). The main reasons for this phenomenon are actuators' limitations or switching delays in the controller. These commutations deteriorate the controller's precision and can cause premature failure of the

mechanical systems and a temperature rise in the electrical systems which means a significant loss of energy [131].

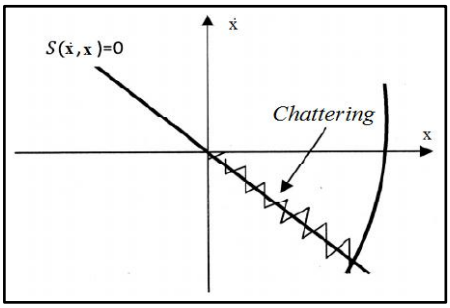

Figure III.5. Chattering phenomenon

Chattering suppression solutions

Chattering is the major inconvenient of SMC, it can cause early deterioration of the control device or excite high-frequency dynamics that have not been considered in the system's modeling, which can degrade the system's performance and even lead to the instability issues. Then, it is necessary to find some solutions to face this problem. It is possible to reduce or to eliminate this phenomenon using many methods [122, 130, 131], such as:

- Replacing the sign function by a smoother continuous approximation like the saturation function and the arctangent function represented in figure (III.6) below, (This solution is named the boundary layer method [122]);
- Using HOSMC [92];
- Combining CSMC with other controllers like backstepping [95], Fuzzy Logic Controller (FLC) [97], adaptive SMC [99, 132], etc.

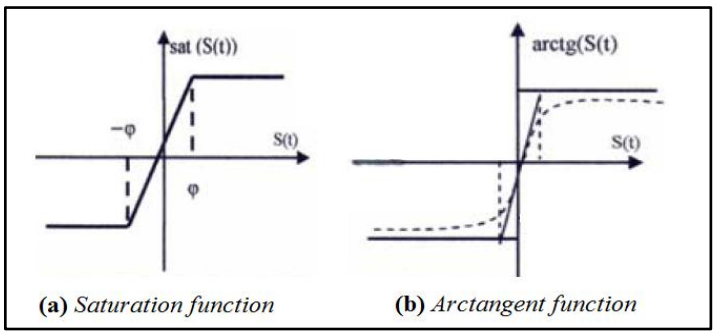

Figure III.6. Commutation functions

In the present work, SMC is combined with a FLC which is used as a tool to have chattering-free systems [97].

III.3. Fuzzy sliding mode control

A Fuzzy Sliding Mode Controller (FSMC) is a combination of SMC and a FLC used in the purpose of taking advantage of both controllers' benefits, where SMC provides robustness, stability and high performance to the studied system and the FLC is used to alleviate or eliminate the chattering phenomenon [97]. The chattering-attenuation's concept here is similar to the previously mentioned boundary layer method, where the FLC varies the SMC efforts (Signal) in order to make it smoother and then to reduce or suppress the undesired chattering [94].

III.3.1. General concept of fuzzy logic control

Since the 1980s, fuzzy-logic-based systems have become one of the most fruitful research areas in automatic control [133, 134]. Contemporary works were inspired by the Mamdani's research on fuzzy control which was motivated by the papers of Lotfi Zadeh about the linguistic approach based on the fuzzy sets theory [135]. Since then, fuzzy logic was widely applied in machine control systems, image processing, artificial intelligence, etc. Lee has given in his two-parted paper [133, 134] a survey that details fuzzy logic control history, principles, and use in control systems.

A FLC uses linguistic information and rule-based algorithms. It has a control structure which is relatively simple to design and does not require a full knowledge of the system's model [101]. It is commonly used in several domains and for different aims [101- 105]. The importance of fuzzy logic resides in its ability to deal with imprecision and uncertainty. This logic was introduced in the purpose of approaching the human reasoning via an adequate representation of knowledge where human concepts (That are used to define the fuzzy sets, like big, small, hot, cold, etc.) are translated in a form that can be used by computers. The fuzzy-control's success lies then in its ability to translate a control strategy into a set of easily-interpretable "If…then" linguistic rules (Fuzzy rules) [133]. The basic structure of a fuzzy system is divided into three main parts [136] as shown in figure (III.7) herein.

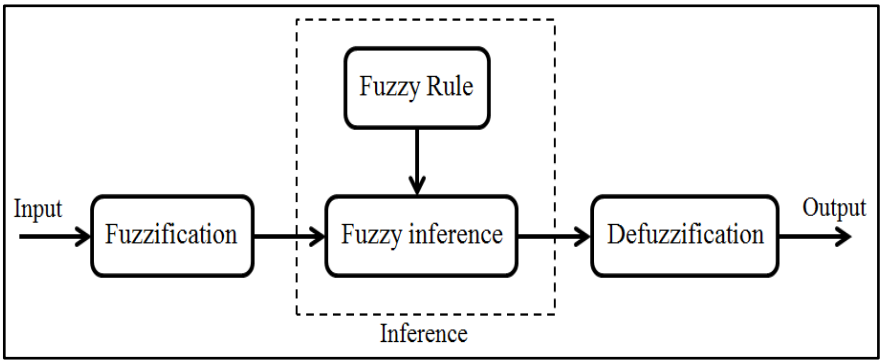

Figure III.7. The FLC structure

Fuzzification:

It is the operation of converting inputs (Crisp numbers that are measured by sensors and passed into the control system for processing, such as speed, temperature, etc.) into fuzzy sets. In other words, fuzzification consists in assigning to a real variable of each input, a linguistic variable characterized by its membership function in each of the fuzzy sets.

Inference:

It is the stage where fuzzy rules are established. These rules link between output and input variables in order to draw fuzzy inferences and conclusions that lead to decisions.

From the fuzzy rules and the fuzzy sets that correspond to the inputs' fuzzification, the inference mechanism calculates the expression "**If** premise **Then** conclusion", where the premise is a set of conditions linked together by fuzzy operators (And/Or), and the conclusion can be a description of evolution in the case of an identification or an action in the case of control.

Defuzzification:

It is the reverse operation of fuzzification, it aims to transform the linguistic variable defined by the inference mechanism into a real (non-fuzzy or crisp) value, allowing then the effective control of the system. To carry out this operation, many methods can be found in literature, like the gravity center method, mean of maximum, and center average methods.

III.3.2. FSMC examples

SMC has been modified in literature by introducing FLC in several ways. Liu and Wang [97] detailed some kinds of fuzzy sliding mode controllers with their descriptions, control laws' design, and simulations. Herein some examples of FSMC:

- FSMC based on equivalent control, where the equivalent control in the CSMC law is replaced by a FLC ;
- SMC based on fuzzy switch-gain regulation, where The discontinuous switch gain in the CSMC is substituted by a FLC ; and
- SMC based on fuzzy system approximation, which is a concept supported by previous research like in the paper of Kosko [137], affirming that a fuzzy system can approximate any nonlinear function over a compact set with random precision.

In the present work, FLC is introduced in the switching control expression $\boldsymbol{\Delta U}$, where it replaces the switching gain that exists in the CSMC law. The idea is to design a FLC that has the sliding surface S as an input, and the variant membership M as an output. After that, the designed controller is inserted in the CSMC law in order to remove the chattering phenomenon. The FSMC expression's establishment will be detailed in the coming sections.

III.4. Observer-based sliding mode control

III.4.1. Observers and observability for nonlinear systems

An observer is a dynamic system that uses the system's inputs, the measured outputs, as well as a priori knowledge of the model, to provide estimated states which have to converge towards the actual states' values [122]. It allows following the evolution of the states' information, and optimizing the number of needed sensors', hence its economic benefit in industry.

By definition, nonlinear systems are of so varied features, and require different approaches compared to linear systems [120]. Therefore, the concepts of observers and observability for nonlinear systems are also different (See appendix B), where the estimators' synthesis is still an open problem, and the observers' design for nonlinear systems is a problem where research work remains very intensive [122].

The observability of a process is an important concept in the field of state estimation. Indeed, to reconstruct the inaccessible system's states, it is necessary to know whether the state variables are observable or not, i.e. if it is possible or not, to determine the states using only the input and output signals. In the case of nonlinear systems, the observability notion depends on the inputs and the initial conditions [138]. It is based on the possibility of distinguishing two initial conditions, this is equivalent to saying that it is defined from an indistinguishability relation, where a nonlinear system is observable if it does not admit

indistinguishable pairs, in simpler words, if for two different initial conditions, two different outputs are obtained [120, 122].

III.4.2. Sliding mode observers' structure

One of the well-known classes of robust nonlinear observers is that of sliding mode ones (Observer-based SMC). This type of observers is also based on the VSS theory [122]. The choice of this type of observers is explained by its properties such as the convergence in finite time towards a sliding surface, the possibility of downsizing the observation system, and the robustness against errors and disturbances [120]. For a nonlinear system, there are several types of sliding mode observers, such as [97, 139]:

- Sliding Mode with High Gain Observer (SMHGO);
- The sliding mode integral-chain differentiator ;
- The sliding mode disturbance observer ; and
- The sliding mode delayed-output observer.

A sliding mode observer's general structure is illustrated in figure (III.8) below and described as follows.

$$\dot{\hat{x}}(t) = f(\hat{x}(t), u(t)) - l\, Sign(y(t) - \hat{y}(t))$$
$$\hat{y}(t) = h(\hat{x}(t)) \qquad \text{(III.10)}$$

$\hat{x}(t)$ and $\dot{\hat{x}}(t)$ are respectively, the estimated state value and its derivative, $x(t)$ is the actual state value, $y(t)$ and $\hat{y}(t)$ are respectively, the actual system's output and the estimated one, f and h are nonlinear functions.

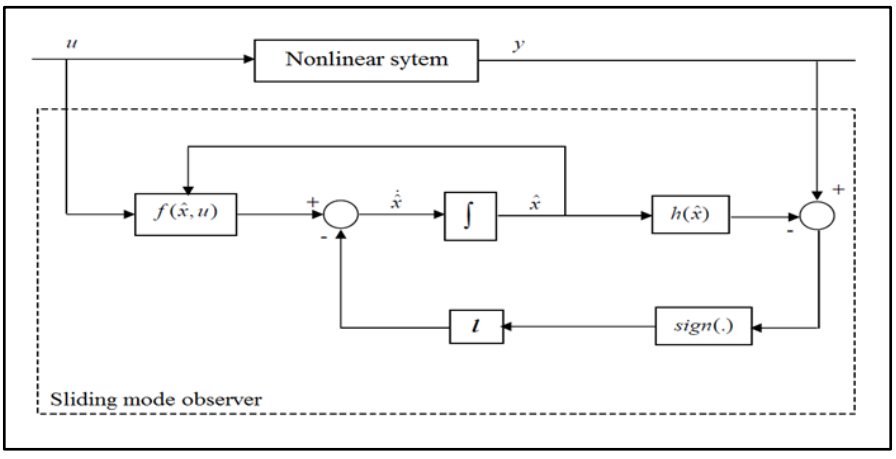

Figure III.8. Sliding mode observers' general structure

One can notice that the obtained estimator's structure is similar to the system's model with a correction term introduced to guarantee the convergence of $\hat{x}(t)$ towards $x(t)$. In this case $S = E_y = y - \hat{y}$ is the sliding surface, and l is a correction term which is proportional to the $Sign$ function [120].

The dynamic for sliding mode observers concerns the observation error $E(t) = x(t) - \hat{x}(t)$. This error converges from its initial value to the equilibrium position in two steps [120]:

- At the beginning, the observation error trajectory evolves towards the sliding surface on which the output error $E_y(t)$ is null. This step is known as the "reaching mode".
- Then, the observation error's trajectory slides on the sliding surface with imposed dynamics so as to suppress all the observation errors, it is called the "sliding mode". The corrective term acts in such a way to satisfy the following invariance condition: $S = 0$ and $\dot{S} = 0$ so that the estimated states converge towards the real ones.

III.4.3. High gain observer

The type of observers that is associated with SMC in this work is the High Gain Observer (HGO) thanks to its advantageous features of stability, robustness, and disturbance rejection. HGO is a nonlinear robust estimator that has a simple structure making it unchallenging to design, it has been investigated and used firstly by Doyle in 1979 [140] as a robust-observer design tool in linear control until the late 1980's where HGO started to be used in nonlinear feedback control like in [141- 143]. Further details are presented in the works of Khalil [144, 145] where HGO has been extensively explained, including history, definitions, examples, and Matlab/Simulink simulations, and also in the book of Liu and Wang [97].

The HGO's general expression is the following

$$\left.\begin{aligned} \dot{\hat{x}}_1 &= \hat{x}_2 - \frac{q_n}{\varepsilon^1}(\hat{x}_1 - x) \\ \dot{\hat{x}}_2 &= \hat{x}_3 - \frac{q_{n-1}}{\varepsilon^2}(\hat{x}_1 - x) \\ &\vdots \\ \dot{\hat{x}}_{n-1} &= \hat{x}_n - \frac{q_2}{\varepsilon^{n-1}}(\hat{x}_1 - x) \\ \dot{\hat{x}}_n &= -\frac{q_1}{\varepsilon^n}(\hat{x}_1 - x) \end{aligned}\right\} \qquad \text{(III.11)}$$

Where:

$[x_1 \ x_2 \ldots x_n]^T$ is the actual states' vector of the system ;

$[\hat{x}_1 \ \hat{x}_2 \dots \hat{x}_n]^T$ is the estimated states' vector of the system ;

x is the measured state's trajectory ;

ε is a sufficiently small constant, where the smaller it gets the faster is the HGO's convergence [122]. It is usually taken 0.001 (Like in [97]) ;

$q_i (i = 1, 2, \dots, n)$ are constants chosen so that $s^n + q_n s^{n-1} + \cdots + q_2 s + q_1 = 0$ is a Hurwitz polynomial, i.e. so that the eigenvalues of this equation are of negative real parts.

The sliding surface in this case is of the following form.

$$S(\hat{x}) = k E_1 + E_2 \tag{III.12}$$

$E_1 = \hat{x}_1 - {x_1}^d$ and $E_2 = \hat{x}_2 - \dot{x}_1{}^d$, ${x_1}^d$ is the desired value of x_1 ; and k is a coefficient that represents the slope of the sliding surface.

In general, the laws established for the calculation of the sliding surface, the equivalent control, and the switching control for the sliding mode remain applicable for the Sliding Mode with High Gain Observer Controller (SMHGOC), the only difference is that in this case, the formulas are established using states' values which can be measured and those estimated by the observer, and which are approximate values that have to converge towards the real values.

III.5. The controllers' establishment

The nonlinear studied system has the following form.

$$\begin{cases} \dot{x}(t) = f\big(x(t), u(t)\big) \\ y(t) = h\big(x(t)\big) \end{cases} \tag{III.13}$$

f and h are two nonlinear functions.

$x(t)$ is the state vector, where:

$$x(t) = [x_1 \ x_2 \ x_3 \ x_4 \ x_5 \ x_6 \ x_7 \ x_8]^T = [\mathrm{h} \ \dot{\mathrm{h}} \ \alpha \ \dot{\alpha} \ \mathrm{w}_1 \ \mathrm{w}_2 \ \mathrm{w}_3 \ \mathrm{w}_4]^T \tag{III.14}$$

$u(t)$ is the control vector, where:

$$u(t) = \begin{pmatrix} U_1 \\ U_2 \end{pmatrix} = \begin{pmatrix} b_{31} & b_{32} \\ b_{41} & b_{42} \end{pmatrix} \begin{pmatrix} \beta \\ \gamma \end{pmatrix} \tag{III.15}$$

In other words:

$$\begin{cases} U_1 = b_{31}\beta + b_{32}\gamma \\ U_2 = b_{41}\beta + b_{42}\gamma \end{cases} \tag{III.16}$$

$y(t)$ is the output vector.

Then:

$$\dot{x}(t) = [\dot{x_1}\ \dot{x_2}\ \dot{x_3}\ \dot{x_4}\ \dot{x_5}\ \dot{x_6}\ \dot{x_7}\ \dot{x_8}]^T = [\dot{h}\ \ddot{h}\ \dot{\alpha}\ \ddot{\alpha}\ \dot{w}_1\ \dot{w}_2\ \dot{w}_3\ \dot{w}_4]^T \quad \text{(III.17)}$$

Where:

$$\begin{aligned}
\dot{x_1} &= \dot{h} = x_2 \\
\dot{x_2} &= \ddot{h} = a_{31}x_1 + a_{32}x_3 + a_{33}x_2 + a_{34}x_4 + a_{35}x_5 + a_{36}x_6 + a_{37}x_7 + a_{38}x_8 + U_1 \\
\dot{x_3} &= \dot{\alpha} = x_4 \\
\dot{x_4} &= \ddot{\alpha} = a_{41}x_1 + a_{42}x_3 + a_{43}x_2 + a_{44}x_4 + a_{45}x_5 + a_{46}x_6 + a_{47}x_7 + a_{48}x_8 + U_2 \\
\dot{x_5} &= \dot{w_1} = x_1 - \varepsilon_1 x_5 \\
\dot{x_6} &= \dot{w_2} = x_1 - \varepsilon_2 x_6 \\
\dot{x_7} &= \dot{w_3} = x_3 - \varepsilon_1 x_7 \\
\dot{x_8} &= \dot{w_4} = x_3 - \varepsilon_2 x_8
\end{aligned} \quad \text{(III.18)}$$

The coming sections show the steps of the proposed control laws' establishment, in order to stabilize the built nonlinear aeroelastic model, and to enhance its performance.

III.5.1. Conventional sliding mode control law

In order to establish the CSMC law, i.e. to define the expressions of U_1 and U_2; the studied system can be subdivided into two second-order subsystems as follows.

First subsystem:

$$\begin{cases} \dot{x_1} = \dot{h} = x_2 \\ \dot{x_2} = \ddot{h} = a_{31}x_1 + a_{32}x_3 + a_{33}x_2 + a_{34}x_4 + a_{35}x_5 + a_{36}x_6 + a_{37}x_7 + a_{38}x_8 + U_1 \end{cases} \quad \text{(III.19)}$$

Replacing k_α and a_{32} by their expressions given in chapter II, the following writing of equation (III.19) is obtained.

$$\begin{cases} \dot{x_1} = x_2 \\ \dot{x_2} = a_{31}x_1 + a_{33}x_2 + \left(\frac{B}{D}\ 12{,}77 + G_1 - G_2\right)x_3 + \frac{B}{D}53{,}47\ {x_3}^2 + \frac{B}{D}1003\ {x_3}^3 + a_{34}x_4 + \\ \qquad a_{35}x_5 + a_{36}x_6 + a_{37}x_7 + a_{38}x_8 + U_1 \end{cases} \quad \text{(III.20)}$$

The equation (III.1) proposed by Slotine is used to define the sliding surface, where the subsystem is of second order which means that $r = 2$, and the desired state value is $x^d = 0$. Then, the sliding surface for the first subsystem S_1 has the following expression.

$$S_1(x) = k_1x_1 + \dot{x_1} = k_1x_1 + x_2 \quad \text{(III.21)}$$

Referring to equation (III.7), the control law for the 1st subsystem is of the following form.

$$U_1 = U_{1eq} + \Delta U_1 \quad \text{(III.22)}$$

Using equations (III.20) and (III.21), the sliding surface derivative is the following.

$\dot{S_1}(x) = k_1\dot{x_1} + \ddot{x_1} = k_1 x_2 + \dot{x_2}$ which means:

$$\dot{S_1}(x) = a_{31}x_1 + (k_1 + a_{33})x_2 + \left(\frac{B}{D}\,12{,}77 + G_1 - G_2\right)x_3 + \frac{B}{D}53{,}47\,{x_3}^2 + \frac{B}{D}1003\,{x_3}^3 + a_{34}x_4 + a_{35}x_5 + a_{36}x_6 + a_{37}x_7 + a_{38}x_8 + U_1 \quad \text{(III.23)}$$

Using the equivalent control definition mentioned in section (III.2.1) of the current chapter, and equation (III.23), in order to have $\dot{S_1}(x) = 0$ which means:

$$a_{31}x_1 + (k_1 + a_{33})x_2 + \left(\frac{B}{D}\,12{,}77 + G_1 - G_2\right)x_3 + \frac{B}{D}53{,}47\,{x_3}^2 + \frac{B}{D}1003\,{x_3}^3 + a_{34}x_4 + a_{35}x_5 + a_{36}x_6 + a_{37}x_7 + a_{38}x_8 + U_{1eq} = 0 \quad \text{(III.24)}$$

The expression of U_{1eq} should have the following form:

$$U_{1eq} = -a_{31}x_1 - (k_1 + a_{33})x_2 - \left(\frac{B}{D}\,12{,}77 + G_1 - G_2\right)x_3 - \frac{B}{D}53{,}47\,{x_3}^2 - \frac{B}{D}1003\,{x_3}^3 - a_{34}x_4 - a_{35}x_5 - a_{36}x_6 - a_{37}x_7 - a_{38}x_8 \quad \text{(III.25)}$$

According to equation (III.8), the commutation controller is right below.

$$\Delta U_1 = -l_1\, Sign(S_1) \quad \text{(III.26)}$$

Then, the CSMC expression for the first subsystem is as follows.

$$U_1 = -a_{31}x_1 - (k_1 + a_{33})x_2 - \left(\frac{B}{D}\,12{,}77 + G_1 - G_2\right)x_3 - \frac{B}{D}53{,}47\,{x_3}^2 - \frac{B}{D}1003\,{x_3}^3 - a_{34}x_4 - a_{35}x_5 - a_{36}x_6 - a_{37}x_7 - a_{38}x_8 - l_1\, Sign(S_1) \quad \text{(III.27)}$$

In the aim of satisfying the Lyapunov stability criterion, the Lyapunov function $V_1(x)$ and its derivative $\dot{V}_1(x)$ are considered as follows.

$$V_1(x) = \frac{1}{2}\,{S_1}^2(x) > 0 \quad \text{(III.28)}$$

$$\dot{V}_1(x) = \dot{S}_1(x)S_1(x) \quad \text{(III.29)}$$

$$\dot{V}_1(x) = S_1\,[-l_1\, Sign(S_1)\,] = S_1\left[-l_1\,\frac{S_1}{|S_1|}\right] \quad \text{(III.30)}$$

$$\dot{V}_1(x) = -l_1\,\frac{S_1^2}{|S_1|} < 0 \quad \text{(III.31)}$$

So, the Lyapunov stability criterion is satisfied for the first aeroelastic subsystem.

Second subsystem:

$$\begin{cases} \dot{x_3} = \dot{\alpha} = x_4 \\ \dot{x_4} = \ddot{\alpha} = a_{41}x_1 + a_{42}x_3 + a_{43}x_2 + a_{44}x_4 + a_{45}x_5 + a_{46}x_6 + a_{47}x_7 + a_{48}x_8 + U_2 \end{cases} \quad \text{(III.32)}$$

Replacing k_α and a_{42} by their expressions given in chapter II, the following form of equation (III.32) is obtained.

$$\begin{cases} \dot{x_3} = x_4 \\ \dot{x_4} = a_{41}x_1 + a_{43}x_2 + \left(G_3 - \frac{A}{D}12{,}77 - G_4\right)x_3 - \frac{A}{D}53{,}47\ {x_3}^2 - \frac{A}{D}\ 1003\ {x_3}^3 + a_{44}x_4 + \\ \qquad a_{45}x_5 + a_{46}x_6 + a_{47}x_7 + a_{48}x_8 + U_2 \end{cases} \quad \text{(III.33)}$$

Following the same procedures used for the first subsystem leads to acquire these results.

$$S_2(x) = k_2x_3 + \dot{x_3} = k_1x_3 + x_4 \quad \text{(III.34)}$$

$$\dot{S_2}(x) = k_1\dot{x_3} + \ddot{x_3} = k_1x_4 + \dot{x_4} \quad \text{(III.35)}$$

$$U_{2eq} = -a_{41}x_1 - a_{43}x_2 - \left(G_3 - \frac{A}{D}12{,}77 - G_4\right)x_3 + \frac{A}{D}53{,}47\ {x_3}^2 + \frac{A}{D}\ 1003\ {x_3}^3 - (k_2 + a_{44})\ x_4 - a_{45}x_5 - a_{46}x_6 - a_{47}x_7 - a_{48}x_8 \quad \text{(III.36)}$$

$$\Delta U_2 = -l_2\ Sign(S_2) \quad \text{(III.37)}$$

Then, the CSMC expression for the second subsystem is as follows.

$$U_2 = -a_{41}x_1 - a_{43}x_2 - \left(G_3 - \frac{A}{D}12{,}77 - G_4\right)x_3 + \frac{A}{D}53{,}47\ {x_3}^2 + \frac{A}{D}\ 1003\ {x_3}^3 - (k_2 + a_{44})\ x_4 - a_{45}x_5 - a_{46}x_6 - a_{47}x_7 - a_{48}x_8 - l_2\ Sign(S_2) \quad \text{(III.38)}$$

The Lyapunov stability criterion is satisfied for the second aeroelastic subsystem in the same method applied for the first subsystem.

Determination of the angles β and γ:

Using equation (III.15) and the Cramer rule, the following equations are found:

$$\begin{cases} \beta = \dfrac{det\begin{vmatrix} U_1 & b_{32} \\ U_2 & b_{42} \end{vmatrix}}{det\begin{vmatrix} b_{31} & b_{32} \\ b_{41} & b_{42} \end{vmatrix}} \\ \gamma = \dfrac{det\begin{vmatrix} b_{31} & U_1 \\ b_{41} & U_2 \end{vmatrix}}{det\begin{vmatrix} b_{31} & b_{32} \\ b_{41} & b_{42} \end{vmatrix}} \end{cases} \quad \text{(III.39)}$$

These calculations can be carried out numerically using appropriate software.

III.5.2. Fuzzy sliding mode control law

The idea here is to develop a FLC with the sliding surface S as input and the variant membership M as output, and to combine it with the CSMC aiming to eliminate the chattering phenomenon [146].

First subsystem:

The SMC law for the first subsystem described by equation (III.22) becomes then:

$$U_1 = U_{1eq} + M_1 \, \Delta U_1 \qquad \text{(III.40)}$$

With M_1 is the variant membership for the first subsystem.

Considering the following fuzzy sets:

- For the input S_1: NG (Negative and large); N (Negative); Z (Zero); P (Positive); PG (Positive and large).
- For the output M_1: NG ; N ; Z ; P ; PG.

The fuzzy rules are chosen as follows:

1. If S_1 is *NG* Then M_1 is *PG* ;
2. If S_1 is *N* Then M_1 is *P* ;
3. If S_1 is *Z* Then M_1 is *Z* ;
4. If S_1 is *P* Then M_1 is *P* ;
5. If S_1 is *PG* Then M_1 is *PG.*

The membership functions of the input S_1 and the output M_1 are showed in the following figures (III.9) and (III.10) respectively. These figures describe the properties of the input and the output of the designed FLC.

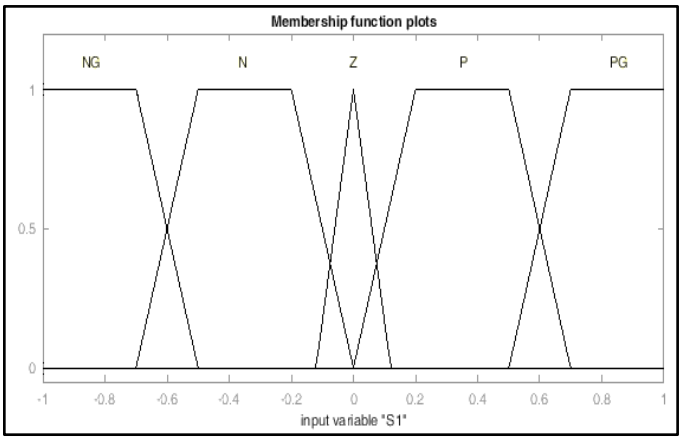

Figure III.9. The membership function of S_1

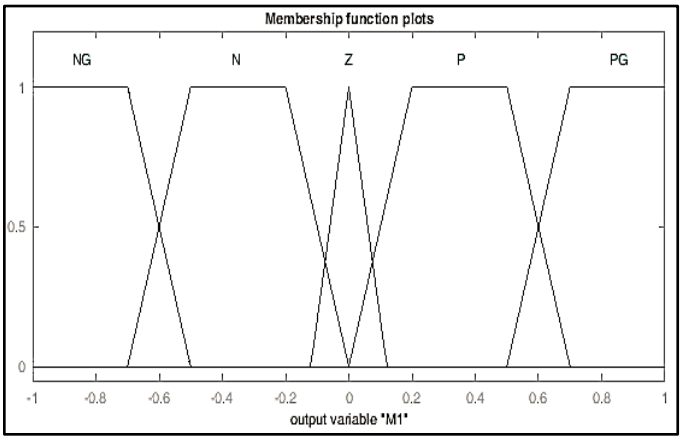

Figure III.10. The membership function of M_1

The FLC and the fuzzy rules are designed so that:

- The FSMC law is equal to the equivalent control expression if M_1 is null ;
- The FSMC law is equal to the CSMC if M_1 is equal to one ;
- Else, the chattering is reduced or eliminated via the variation of M_1 in equation (III.40).

Since $M_1 \geq 0$ then, the Lyapunov stability criterion remains satisfied.

Second subsystem:

In the same way, the FSMC law for the second subsystem is built, where:

$$U_2 = U_{2eq} + M_2 \, \Delta U_2 \tag{III.41}$$

III.5.3. Sliding mode with high gain observer control law

The so-called high-gain techniques can be applied without transforming the initial system. In this case, the design of the observer is done directly from the structure of the system [120].

First subsystem:

Applying the general formula (III.11) on the studied second-order subsystem with $x = x_1$ leads to have the following expression of the HGO [147].

$$\begin{cases} \dot{\hat{x}}_1 = \hat{x}_2 - \frac{q_2}{\varepsilon} \, (\hat{x}_1 - x_1) \\ \dot{\hat{x}}_2 = - \frac{q_1}{\varepsilon^2} \, (\hat{x}_1 - x_1) \end{cases} \tag{III.42}$$

q_1 and q_2 are two coefficients chosen so that the eigenvalues of the following equation for the second-order subsystem have negative real parts [97].

$$s^2 + q_2 \, s + q_1 = 0 \tag{III.43}$$

According to the equation (III.12), and for $x_1^d = 0$, the sliding surface is obtained.

$$S_1(\hat{x}) = k_1\hat{x}_1 + \hat{x}_2 \quad \text{(III.44)}$$

Then, the control law is of the following form.

$$U_1 = U_{1eq} + \Delta U_1 \quad \text{(III.45)}$$

In CSMC: $S_1(x) = k_1 x_1 + x_2$ then: $\dot{S}_1(x) = k_1 x_2 + \ddot{h}$

The equivalent controller is chosen as follows.

$$U_{1eq} = -k_1\hat{x}_2 \quad \text{(III.46)}$$

The switching controller is of the following form.

$$\Delta U_1 = -l_1\, Sign(S_1(\hat{x})) \quad \text{(III.47)}$$

Then, the expression of the SMHGOC for the first subsystem is right below.

$$U_1 = -k_1\hat{x}_2 - l_1\, Sign(S_1(\hat{x})) \quad \text{(III.48)}$$

To fulfill the stability criterion in the sense of Lyapunov, Liu and Wang have provided a demonstration in [97] for the SMHGOC case. From which the following demonstration is derived. Considering the following Lyapunov function for the first subsystem.

$$V_1(x) = \frac{1}{2}\, {S_1}^2(x) \quad \text{(III.49)}$$

$$\dot{V}_1(x) = \dot{S}_1(x)S_1(x) \quad \text{(III.50)}$$

$$\dot{V}_1(x) = S_1[k_1(\dot{x}_1 - \dot{\hat{x}}_1) + f_1(x) - l_1\, Sign(\hat{S}_1)] \quad \text{(III.51)}$$

$f_1(x) = a_{31}x_1 + a_{32}x_3 + a_{33}x_2 + a_{34}x_4 + a_{35}x_5 + a_{36}x_6 + a_{37}x_7 + a_{38}x_8$ is bounded, in other words: $|f_1(x)| \leq l_{f1}$

$$\dot{V}_1(x) = (\hat{S}_1 + S_1 - \hat{S}_1)k_1(\dot{x}_1 - \dot{\hat{x}}_1) + (\hat{S}_1 + S_1 - \hat{S}_1)f_1(x) - (\hat{S}_1 + S_1 - \hat{S}_1)\, l_1\, Sign(\hat{S}_1) \quad \text{(III.52)}$$

$$\dot{V}_1(x) \leq -\hat{S}_1\, l_1 Sign(\hat{S}_1) + l_1|S_1 - \hat{S}_1| + (|f_1(x)| + k_1|x_2 - \hat{x}_2|)|\hat{S}_1| + |S_1 - \hat{S}_1|(|f_1(x)| + k_1|x_2 - \hat{x}_2|) \quad \text{(III.53)}$$

$$\dot{V}_1(x) \leq -l_1|\hat{S}_1| + l_1|S_1 - \hat{S}_1| + (|f_1(x)| + k_1|x_2 - \hat{x}_2|)|\hat{S}_1| + |S_1 - \hat{S}_1|(|f_1(x)| + k_1|x_2 - \hat{x}_2|) \quad \text{(III.54)}$$

$$\dot{V}_1(x) \leq -l_1|\hat{S}_1| + (l_{f1} + k_1|x_2 - \hat{x}_2|)|\hat{S}_1| + \Delta \quad \text{(III.55)}$$

$$\Delta = \left|S_1 - \hat{S}_1\right|(l_1 + l_{f1} + k_1|x_2 - \hat{x}_2|) \quad \text{(III.56)}$$

Because of the observer's convergence **[97]**, the expressions $|x_2 - \hat{x}_2|$ and $\left|S_1 - \hat{S}_1\right|$ are bounded and sufficiently small. Therefore, Δ is sufficiently small to have $\dot{V}_1(x) < 0$ and then to satisfy the desired stability criterion. In the same way, the Lyapunov stability criterion verification is demonstrated for the second subsystem.

Second subsystem:

Applying the general formula (III.11) on the studied second-order subsystem, with $x = x_3$ leads to have the following expression of the HGO.

$$\begin{cases} \dot{\hat{x}}_3 = \hat{x}_2 - \frac{q_4}{\varepsilon}(\hat{x}_3 - x_3) \\ \dot{\hat{x}}_4 = -\frac{q_3}{\varepsilon^2}(\hat{x}_3 - x_3) \end{cases} \quad \text{(III.57)}$$

q_3 and q_4 are two coefficients chosen so that the eigenvalues of the following equation for the second-order subsystem have negative real parts.

$$s^2 + q_4 s + q_3 = 0 \quad \text{(III.58)}$$

According to the equation (III.12), and for $x_3^d = 0$, the sliding surface is obtained.

$$S_2(\hat{x}) = k_3\hat{x}_3 + \hat{x}_4 \quad \text{(III.59)}$$

Then, the control law is of the following form.

$$U_2 = U_{2eq} + \Delta U_2 \quad \text{(III.60)}$$

In CSMC: $S_2(x) = k_2 x_3 + x_4$ then: $\dot{S}_2(x) = k_2 x_3 + \ddot{\alpha}$

The equivalent controller is chosen as follows.

$$U_{2eq} = -k_2\hat{x}_4 \quad \text{(III.61)}$$

The switching controller is of the following form.

$$\Delta U_2 = -l_2\, Sign(S_2(\hat{x})) \quad \text{(III.62)}$$

Then, the expression of the SMHGOC for the second subsystem is right below.

$$U_2 = -k_2\hat{x}_4 - l_2\, Sign(S_2(\hat{x})) \quad \text{(III.63)}$$

III.5.4. Fuzzy sliding mode with high gain observer control law

This section explains the FSMHGO control plant which combines CSMC with a FLC and a HGO, aiming to have a stabilized and chattering free system using only some states of the

nonlinear aeroelastic model. The control law is then designed using the SMHGOC with the FLC exposed in the sections right above.

First subsystem:

The structure of the HGO used for this controller is described by equation (III.42), and the sliding surface is given by equation (III.44). The control law is built by introducing the FLC described in section (III.5.2.) in the SMHGOC plant given in equation (III.48). Then, the desired control law has the following form.

$$U_1 = -k_1\hat{x}_2 - M_1\, l_1\, Sign(S_1(\hat{x})) \quad \text{(III.64)}$$

The criterion of the controller's stability stays satisfied since the introduced membership M_1 that is multiplied by the positive switching coefficient l_1 is always positive.

Second subsystem:

In the same way, the following control law for the second subsystem is derived.

$$U_2 = -k_2\hat{x}_4 - M_2\, l_2\, Sign(S_2(\hat{x})) \quad \text{(III.65)}$$

Since $M_2 \geq 0$ then, the Lyapunov stability criterion remains satisfied.

III.6. Conclusion

This chapter is dedicated to the definition and development of control laws for the nonlinear aeroelastic systems' stability, presenting in some detail CSMC, FSMC, SMHGOC, and FSMHGOC. The designed controllers are applied on the studied aeroelastic model, and the effectiveness of these control laws will be investigated by the simulation of these techniques in the next chapter in order to drive conclusions about their advantages and limits.

CHAPTER IV:

Simulation results and discussion

Contents

IV.1. Introduction

This important part of the present thesis consists in evaluating and comparing the four robust combinations of SMC that have been built in the previous chapter and applied on the nonlinear aeroelastic TAMU II wing model designed in chapter II, in the aim of regulating the system's states in a way that ensures fast stabilization and improved performance for the considered system, and pushes the critical flutter speed margins as far as possible compared to the free-motion case, having consequently safe flight conditions.

The system's responses will be studied in open loop and in closed loop (After applying the controllers). Also, the results obtained using each controller will be compared to those in open loop and then to the other controllers for different speed values, in order to visualize the effect of every control plant on the stability and performance of the system.

The vertical displacement (h), the pitch angle (α), trailing edge flap deflection angle (β), and leading edge flap deflection angle (γ), will be shown and studied graphically, and the critical flutter velocity will be identified for every case.

In order to solve the differential equations of the established model, fourth order variable-step Runge-Kutta method (RK 4(5)) is adopted as the numerical method in this work. This method is commonly used to solve such engineering problems [148].

IV.2. Open loop simulation results

In this section, the wing-model stability in free-motion (Open loop) will be investigated, by visualizing the behavior of the vertical displacement of the wing (h), as well as its pitch angle (α). It is known from the system's governing equations that the wing model depends on the airflow velocity. Then, the stability of this model is tested for different airspeed values.

The following figure (IV.1) presents the Simulink program that has been established in the purpose of having the results' graphical representations for the considered nonlinear model in open loop, and in closed loop thereafter.

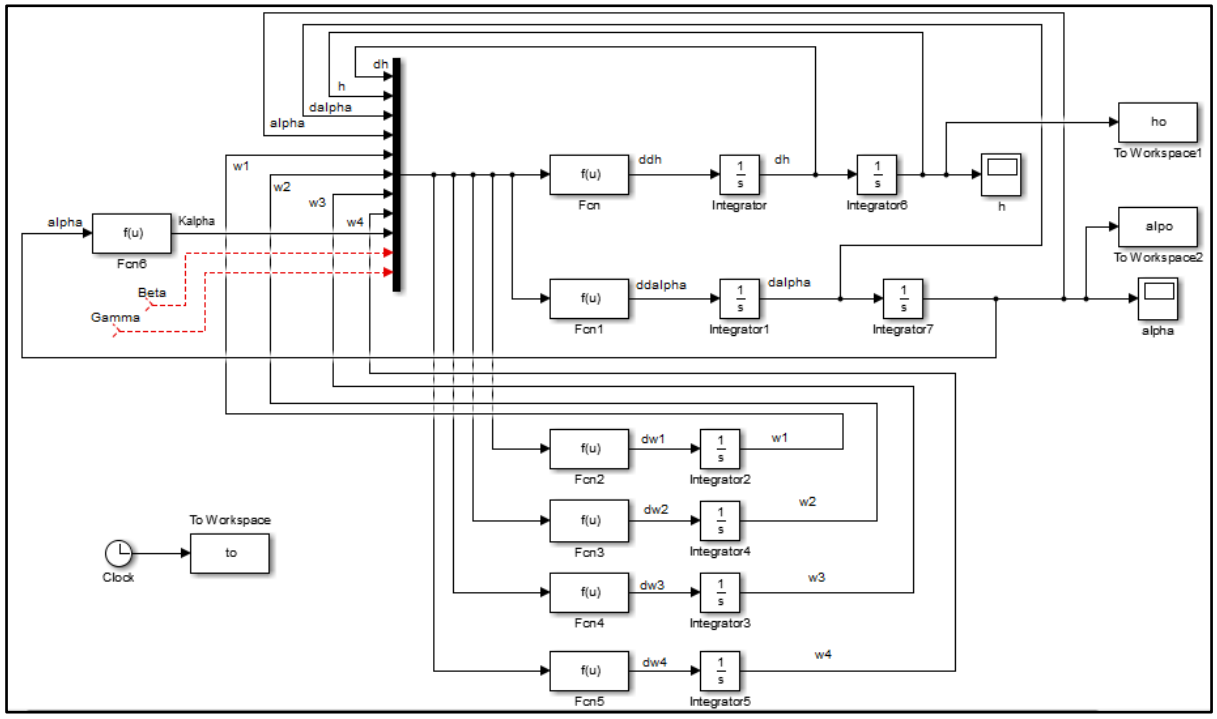

Figure IV.1. Simulink system's implementation in open loop

Simulation results for the nonlinear studied system in open loop are obtained under the initial conditions $[h\ \dot{h}\ \alpha\ \dot{\alpha}\ w_1\ w_2\ w_3\ w_4]^T = [0.01\ 0\ 0.2\ 0\ 0\ 0\ 0]^T$.

These results are shown in figures (IV.2) and (IV.3) where figure (IV.2) presents the Open-Loop (OL) time responses for a velocity of 8 m/s, and figure (IV.3) presents the open-loop time responses for a speed of 14 m/s.

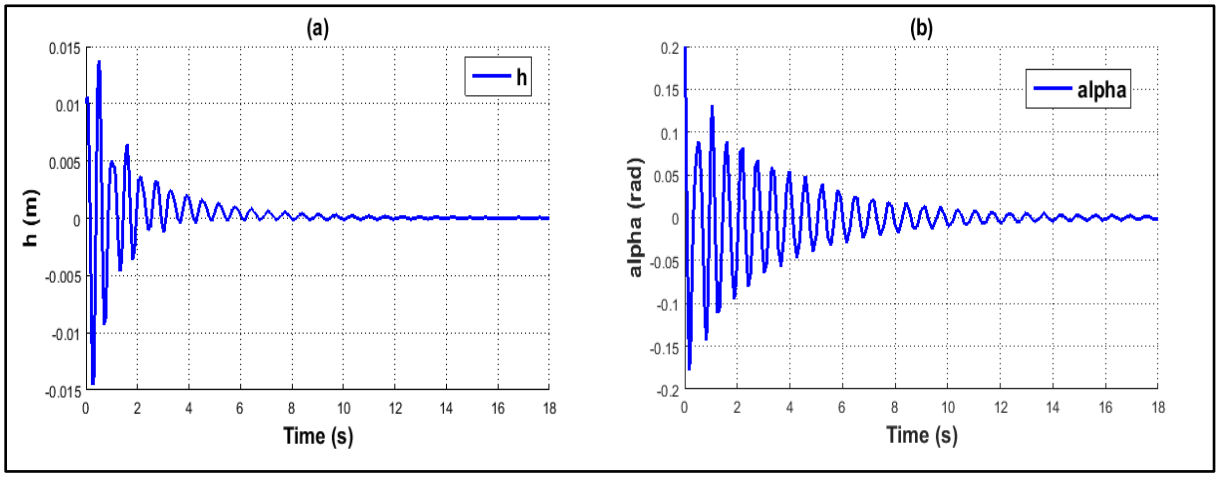

Figure IV.2. Open Loop time responses for V = 8 m/s

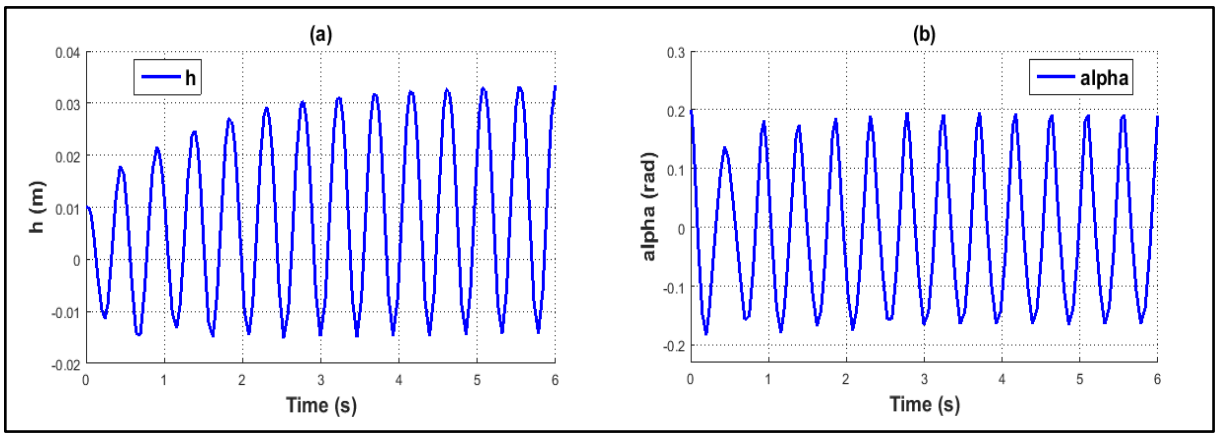

Figure IV.3. Open Loop time responses for V = 14 m/s

The open-loop simulation results show that at the speed of $8\,m/s$ (Figure (IV.2)), the system exhibits oscillations of low amplitudes that converge slowly towards the equilibrium position, i.e. the system in this case is stable but poorly damped, where more than 10 seconds were needed to these oscillations to be removed.

At the airspeed of $14\,m/s$, the nonlinear open-loop model becomes unstable as can be seen in figure (IV.3) that presents large-amplitudes oscillations that become periodic after few seconds with a constant amplitude, which means in other words the appearance of the undesired Limit Cycle Oscillations (LCOs) due to structural and aerodynamic nonlinearities, and generally considered as the beginning of the flutter phenomenon. This explains the importance of the active control-plant introduction. It can be noticed also from these figures, that there is a transition velocity between the two previous airspeeds known as the flutter velocity, and in which the system passes from a stable to an instable state.

After successive simulations, the flutter velocity for the open-loop case was identified at:

$$\boldsymbol{V_{F1} = 10.70\,m/s}$$

IV.3. Classical Sliding Mode Control (CSMC)

In this section, the system's stability and time-responses behavior will be investigated after applying a classical sliding mode control plant. The plunge displacement h and the pitch angle α time variations will be visualized as well as the TLECS deflections β and γ. These deflections has been limited between $\pm$ 0.5 rad (About $\pm$ 28°) in order to keep their values among the actuator's physical capabilities.

Simulation results are obtained under the same initial conditions as the open-loop case, and for the following controller's parameters: $k_1 = k_2 = 15$ and $l_1 = l_2 = 5$.

Figure (IV.4) shows the system's time-responses behavior after applying the CSMC law, compared to the open-loop case, for a free-stream velocity of 35 m/s. It can be observed in figure IV.4 (a) and (b) that the established controller has successfully removed the harmful LCOs and stabilized the system in less than half-a-second ($< 0{,}5$ s), while in the OL case the system presented instability expressed by the appearance of LCOs as shown in figure IV.4 (c) and (d).

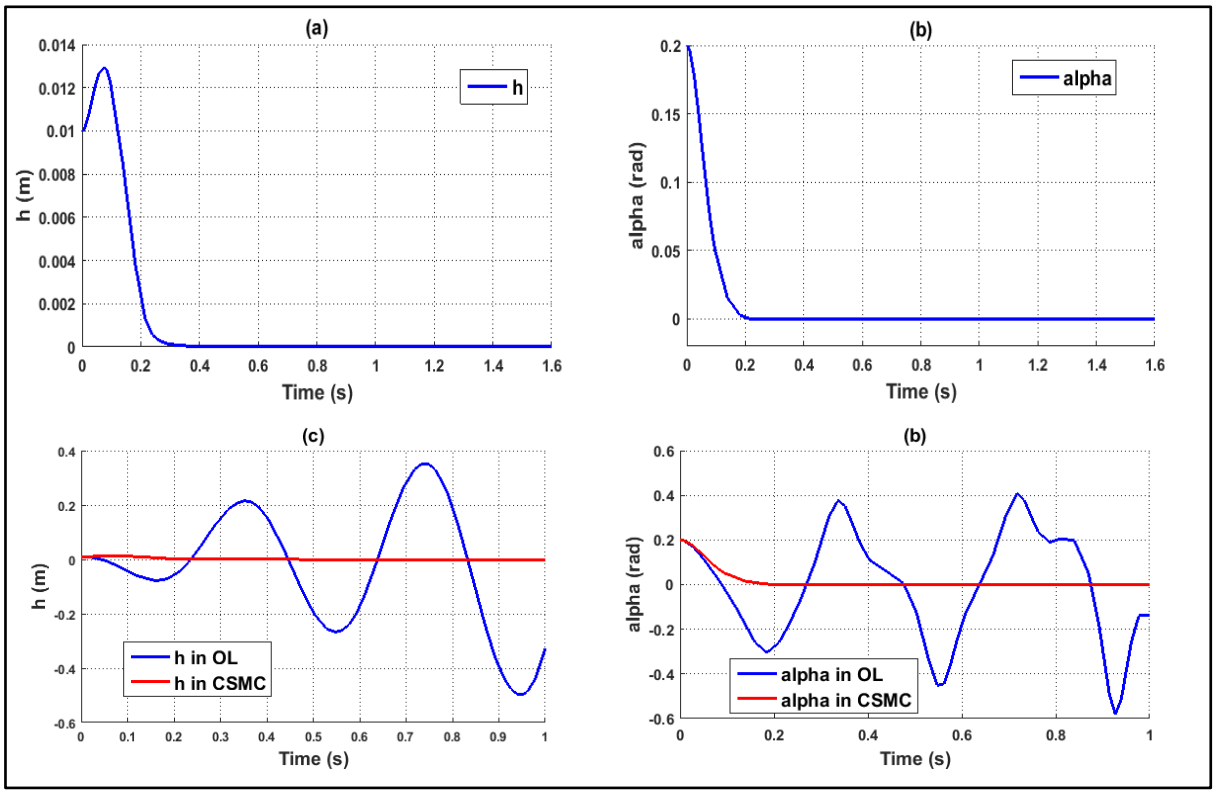

Figure IV.4. CSMC time responses compared to the OL case for V = 35 m/s

Figure (IV.5) illustrate the TLECS deflections and the sliding surfaces time responses in CSMC for the same airspeed, where one can notice that these parameters convergence smoothly towards the equilibrium position.

The CSMC plant has then guaranteed a fast system's stabilization with improved performance in spite of the existing nonlinearities and unsteady aerodynamic loads, and for an airspeed that is much higher than the OL critical flutter velocity.

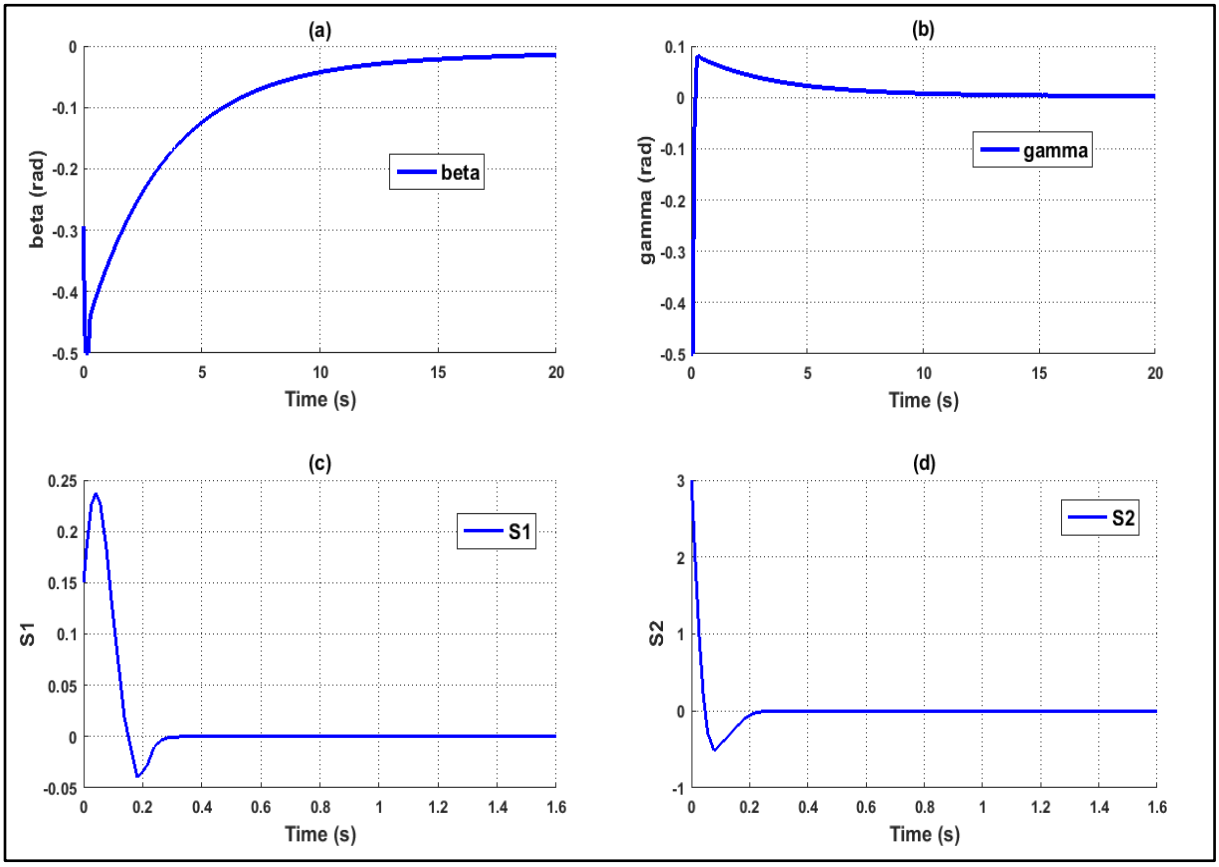

Figure IV.5. TLECS deflections and sliding surfaces time responses in CSMC for V = 35 m/s

The system's time-responses variations for the airspeed of 39 m/s are presented in figure (IV.6). Both plunge and pitch motions have exhibited LCOs which means that the airspeed has exceeded the critical flutter velocity for the CSMC case.

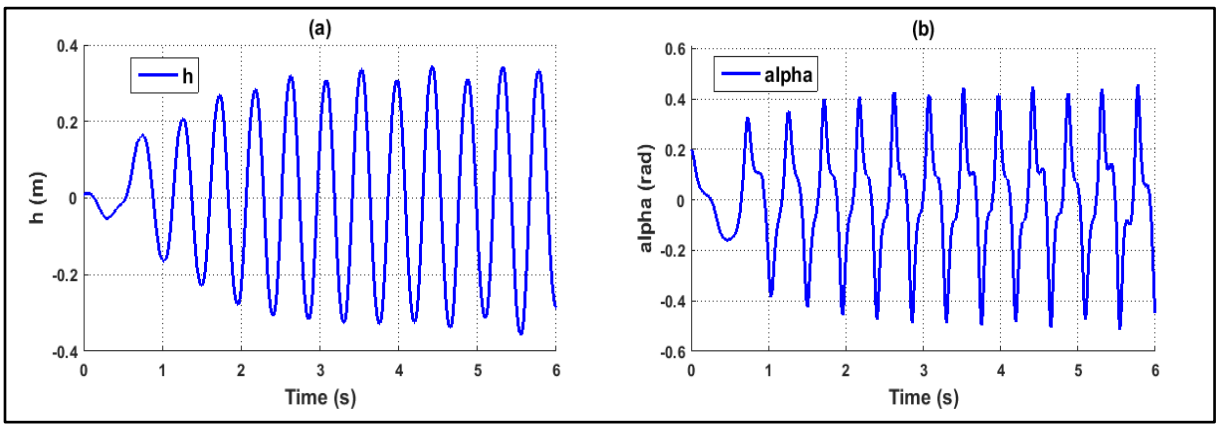

Figure IV.6. CSMC time responses for V = 39 m/s

After successive simulations, the flutter velocity for the CSMC case was found at:

$$\boldsymbol{V_{F2} = 38,27\ m/s}$$

In order to further test the controller's efficiency, the system's responses variations are visualized when the controller is activated at $t = 2\,s$ for the same initial conditions and controller's parameters, and for a free-stream velocity of $20\,m/s$. These variations are shown in figures (IV.7) and (IV.8). It is remarked from figure (IV.7) that the proposed control plant was able to stabilize the system smoothly and rapidly at the moment in which it was turned on, even after the system has entered in limit cycle oscillatory. Although, the chattering phenomenon is clearly seen in the deflections of TLECS as shown in fig. IV.8 (a) and (b).

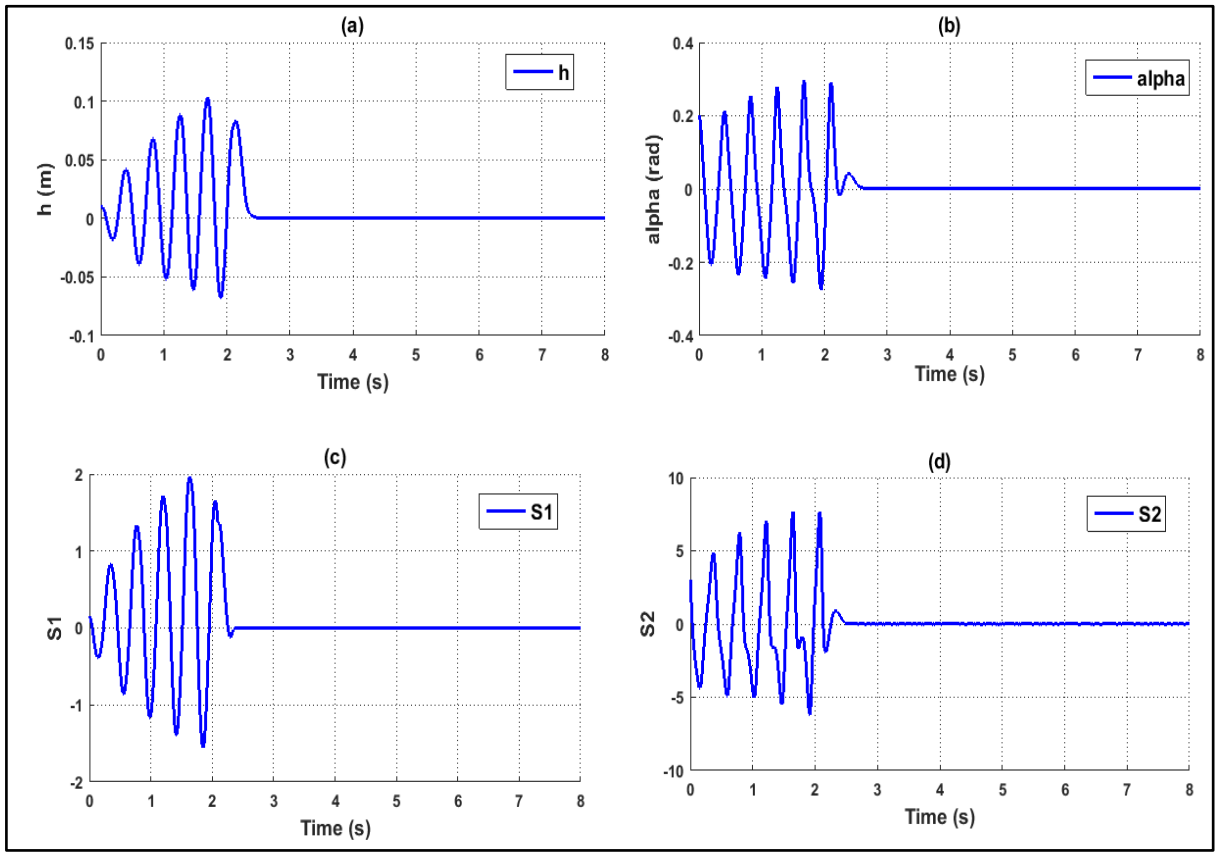

Figure IV.7. CSMC time responses, controller activated at t = 2 s

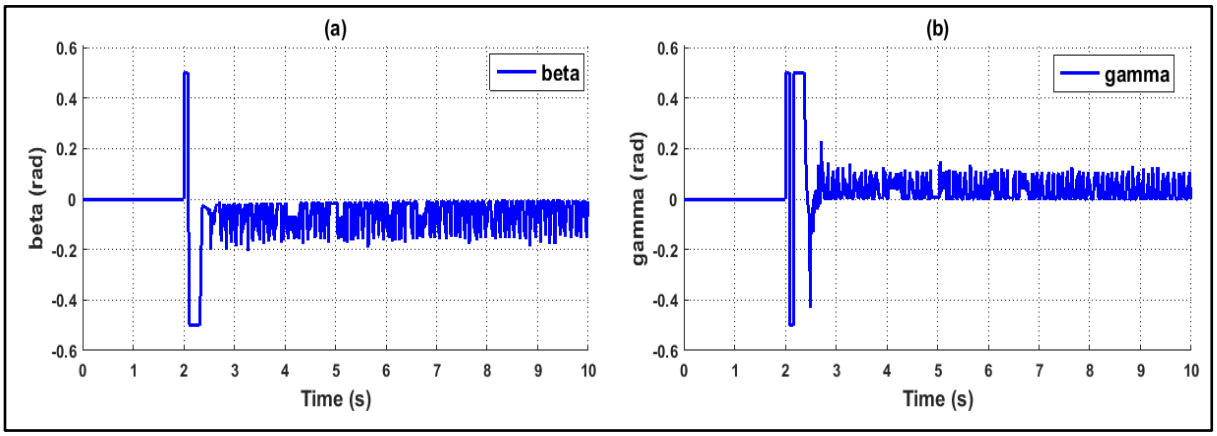

Figure IV.8. TLECS deflections responses in CSMC, controller activated at t = 2 s

IV.4. Fuzzy Sliding Mode Control (FSMC)

In order to eliminate any eventual appearance of the chattering phenomenon like the case that has been noticed in the previous section, CSMC is associated with a fuzzy logic controller in this section. The established FSMC law is designed with the same CSMC parameters and for the same initial conditions.

The figure (IV.9) right below presents the variations of the nonlinear system's responses after applying the designed fuzzy sliding controller, for a free-stream velocity of $35\ m/s$. It shows that the use of FSMC leads to have smooth and fast stabilized system's responses for high speeds. It's also noticed comparing this figure to figures (IV.4) and (IV.5) that FSMC maintains nearly the same system's performance guaranteed by the CSMC.

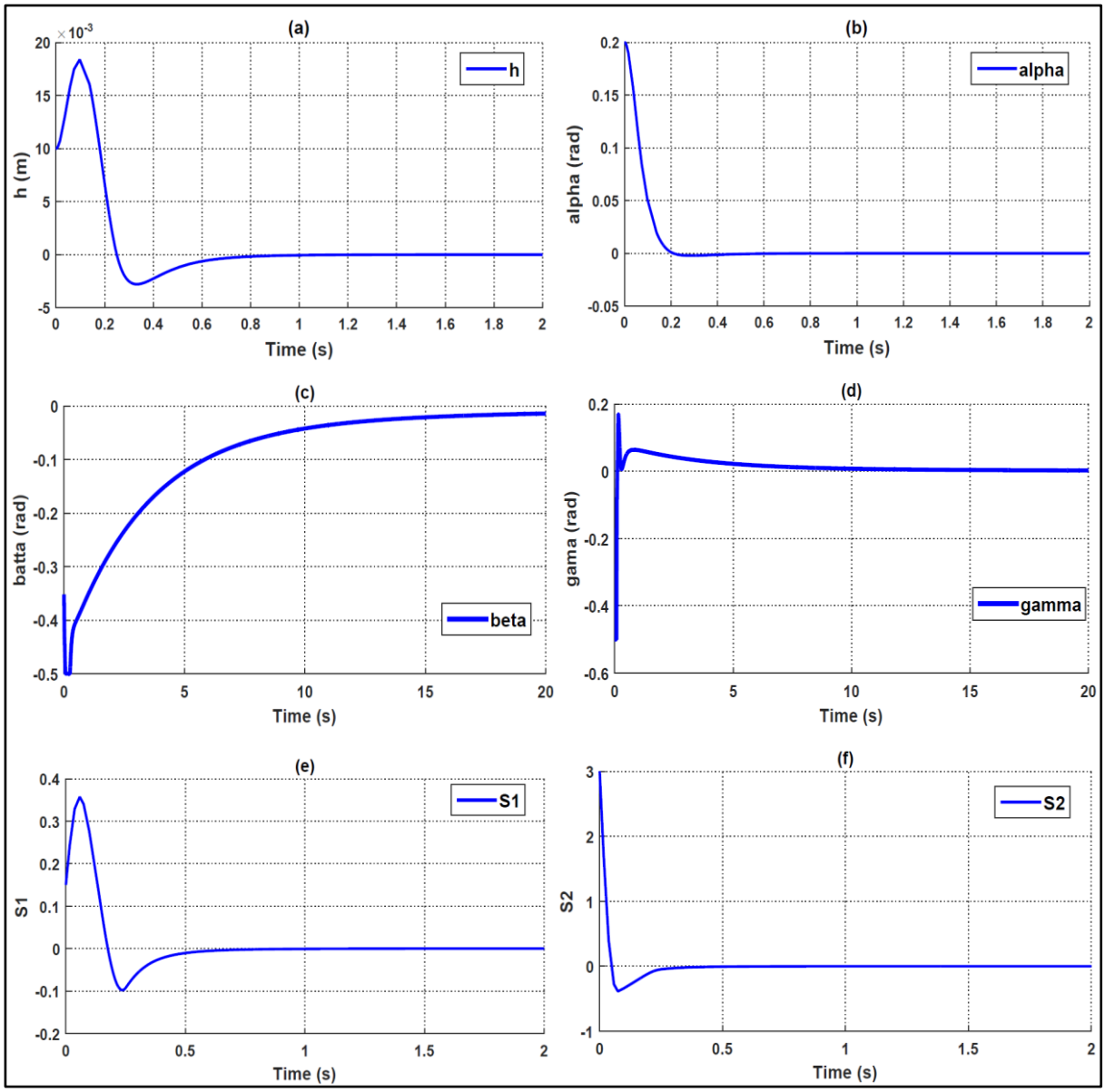

Figure IV.9. FSMC time responses for V = 35 m/s

The memberships M1 and M2 time-variations are given in figure IV.10 (a) and (b), where it is visualized that these memberships converge to the equilibrium position in a smooth way.

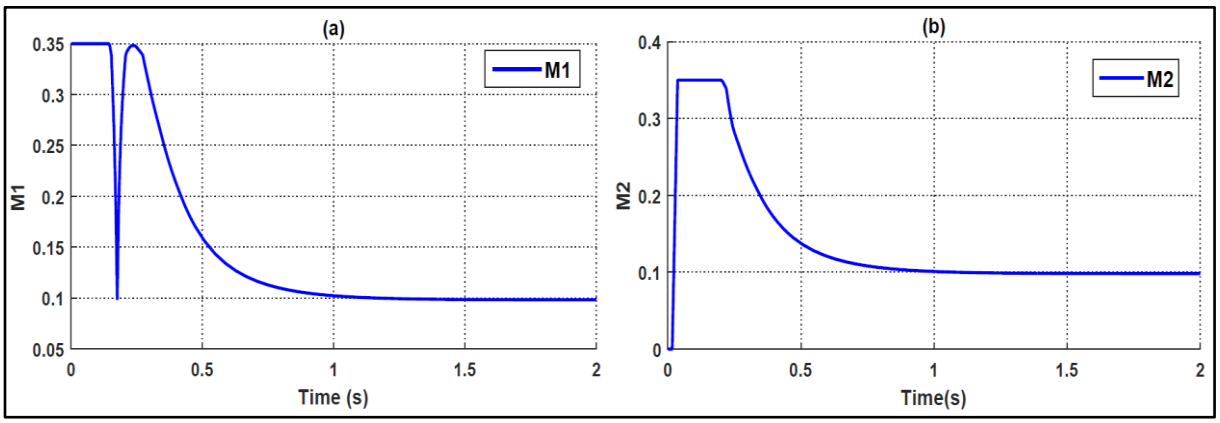

Figure IV.10. The memberships M1 and M2 time variations for V = 35 m/s

For the airspeed of 38 m/s, the system becomes instable as presented in figure (IV.11).

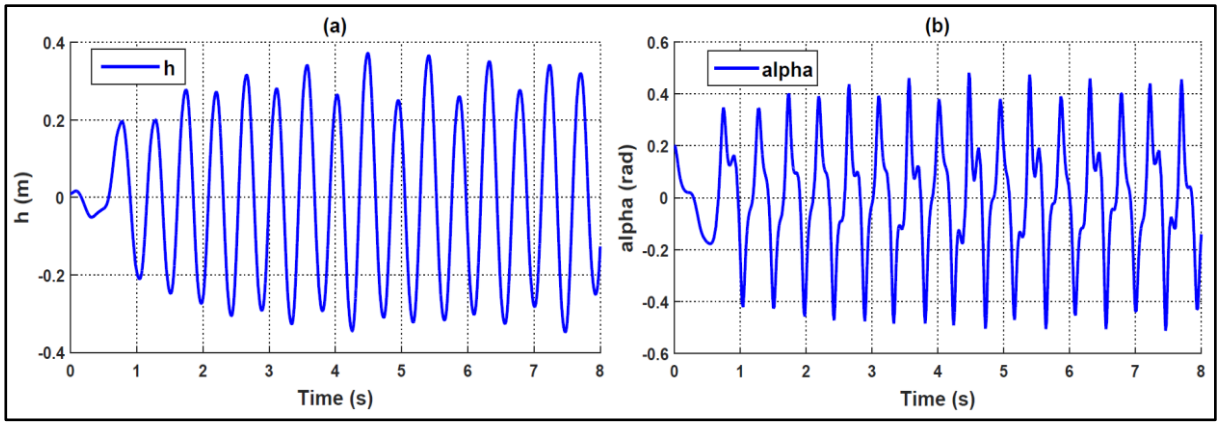

Figure IV.11. FSMC time responses for V = 38 m/s

After multiple simulations, the critical flutter speed for the FSMC case was spotted at:

$$\boldsymbol{V_{F3} = 36,99\ m/s}$$

For a speed of $20\,m/s$, the system's time-responses behavior, the memberships time variations, and the TLECS deflections responses compared to those in the CSMC case when the controller is activated at $t = 2\,s$ are respectively illustrated in figures (IV.12), (IV.13), and (IV.14). From these figures, one can remark that in addition to the quick stabilization of the system despite the LCOs' appearance, the introduction of FSMC has successfully and efficiently removed the chattering phenomenon that took place in the CSMC case.

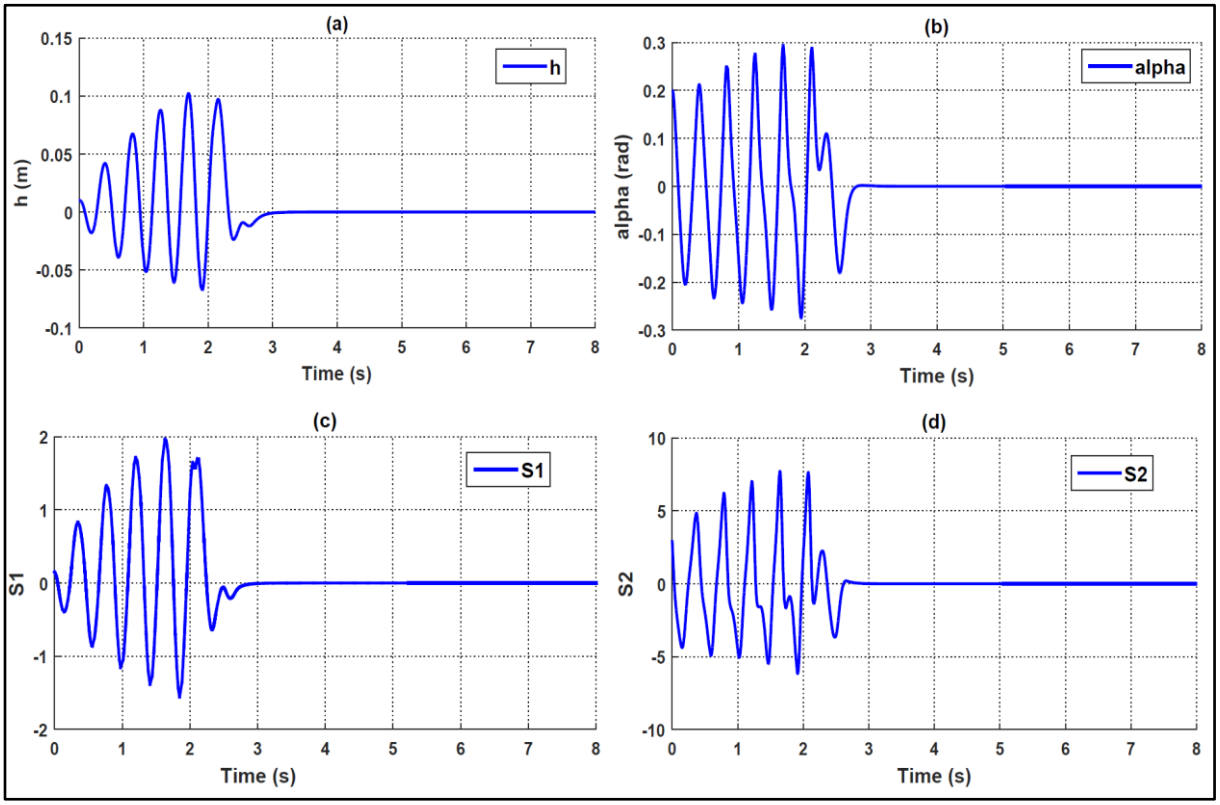

Figure IV.12. FSMC time responses, controller activated at t = 2 s

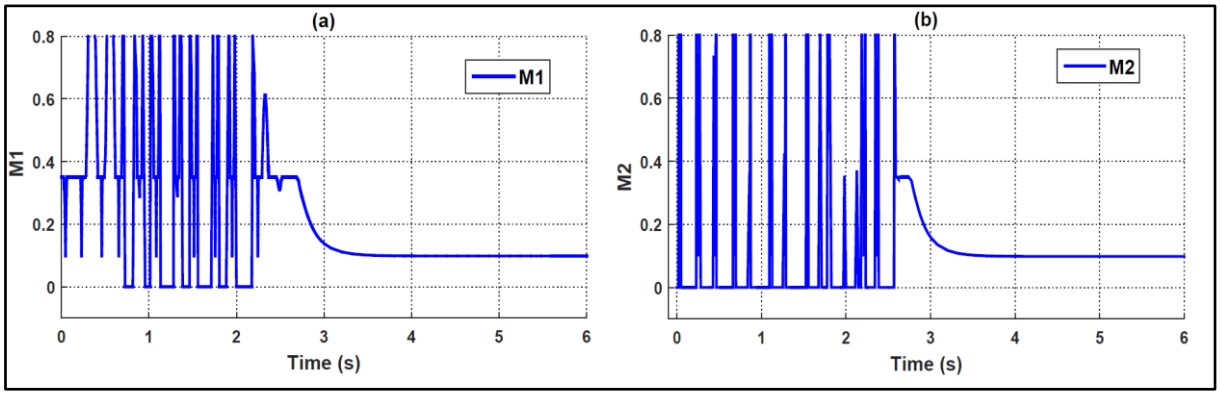

Figure IV.13. The memberships M1 and M2 time variations, controller activated at t = 2 s

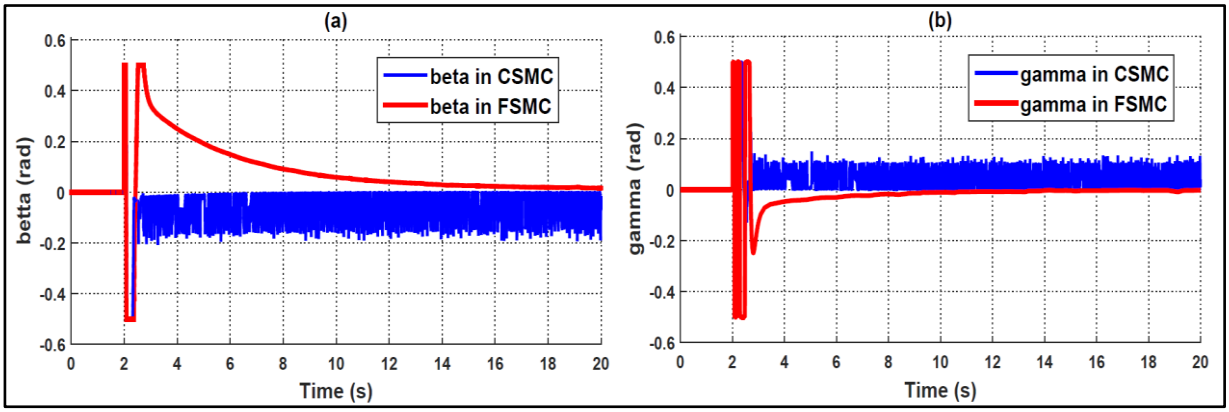

Figure IV.14. FSMC/CSMC comparison for TLECS deflections, controller turned on at t = 2 s

IV.5. Sliding Mode with High Gain Observer Controller (SMHGOC)

In this section, CSMC is combined with a High Gain Observer (HGO) that provides estimated states' values using some measured states. The system's stability and performance will be investigated after applying the SMHGOC. The plunge and pitch motions variations, the TLECS deflections, and the error between the actual and the estimated states will also be shown and discussed.

Simulation results are obtained under the initial conditions: $[h\ \dot{h}\ \alpha\ \dot{\alpha}\ w_1\ w_2\ w_3\ w_4]^T = [0.005\ 0\ 0.2\ 0\ 0\ 0\ 0]^T$, for the controller's parameters: $k_1 = k_2 = 15$, $l_1 = 32$, $l_2 = 18$, and for the HGO's parameters: $\varepsilon_1 = \varepsilon_2 = 0.001$, $q_1 = q_3 = 3$ and $q_2 = q_4 = 2$, chosen in a way to have negative real-parts for the eigenvalues of the following equations:

$s^2 + q_1 s + q_2 = 0$ and $s^2 + q_3 s + q_4 = 0$.

Figure IV.15 (a), (b), (c) and (d) represents the system's time response after the implementation of the SMHGOC for a velocity of $31\ m/s$, where (c) and (d) are zoomed parts of (a) and (b) respectively. And figure IV.15 (e) and (f) shows the variation of the error between the actual states' values (h and α) and the estimated ones. It can be seen from this figure that the plunge and pitch motions have been stabilized within some fractions of a second. It is also noticed that the estimated-state graph has joined the graphical representation of the actual state for both plunge and pitch motions in a short period of time, as pointed in the figure IV.15 (c) and (d), where the error between the actual and estimated values converged rapidly to zero as illustrated in figure IV.15 (e) and (f).

Figure (IV.16) visualizes the sliding surfaces time variations for an airspeed of $31\ m/s$, and it shows that these variations tend towards the equilibrium position in finite time.

These results mean a performant controller with a well-designed observer and important critical flutter velocity margins.

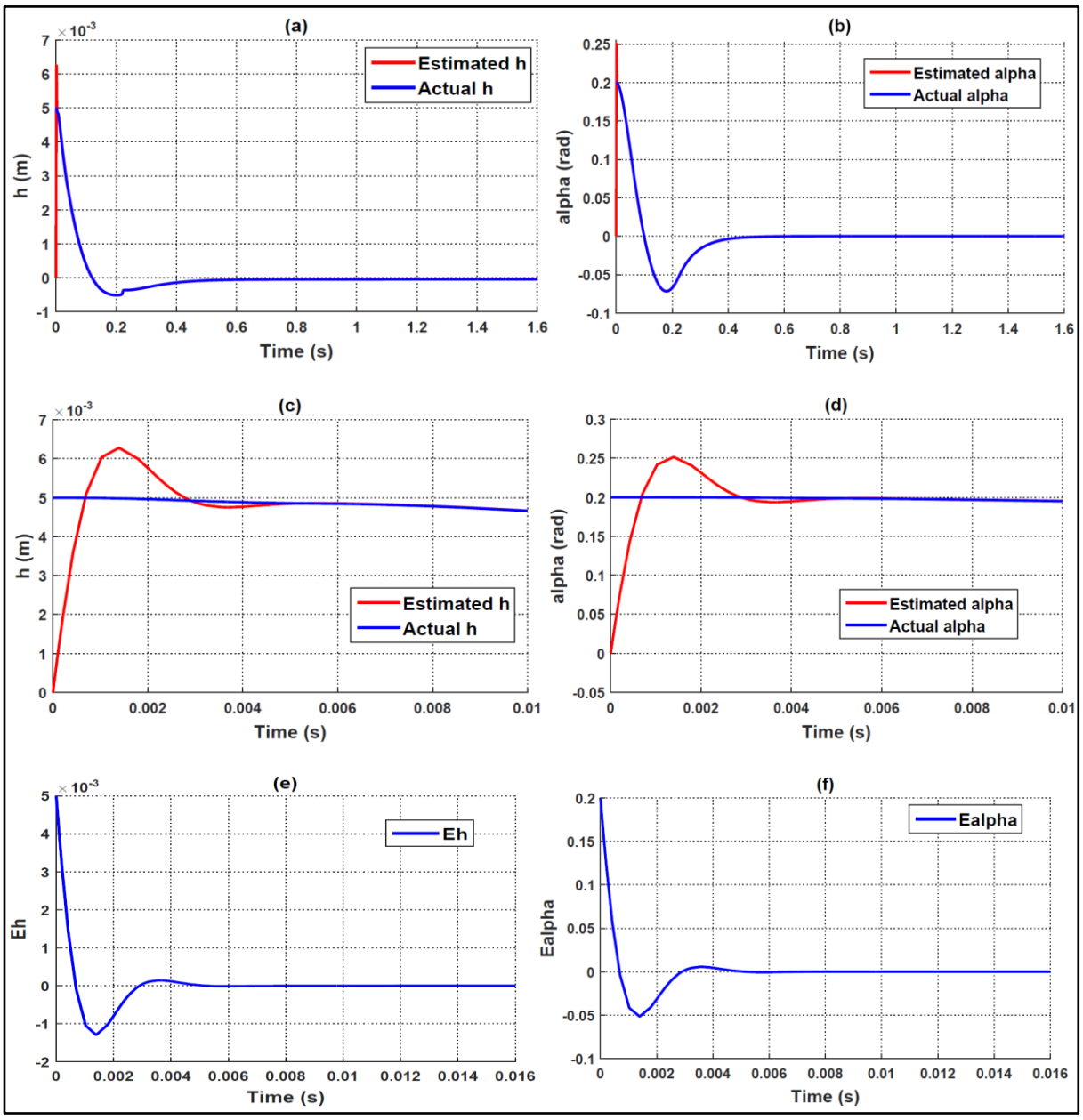

Figure IV.15. SMHGOC time responses for V = 31 m/s

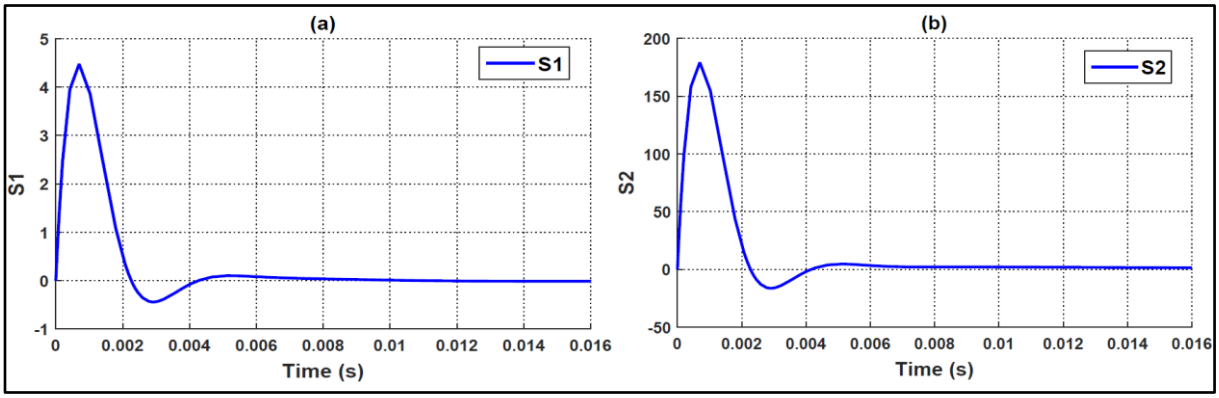

Figure IV.16. Sliding surfaces time variations for V = 31m/s

The following figure (IV.17) shows the behavior of the TLECS deflections for the airspeed of 31 m/s. As noticed in the parts (a) and (b), the deflections tend towards zero in finite time, but, they present an oscillating behavior which is the well-known chattering phenomenon, clearly seen in figure IV.17 (c) and (d) that are zoomed parts of (a) and (b).

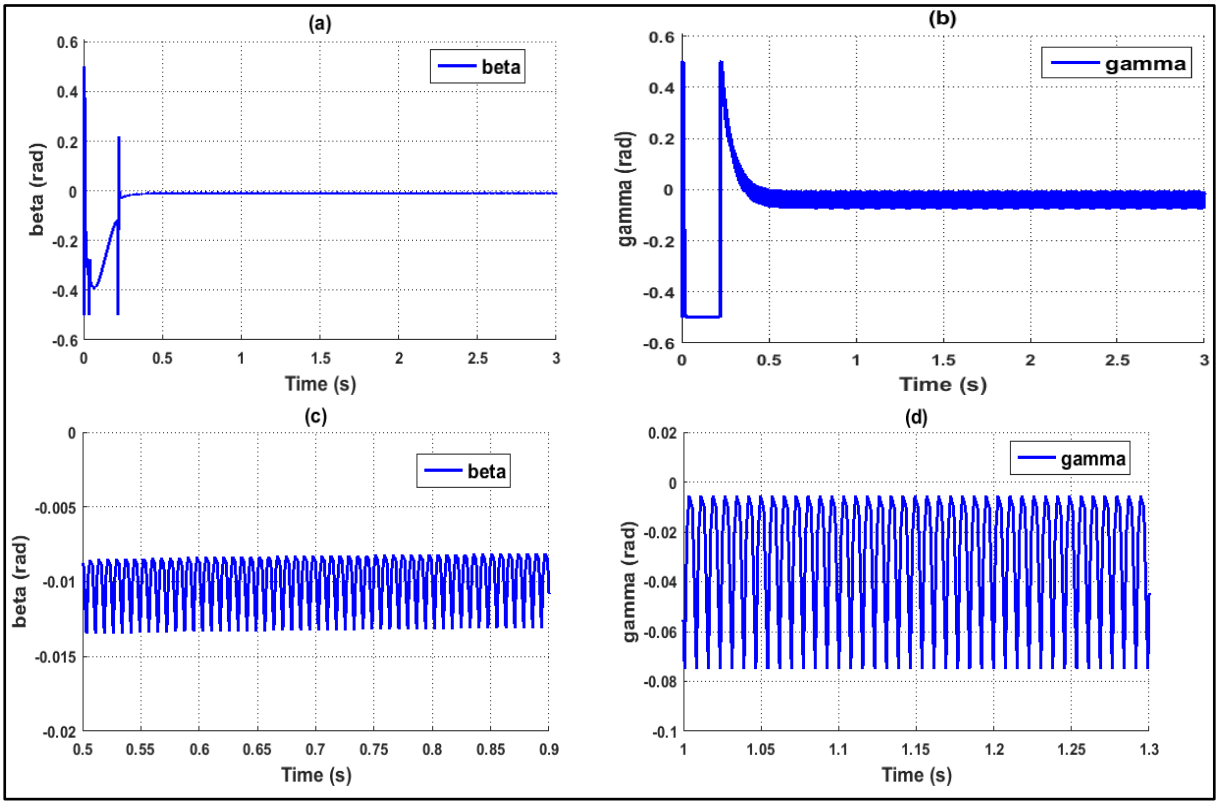

Figure IV.17. TLECS deflections time variations for V = 31 m/s

The plunge displacement and the pitch angle variations for a speed of 44 m/s are illustrated in figure (IV.18), where the system's instability was expressed by the apparition of LCOs in both motions. After simulations, the flutter velocity has been found at:

$$\boldsymbol{V_{F4} = 42,59\ m/s}$$

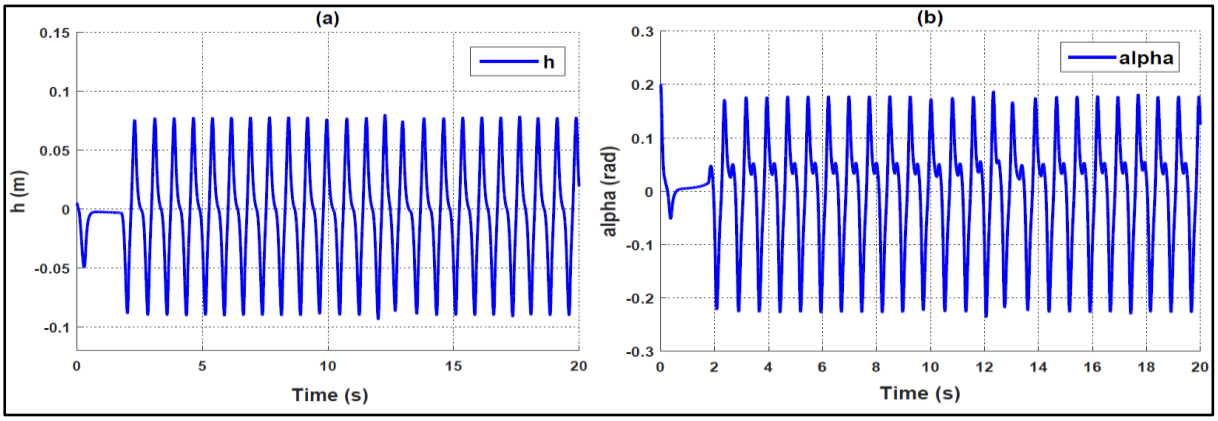

Figure IV.18. The system's time responses for V = 44 m/s

IV.6. Fuzzy Sliding Mode with High Gain Observer Controller (FSMHGOC)

In the previous part, simulation results showed the apparition of chattering after using SMHGOC. In this part, this controller will be combined with a FLC in order to eliminate this harmful phenomenon. The FSMHGOC is built and implemented under the initial conditions and with the same controller's and observer's parameters as in the SMHGOC case.

Figure (IV.19) describes the system's time responses after applying the FSMHGOC for the same initial conditions and controller's parameters in the previous section, and for a free-stream velocity of 37 m/s. According to this figure, the use of this controller led to stabilize the aeroelastic system in a short period of time, with an accurate estimation of the system's states where the error between the estimated and the actual states' values tend rapidly to zero, proving the controller's effectiveness and the observer's accuracy.

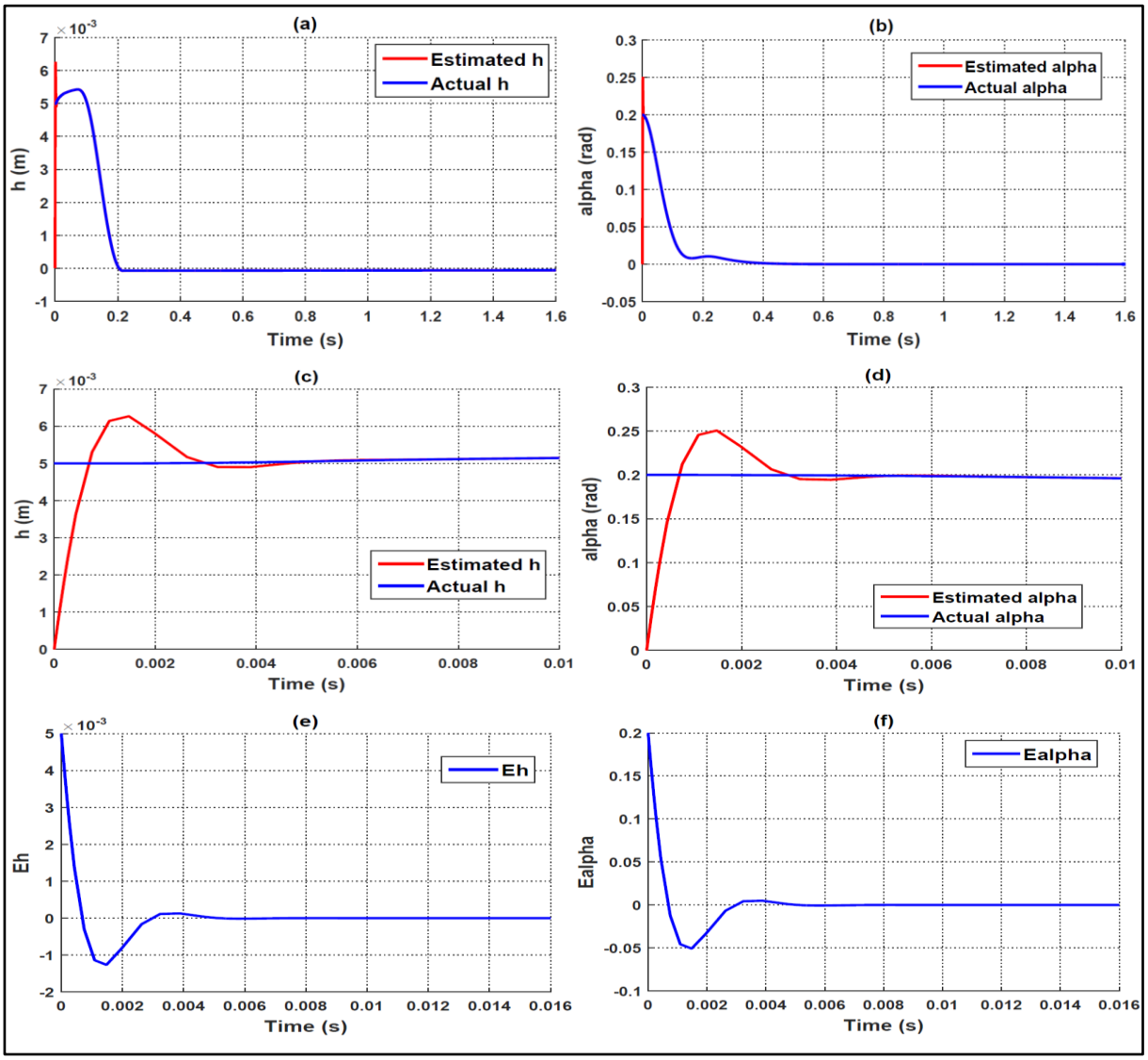

Figure IV.19. FSMHGOC time responses for V = 37 m/s

Figure (IV.20) is the graphical representation of the sliding planes and the membership functions time responses in a speed of 37 m/s. These responses converge steadily to the position of equilibrium in short time.

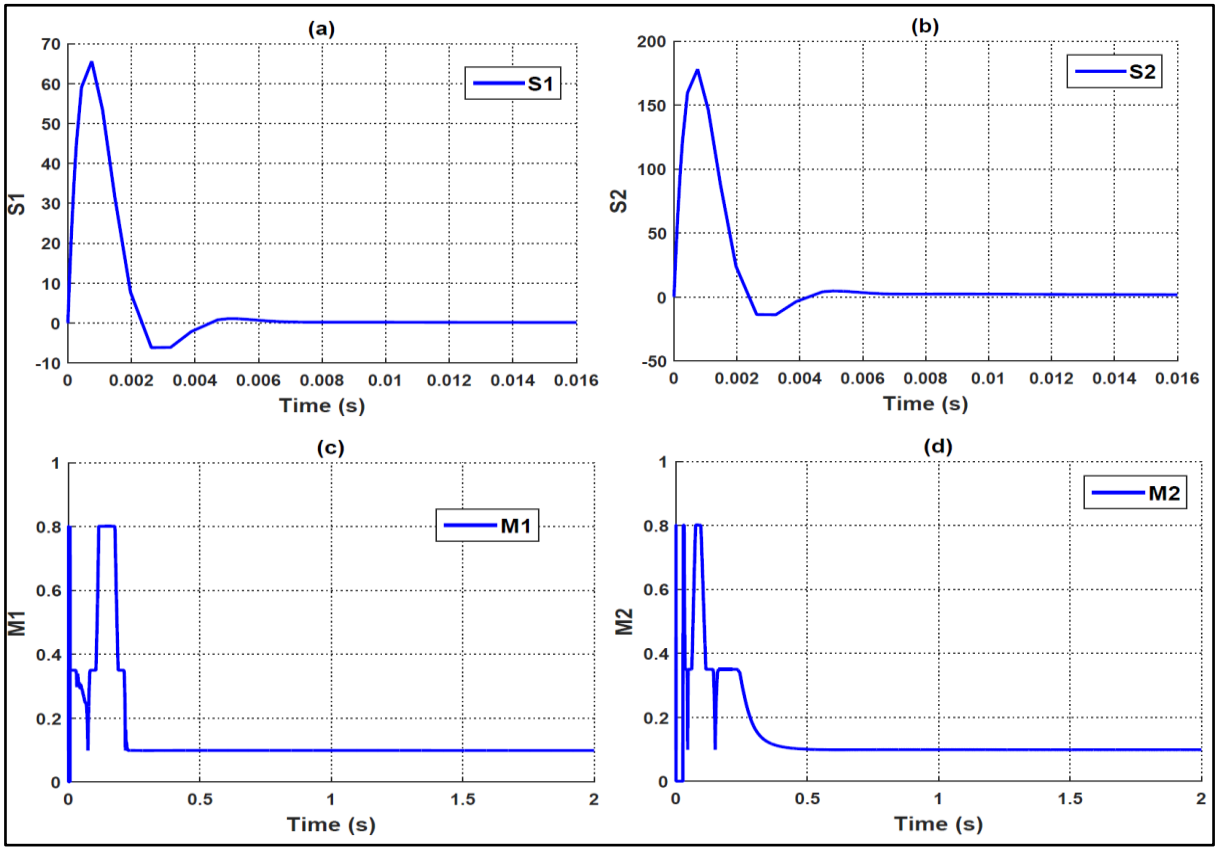

Figure IV.20. Sliding surfaces and membership functions time variations for V = 37 m/s

For the same airspeed, the TLECS deflections' time changes compared to the SMHGOC case are illustrated in figure (IV.21) from which one can see that in the case of FSMHGOC, the deflections tend in a steady way towards the equilibrium position in finite time, with no apparition of the chattering as in the case of SMHGOC.

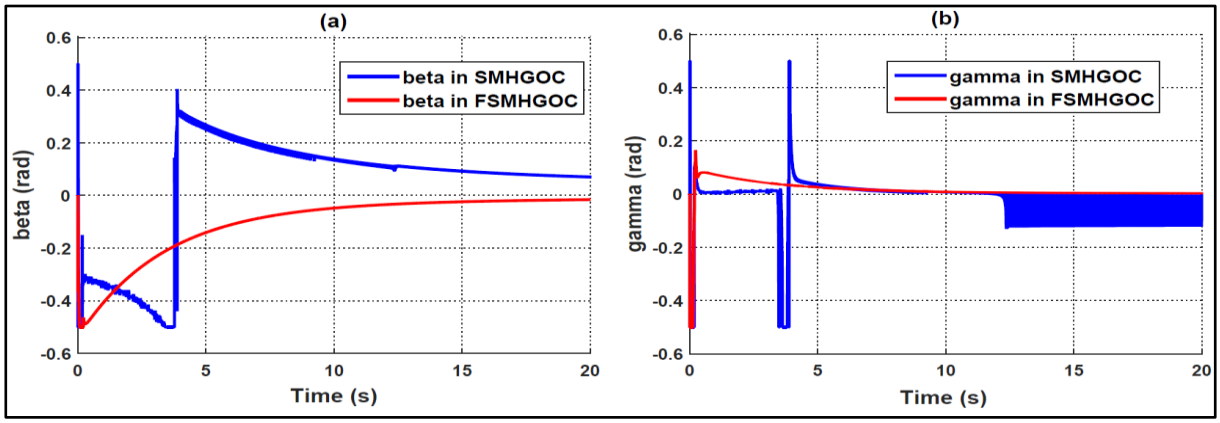

Figure IV.21. TLECS deflections time variations for V = 37 m/s

For a speed of 41 m/s, the aeroelastic system became instable exhibiting LCOs as shown in figure (IV.22) below.

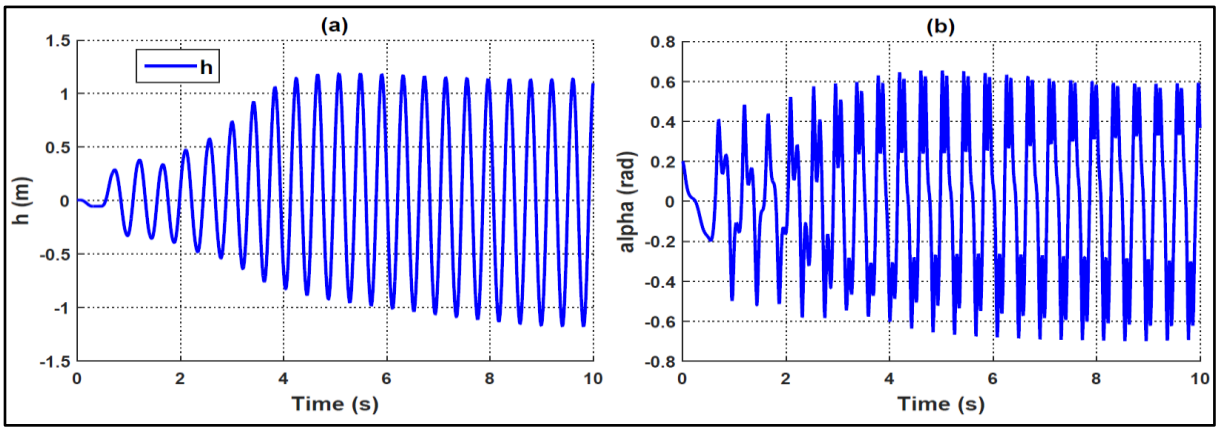

Figure IV.22. The system's time responses for V = 41 m/s

The critical flutter speed has been observed after many simulations at:

$$\boldsymbol{V_{fsmc} = 39,67 m/s}$$

IV.7. A comparative study

This part exposes a comparison between the open-loop case and the designed controllers in terms of system's performance, flutter velocity value, critical flutter speed gain and chattering existence or removal. This comparison is summarized in the following table (IV.1).

Table IV.1. A summarizing comparison

	Open-loop	***CSMC***	***FSMC***	***SMHGOC***	***FSMHGOC***
Performance	Degraded	Enhanced	Enhanced	Enhanced	Enhanced
Flutter speed	10,70 m/s	38,27 m/s	36,99 m/s	42,59 m/s	39,67 m/s
Flutter speed margins	/	+ 27,57 m/s	+ 26,29 m/s	+ 31,89 m/s	+ 28,97 m/s
Chattering	Instability	Exists	Removed	Exists	Removed

The table shows that the proposed controllers have effectively enhanced the system's performances in short periods of time even with the system's structural and aerodynamic nonlinearities and gust loads, and led to have increased flutter velocity margins. It shows also that the introduction of the FLC led to remove any eventual appearance of the chattering phenomenon as has been noticed in the CSMC and SMHGOC cases. Then, these controllers

have provided robustness and accuracy thanks to the SMC, the chattering removal ensured by the FLC, and the precise states' estimation by the HGO which means less expansive sensors.

IV.8. Conclusion

In this chapter, the simulations' results have been exposed and discussed. The numerical and graphical results presented in this chapter have shown the effectiveness of the robust control plants in improving the system performance, increasing the flutter speed margins in a significant way, removing the chattering phenomenon and providing precise estimations for the nonlinear aeroelastic systems' states, in spite of nonlinearities in the system and unsteady aerodynamic charges.

CONCLUSIONS AND PERSPECTIVES

The objective of the work presented in this thesis is based on the mathematical modeling of an aeroelastic wing section for an unsteady aerodynamic regime via the Wagner's function, which is a recent direction in this research field. The obtained dynamic model has two degrees of freedom since it considers the pitch movement and the plunge displacement with two control surfaces.

Characterized by its non-linearity, the dynamic motion of the model in open loop has badly-damped or unstable oscillations for given flow velocities. Therefore, four types of controllers have been used for the stabilization and the control of the considered model: The CSMC, FSMC, SMHGOC, and FSMHGOC, exploited in order to limit the vibrations and to delay the appearance of the flutter phenomenon.

To start with, a general overview was presented in the first chapter concerning ASE and aeroelasticity phenomena, particularly that of flutter. For the physical system, an essential part of the study which is the mathematical development of the dynamic model was built in the second chapter, and an application was made on the wing model TAMU II in order to get its space state representation. The latter allowed the development of control laws for the stability of the aeroelastic system in the third chapter where the designed controllers' definition and establishment-steps were presented in some detail.

The mathematical model as well as the developed control laws made it possible; in the fourth chapter; to simulate the dynamic behavior of the system in terms of pitch and vertical movements in open loop as well as by applying the controllers.

The open-loop simulation led to visualize the flutter phenomenon which corresponds to a critical velocity known as the flutter speed which was relatively low in this case. This unwanted phenomenon leads generally to problems of structural fatigue, passengers' discomfort, performance deterioration, and even catastrophic structural failures. Then, the considered controllers have been proposed in order to deal with this phenomenon. The common point about these control laws is the use of the first-order CSMC which is a robust control plant for VSS, with a simple structure and a high precision. This controller is characterized by the choice of a switching function that ensures the convergence of the state trajectory towards the equilibrium position while remaining in the vicinity of a sliding surface with insensitivity towards perturbations and parameters changes. However, the use of SMC can cause the apparition of the chattering phenomena which is very high-frequency

oscillations that affect the system's performances and harm the associated actuators. Indeed, this phenomenon has been noticed in the simulation results of the CSMC and the SMCHGOC. For that, a solution was required to alleviate this SMC inconvenience. Thus, a FLC has been proposed, it is a simply-designed controller that uses linguistic information and rule-based algorithms, and commonly used to deal with chattering cases.

In order to deal with the concern of having a complicated model with an increased number of system states (From which some may be unmeasurable) due to the consideration of unsteady aerodynamic charges and the different nonlinearities that exist in the aeroelastic system, a HGO is introduced with the CSMC and also with the FSMC, this type of controllers relies on the right choice of the control parameters in order to guarantee the convergence of the estimated state trajectory towards the real ones, and to ensure a robust and stable model even with some unmeasurable systems' states.

The simulation results have shown that the application of the built controllers has efficiently accomplished the system's stabilization in spite of nonlinearities and unsteady aerodynamic loads, resulting in a significant increase of the flutter speed margins. These results have visualized also the chattering phenomenon in the cases of CSMC and SMHGOC, and the introduction of the FLC has led to a full suppression of this undesired phenomenon.

Therefore, the obtained results and conclusions that have been derived from this work can confirm that the study may serve as a robust, effective, and accurate solution for stability problems in the active control domain for nonlinear aeroelastic systems, even under unsteady gust charges. Furthermore, it can be an economic tool to develop nonlinear aeroelastic airfoils in wind tunnels or for fixed-wing drones. All of this, in addition to the rich bibliography that it provides, and that may help as a departure point for further research in ASE.

Perspectives:

This study remains open for more research items in all the ASE directions, in the aim of having the best compromise between the system's stability with high performances, and less complexities in systems' models and controllers' designs. Here are some examples:

- In the modeling direction, the system's modeling can be extended to a three-dimensional complete aeroelastic wing model or full flexible aircraft with unsteady aerodynamics ;
- In the control side, many controllers may be proposed such as SMC based on neural networks (Deep learning), or adaptive SMC, applied on the studied model, or on the suggested models right above.

BIBLIOGRAPHY

[1] A. Tewari, Aeroservoelasticity: Modeling and control, Springer, New York, 2015.

[2] A. Tewari, Adaptive aeroservoelastic control, John Wiley & Sons, 2016.

[3] S. Dilmi, Elaboration des lois de commande dédiées au guidage d'un avion souple, (Ph. D. thesis), Institute of Aeronautics and Spatial Studies, University of Blida 1, Algeria, 2017.

[4] Y. C. Fung, An Introduction to the Theory of Aeroelasticity, Dover Publications, New York, 1993.

[5] E. H. Dowell, A Modern Course in Aeroelasticity, 6th edition, Springer, 2022.

[6] A. R. Collar, The Expanding Domain of Aeroelasticity, The Aeronautical Journal, Vol. 50, No. 428, (1946), 613–636.

[7] P. Singh, An Introduction to Aeroelasticity, Indian institute of Engineering Science and Technology, 2021.

[8] C. Mertens, T. de Rojas Cordero, J. Sodja, A. Sciacchitano, B. Van Oudheusden, Determination of Collar's Triangle of Forces on a Flexible Wing based on Particle Tracking Velocimetry Measurements. In AIAA Scitech 2021 Forum, (January 2021), 11–15 & 19–21.

[9] S. Nithin, B. K. Vijayalakshmi, Review on aeroelasticity, International Journal of Engineering Applied Sciences and Technology, Vol. 4, No 8, (2019), 271 -274.

[10] Q. Rendu, Modélisation des écoulements transsoniques décollées pour l'étude des interactions fluide-structure, (Ph. D. thesis), University of Lyon, 2016.

[11] A. Malher, O. Doaré, C. Touzé, Passive control of the flutter instability on a two-degrees-of-freedom system with pseudoelastic shape-memory alloy springs, In International Conference on Structural nonlinear dynamics and diagnosis, (CSNDD 2014), 2014.

[12] R. L. Bisplinghoff, H. Ashley, R. L. Halfman, Aeroelasticity, Dover Publications, 1996.

[13] E. L. Houghton, P. W. Carpenter, S. H. Collicott, D. T. Valentine, Basic Concepts and Definitions, In: Aerodynamics for Engineering Students, (Book chapter), Elsevier, (2017), 1–86.

[14] J. Kou, W. Zhang, Data-driven modeling for unsteady aerodynamics and aeroelasticity, Progress in Aerospace Sciences, Vol. 125, (2021), 100725.

[15] J. R. Wright, J. E. Cooper, Introduction to Aircraft Aeroelasticity and Loads, John Wiley & Sons, 2008.

[16] R. Kamakoti, W. Shyy, Fluid–structure interaction for aeroelastic applications, Progress in Aerospace Sciences, Vol. 40, No. 8, (2004), 535-558.

[17] F. Afonso, J. Vale, E. Oliveira, F. Lau, A. Suleman, A review on non-linear aeroelasticity of high aspect-ratio wings, Progress in Aerospace Sciences Vol. 89, (2017), 40–57.

[18] I. E. Garrick, W. H. Reed III, Historical development of aircraft flutter, Journal of Aircraft, Vol. 18, No. 11, (1981), 897-912.

[19] I. Zentner, Investigation of stability of aeroleastic systems excited by multiplicative noise, (Ph. D. thesis), Ecole des Ponts ParisTech, France, 2005.

[20] J. G. Marshall, M. Imregun, A review of aeroelasticity methods with emphasis on turbomachinery applications, Journal of fluids and structures, vol. 10, No. 3, (1996), 237-267.

[21] M. U. D. S. Rajput, Evaluation of experimental forced response data of a turbine stage with respect to different stator blade damages, (Ph. D. thesis), Royal Institute of Technology, Stockholm, Sweden, 2013.

[22] A. Akmeşe, Aeroservoelastic analysis and robust controller synthesis for flutter suppression of air vehicle control actuation systems, (Ph. D. thesis), Department of Mechanical Engineering, The Middle East Technical University, Turkey, 2006.

[23] R. L. Bisplinghoff, H. Ashley, Principles of Aeroelasticity, Dover publications, New York, 1962.

[24] I. E. Garrick, Aeroelasticity – Frontiers and Beyond, Journal of Aircraft, Vol. 9, No. 9, (1976), 641-657.

[25] L. R. Felt, L. J. Huttsell, T. E. Noll, D. E. Cooley, Aeroservoelastic Encounters, Journal of Aircraft, Vol. 16, No. 7, (1979), 471-483.

[26] A. R. Collar, The first 50 years of aeroelasticity, Aerospace (Royal Aeronautical Society, London),Vol. 5, (1978), 12–20.

[27] P. P. Friedmann, Renaissance of aeroelasticity and its future, Journal of Aircraft, Vol. 36, No. 1, (1999), 105–21.

[28] E. Livne, Future of airplane aeroelasticity, Journal of Aircraft, Vol. 40, No. 6, (2003), 1066-1092.

[29] J. Čečrdle, Introduction to aircraft aeroelasticity and whirl flutter, In: Whirl Flutter of Turboprop Aircraft Structures, (Book chapter), Woodhead Publishing, (2015), 1–12.

[30] D. H. Hodges, G. A. Pierce, Introduction to structural dynamics and aeroelasticity, Cambridge University press, Vol. 15, 2002.

[31] M. D. C. Henshaw, K. J. Badcock, G. A. Vio, C. B. Allen, J. Chamberlain, I. Kaynes, G. Dimitriadis, J. E. Cooper, M. A. Woodgate, A. M. Rampurawala, D. Jones, C. Fenwick, A. L. Gaitonde, N. V. Taylor, D. S. Amor, T. A. Eccles, C. J. Denley, Non-linear aeroelastic prediction for aircraft applications, Progress in Aerospace Sciences, Vol. 43, No. 4-6, (2007), 65-137.

[32] E. Dowell, J. Edwards, T. Strganac, Nonlinear aeroelasticity, Journal of aircraft, Vol. 40, No. 5, (2003), 857–874.

[33] B. H. K. Lee, S. J. Price, Y. S. Wong, Nonlinear aeroelastic analysis of airfoil: bifurcation and chaos, Progress in Aerospace Sciences, Vol. 35, No. 3,(1999), 205-334.

[34] M. J. Patil, D. H. Hodges, C. E. S. Cesnik, Limit-Cycle Oscillations in high-aspect-ratio wings, Journal of Fluids and Structures, Vol. 15, No. 1, (2001), 107–132.

[35] H. Haddadpour, M. A. Kouchakzadeh, F. Shadmehri, Aeroelastic instability of aircraft composite wings in an incompressible flow, Composite Structures, Vol. 83, No. 1, (2008), 93-99.

[36] S. H. Shams, M. H. S. Lahidjani, H. Haddadpour, Nonlinear aeroelastic response of slender wings based on Wagner function, Thin Walled Structures, Vol. 46, No. 11, (2008), 1192– 1203.

[37] C. M. Shearer, C. E. S. Cesnik, Nonlinear Flight Dynamics of Very Flexible Aircraft, Journal of Aircraft, Vol. 44, No. 5,(2007), 1528–1545.

[38] A. Iannelli, A. Marcos, M. Lowenberg, Aeroelastic modeling and stability analysis : A robust approach to the flutter problem, International Journal of Robust Nonlinear Control, Vol. 28, No. 1, (2018), 342–364.

[39] J. Xiang, Y. Yan, D. Li, Recent advance in nonlinear aeroelastic analysis and control of the aircraft, Chinese journal of aeronautics, Vol. 27, No. 1, (2013), 12-22.

[40] Z. Wan, B. Zhang, C. Yang, Y. Xu, Static aeroelastic analysis of a high-aspect-ratio wing based on wind-tunnel experimental aerodynamic forces, Science China Technological Sciences, Vol. 54, No. 10, (2011), 2716-2722.

[41] D. Tang, E. Dowell, Experimental Aeroelastic Models Design and Wind Tunnel Testing for Correlation with New Theory, Aerospace, Vol. 3, No. 2, (2016), 12.

[42] M. Delavenne, B. Barriety, F. Vetrano, V. Ferrand, M. Salaun, A Static Aeroelastic Analysis of an Active Winglet Concept for Aircraft Performances Improvement, In: Proceedings of the 5th Symposium on Fluid-Structure-Sound Interactions and Control, Springer, Singapore, (2021), 77-82.

[43] M. Sohst, J. L. do Vale, F. Afonso, A. Suleman, Optimization and comparison of strut-braced and high aspect ratio wing aircraft configurations including flutter analysis with geometric non-linearities, Aerospace Science and Technology, Vol. 124, (2022), 107531.

[44] S. Shafaghat, M. A. Noorian, S. Irani, Nonlinear aeroelastic analysis of a HALE aircraft with flexible components, Aerospace Science and Technology, Vol. 127, (2022), 107663.

[45] Y. Liu, C. Xie, Aeroservoelastic stability analysis for flexible aircraft based on a nonlinear coupled dynamic model, Chinese Journal of Aeronautics, Vol. 31, No. 12, (2018), 2185-2198.

[46] E. Garrigues, A review of industrial aeroelasticity practices at dassault aviation for military aircraft and business jets, Aerospace Lab, Vol. 14, (2018), 1–34.

[47] E. Jonsson, C. Riso, C. A. Lupp, C. E. S. Cesnik, J. R. R. A. Martins, B. I. Epureanu, Flutter and post-flutter constraints in aircraft design optimization, Progress in Aerospace Sciences, Vol. 109, (2019), 100537.

[48] M. Lokatt, Aeroelastic flutter analysis considering modeling uncertainties, Journal of Fluids and Structures, Vol. 74, (2017), 247–262.

[49] R. F. Latif, M. K. A. Khan, A. Javed, S. I. A. Shah, S. T. I. Rizvi, A semi-analytical approach for flutter analysis of a high-aspect-ratio wing, The Aeronautical Journal, Vol. 125, No. 1284, (2020), 410-429.

[50] M. Berci, On Aerodynamic Models for Flutter Analysis: A Systematic Overview and Comparative Assessment, Applied Mechanics, Vol. 2, No. 3, (2021), 516–541.

[51] P. A. Meehan, Flutter prediction of its occurrence, amplitude and nonlinear behavior, Journal of Sound and Vibration, Vol. 535, (2022), 117117.

[52] M. W. Kehoe, A historical overview of flight flutter testing, In: AGARD Structures and Materials Panel Meeting (No. NASA Technical Memorandum 4720), 1995.

[53] N. Tsushima, W. Su, Passive and active piezoelectric effects on flutter suppression of highly flexible wings, In: The first international Symposium on Flutter and its Application (ISFA2016), Tokyo, Japan, 2016.

[54] W. Tian, T. Zhao, Y. Gu, Z. Yang, Nonlinear flutter suppression and performance evaluation of periodically embedded nonlinear vibration absorbers in a supersonic FGM plate, Aerospace Science and Technology, Vol. 121, (2021), 107198.

[55] N. Tsushima, W. Su, Flutter suppression for highly flexible wings using passive and active piezoelectric effects, Aerospace Science and Technology, Vol. 65, (2017), 78–89.

[56] B. R. Rose, G. R. Jinu, A Study on Aeroelastic Flutter Suppression and its Control Measures - Past and Future, International Journal of Engineering and Technology (IJET), Vol. 6, No. 2, (2014), 960-973.

[57] G. L. Ghiringhelli, M. Lanz, P. Mantegazza, S. Ricci, Active flutter suppression techniques in aircraft wings, Control and dynamic systems, Vol. 52, (1992), 57-115.

[58] P. Roesch, R. Harlan, A passive gust alleviation system for light aircraft, In: Mechanics and Control of Flight Conference, USA, (1974), 773.

[59] E. Papatheou, N. D. Tantaroudas, A. da Ronch, J. E. Cooper, J. E. Mottershead, Active control for flutter suppression: an experimental investigation, 2013.

[60] A. G. Cunha-Filho, A. M. G. de Lima, M. V. Donadon, L. S. Leão, Flutter suppression of plates subjected to supersonic flow using passive constrained viscoelastic layers and Golla–Hughes–McTavish method, Aerospace Science and Technology, Vol. 52, (2016), 70–80.

[61] S. Guo, Z. W. Jing, H. Li, W. T. Lei, Y. Y. He, Gust response and body freedom flutter of a flying-wing aircraft with a passive gust alleviation device, Aerospace Science and Technology, Vol. 70, (2017), 277–285.

[62] M. Eugeni, F. Saltari, F. Mastroddi, Structural damping models for passive aeroelastic control, Aerospace Science and Technology, Vol. 118, (2021), 107011.

[63] R. V. Doggett Jr, J. L. Townsend, Flutter suppression by active control and its benefits, In: Proceedings of the SCAR Conference, NASA CP-001, Vol. 1, (1976), 303-333.

[64] E. Livne, Aircraft active flutter suppression: State of the art and technology maturation needs, Journal of Aircraft, Vol. 55, No. 1, (2017), 410-452.

[65] S. Waitman, A. Marcos, Active flutter suppression: non-structured and structured H∞ design, IFAC-PapersOnLine, Vol. 52, No. 12, (2019), 146-151.

[66] B. Takarics, B. Patartics, T. Luspay, B. Vanek, C. Roessler, J. Bartasevicius, S. J. Koeberle, M. Hornung, D. Teubl, M. Pusch, M. Wustenhagen, T. M. Kier, G. Looye, P. Bauer, Y. M. Meddaikar, S. Waitman, A. Marcos, Active flutter mitigation testing on the FLEXOP demonstrator aircraft, In: AIAA Scitech 2020 Forum, (2020), 1970.

[67] M. Kassem, Z. Yang, Y. Gu, W. Wang, E. Safwat, Active dynamic vibration absorber for flutter suppression, Journal of Sound and Vibration, Vol. 469, (2019), 115110.

[68] Y. Chai, W. Gao, B. Ankay, F. Li, C. Zhang, Aeroelastic analysis and flutter control of wings and panels: A review, International Journal of Mechanical System Dynamics, Vol. 1, No. 1, (2021), 5-34.

[69] D. Borglund, J. Kuttenkeuler, Active wing flutter suppression using a trailing edge flap, Journal of Fluids and Structures, Vol. 16, No. 3, (2002), 271-294.

[70] J. J. Block, T. M. Strganac, Applied active control for a nonlinear aeroelastic structure, Journal of Guidance, Control, and Dynamics, Vol. 21, No. 6, (1998), 838– 845.

[71] J. Ko, T. W. Strganac, A. J. Kurdila, Stability and control of a structurally nonlinear aeroelastic system, Journal of Guidance, Control, and Dynamics, Vol. 21, No. 5, (1998), 718–725.

[72] S. N. Singh, W. Yim, State feedback control of an aeroelastic system with structural nonlinearity, Journal of Aerospace Science and Technology, Vol. 7, No. 1, (2003), 23–31.

[73] M. Á. Rosique, R. Alamin, J. F. Whidborne, Application of LQG and H∞ Gain Scheduling Techniques to Active Suppression of Flutter, IFAC-PapersOnLine, Vol. 52, No. 12, (2019), 502-507.

[74] D. D. Bueno, C. G. Gonsalez Bueno, E. H. Dowell, A modal approach for designing controllers for active flutter suppression, Journal of the Brazilian Society of Mechanical Sciences and Engineering, Vol. 43, No. 1, (2021), 1-10.

[75] G. Platanitis, T. W. Strganac, Control of a nonlinear wing section using leading- and trailing-edge surfaces, Journal of Guidance, Control, and Dynamics, Vol. 27, (2004), 52–58.

[76] Z. Wang, A. Behal, B. Marzocca, Adaptive and Robust Aeroelastic Control of Nonlinear Lifting Surfaces with Single-Multiple Control Surfaces: A Review, International Journal of Aeronautical & Space Sciences, Vol. 11, No. 4, (2010), 285-302.

[77] S. Gujjula, S. N. Singh, W. Yim, Adaptive and neural control of a wing section using leading- and trailing-edge surfaces, Aerospace Science and Technology, Vol. 9, No. 2, (2005), 161–171.

[78] Y. Teng, Modeling and simulation of aeroservoelastic control with multiple control surfaces using μ- method, (Ph. D. thesis), The Claremont Graduate University, USA, 2005.

[79] M. Fatehi, M. Moghaddam, M. Rahim, Robust flutter analysis and control of a wing, Aircraft Engineering and Aerospace Technology, Vol. 84, No. 6, (2012), 423– 438.

[80] M. Malik, N. Seghal, A Comparative Study of Classical and Modern Controllers, International Journal of Engineering Research & Technology (IJERT), Vol. 5, No. 3, (2017).

[81] Y. Liu, H. Yu, A survey of underactuated mechanical systems. IET Control Theory & Applications, Vol. 7, No. 7, (2013), 921–935.

[82] X. Wei, J. E. Mottershead, Robust passivity-based continuous sliding-mode control for under-actuated nonlinear wing sections, Aerospace Science and Technology, Vol. 60, (2017), 9–19.

[83] K. W. Lee, S. N. Singh, Global Robust Control of an Aeroelastic System Using Output Feedback, Journal of Guidance, Control, and Dynamics, Vol. 30, No. 1, (2007), 271–275.

[84] X. Yan, Development of robust control based on sliding mode for nonlinear uncertain systems, (Ph. D. thesis), École centrale de Nantes, 2016.

[85] Y. Shtessel, C. Edwars, L. Fridman, A. Levant, Sliding Mode Control and Observation, Springer, New York, 2014.

[86] S. Vaidyanathan, C. H. Lien, Applications of Sliding Mode Control in Science and Engineering, Springer, Switzerland, 2017.

[87] A. R. Patel, M. A. Patel, D. R. Vyas, Modeling and Analysis of Quadrotor using Sliding Mode Control, In: Proceedings of the 44th Southeastern Symposium on System Theory (SSST), IEEE, IEEE, USA, (March 2012), 111-114.

[88] H. Xiao, D. Zhao, S. Gao, S. K. Spurgeon, Sliding mode predictive control: A survey, Annual Reviews in Control, 2022.

[89] S. Niu, W. H. Chen, X. Lu, Sliding mode control with integral sliding surface for linear uncertain impulsive systems with time delays, Applied Mathematical Modeling, Vol. 113, (2022), 439–455.

[90] N. Derbel, J. Ghommam, Q. Zhu, Applications of sliding mode control, Vol. 79, Springer Singapore, 2017.

[91] Y. B. Shtessel, L. Fridman, A. Zinober, Higher order sliding modes. International Journal of Robust and Nonlinear Control, Vol. 18, No. (4-5), (2008), 381–384.

[92] V. Utkin, A. Poznyak, Y. Orlov, A. Polyakov, Conventional and high order sliding mode control, Journal of the Franklin Institute, Vol. 357, No. 15, (2020), 10244-10261.

[93] H. Lee, V. Utkin, Chattering analysis, In: Advances in Variable Structure and Sliding Mode Control, (Book chapter), Springer Berlin Heidelberg, (2006), 107–122.

[94] A. Rosales, L. Ibarra, P. Ponce, A. Molina, Fuzzy sliding mode control design based on stability margins, Journal of the Franklin Institute, Vol. 356, No. 10, (2019), 5260-5273.

[95] Z. Song, H. Li, Second-Order Sliding Mode Control with Backstepping for Aeroelastic Systems Based on Finite-Time Technique, International Journal of Control, Automation, and Systems, Vol. 11, No. 2, (2013), 416-421.

[96] S. Dilmi, B. Bouzouia, Improving Performance for Nonlinear Aeroelastic Systems via Sliding Mode Controller, Arabian Journal for Science and Engineering, Vol. 41, (2016), 3739-3748.

[97] J. Liu, X. Wang, Advanced Sliding Mode Control for Mechanical Systems: Design, Analysis and Matlab Simulation, Springer Heidelberg, Tsinghua University Press, Beijing, 2012.

[98] F. Du, G. Li, Z. Li, Y. Sun, J. Kong, G. Jiang, D. Jiang, Simulation of 2-DOF Articulated Robot Control Based on Adaptive Fuzzy Sliding Mode Control, In: Proceedings of the 10th International Conference of Intelligent Robotics and Application, ICIRA 2017, Wuhan, China, Springer International Publishing, (August 2017), 551-559.

[99] Z. Zhao, X. Jin, Adaptive neural network-based sliding mode tracking control for agricultural quadrotor with variable payload, Computers and Electrical Engineering, Vol. 103, (2022), 108336.

[100] B. Gao, Y. J. Liu, L. Liu, Adaptive neural fault-tolerant control of a quadrotor UAV via fast terminal sliding mode, Aerospace Science and Technology, Vol. 129, (2022), 107818.

[101] V. Kumar, S. Kumar, H. Kansal, Fuzzy logic controller based operating room air condition control system, International Journal of Innovative Research in Electrical, Electronics, Instrumentation and Control Engineering, Vol. 2, No. 1, (2014), 510-514.

[102] G. Li, J. Cao, A. Alsaedi, B. Ahmed, Limit cycle oscillation in aeroelastic systems and its adaptive fractional-order fuzzy control, International journal of machine learning and cybernetics, Vol. 9, (2018),1297-1305.

[103] D. Harkut, M. Ali, Adaptive Fuzzy Hardware Scheduler for Real Time Operating System, International Journal of Computing and Digital Systems, Vol. 5, No. 6, (2016), 473-485.

[104] A. Mohammadi, S. H. Javadi, D. Ciuonzo, Bayesian fuzzy hypothesis test in wireless sensor networks with noise uncertainty, Applied Soft Computing Journal, Vol. 77, (2019), 218-224.

[105] A. Mohammadi, S. H. Javadi, D. Ciuonzo, V. Persico, A. Pescapé, Distributed Detection with Fuzzy Censoring Sensors in the Presence of Noise Uncertainty, Neurocomputing, Vol. 351, (2019), 196-204.

[106] S. Zhou, Z. Ju, Y. Liu, H. Zhang, H. R. Karimi, Driver state detection for driver-automation shared control with fuzzy logic, Control Engineering Practice, Vol. 127, (2022), 105294.

[107] N. Patcharaprakiti, S. Premrudeepreechacharn, Y. Sriuthaisiriwong, Maximum power point tracking using adaptive fuzzy logic control for grid-connected photovoltaic system, Renewable Energie, Vol. 30, No. 11, (2004), 1771–1788.

[108] W. Tian, Y. Gu, H. Liu, X. Wang, Z. Yang, Y. Li, P. Li, Nonlinear aeroservoelastic analysis of a supersonic aircraft with control fin free-play by component mode synthesis technique, Journal of Sound and Vibration, 493, (2021), 115835.

[109] F. Zhang, D. Soffker, Active flutter suppression of a nonlinear aeroelastic system using PI observer, Motion and Vibration Control, Springer Netherlands,(2009), 367–376.

[110] N. Qi, C. Zhang, J. Yuan, Observer based sliding mode control for subsonic piezo-composite plate involving time varying measurement delay, Measurement and Control, Vol. 54, No. 5-6, (2021), 983-993.

[111] D. Li, H. Yang, N. Qi, J. Yuan, Observer-based sliding mode control for piezoelectric wing bending-torsion coupling flutter involving delayed output, Journal of Vibration and Control, Vol. 27, No. 15-16, (2020), 1824-1841.

[112] J. G. Leishman, K. Q. Nguyen, State-space representation of unsteady airfoil behavior, AIAA journal, Vol. 28, No. 5, (1990), 836-844.

[113] R. T. Jones, The unsteady lift of a wing of finite aspect ratio, No. NACA-TR-681, Langley Memorial Aeronautical Laboratory, Washington D. C., 1940.

[114] T. T. Darabseh, Nonlinear State Dependent Riccati Equation Controller for 3-DOF Airfoil with Cubic Structural Nonlinearity, International Review of Aerospace Engineering, Vol. 15, No.2, (2022), 97-111.

[115] J. G. Leishman, Principles of Helicopter Aerodynamics, Cambridge Aerospace Series, 2000.

[116] Y. Teng, Comparison of First- and Second-Order EMA Models for an Aeroservoelastic Wing with Multiple Control Surfaces, In: AIAA Guidance, Navigation, and Control Conference and Exhibit, (2006), 6317.

[117] F. I. de Carvalho, R. G. A. da Silva, Increased flutter velocity with use of a passive control system, In: 31st Congress of the International Council of the Aeronautical Sciences, Belo Horizonte, Brazil, (September 2018).

[118] X. Bertrand, Modélisation aérodynamique des surfaces de contrôle de la voilure d'un avion de transport, (Ph. D. thesis), Institut Supérieur de l'Aéronautique et de l'Espace (ISAE), Toulouse, France, 2008.

[119] J. G. Leishman, Challenges in modeling the unsteady aerodynamics of wind turbines, In: Wind Energy Symposium, Vol. 7476, (2002), 141-167.

[120] F. Sallem, Détection et isolation de défauts actionneurs basées sur un modèle de l'organe de commande, (Ph. D. thesis), Paul Sabatier-Toulouse III University, France, 2013.

[121] A. Choukchou-Braham, B. Cherki, M. Djemaï, K. Busawon, Analysis and control of underactuated mechanical systems, Springer Science & Business Media, 2013.

[122] M. C. Sosse Alaoui, Commande et Observateur par Modes glissants d'un système de pompage et d'un bras manipulateur, (Ph. D. thesis), University of Sidi Mohammed Ben Abdellah, Morocco, 2009.

[123] P. Singh, P. LB, A Comparative Performance Analysis of PID Control and Sliding Mode Control of Two Link Robot Manipulator, International Research Journal on Advanced Science Hub, Vol. 2, No. 6, (2020), 43-54.

[124] J. C. Lo, Y. H. Kuo, Decoupled Fuzzy Sliding Mode Control, IEEE Transactions on Fuzzy systems, Vol. 6, No. 3, (1998), 426-435.

[125] L. K. Wong, H. F. Leung, K. S. Tam, A Fuzzy Sliding Controllers for Nonlinear Systems, IEEE Transactions on Industrial Electronics, Vol. 48, No. 1, (2001), 32-37.

[126] A. F. Fillipov, Differential equations with discontinuous right-hand side, Matematicheskii Sbornik, Vol. 51, No. 1, (1960), 99-128.

[127] S. V. Emelyanov, Variable structure control systems, Nauka, Moscow, 1967.

[128] V. I. Utkin, Sliding modes and their application in variable structure systems, Mir, Moscow, 1978.

[129] J. J. Slotine, S. S. Sastry, Tracking control of nonlinear system using sliding surface, with application to robotic manipulators, International Journal of Control, Vol. 38, No. 2, (1983), 465-492.

[130] B. Beltran, M. Benbouzid, T. Ahmed-Ali, O. Benzineb, Commande par modes glissants d'ordre supérieur et observateur grand gain de la génératrice asynchrone double alimentation d'une éolienne, In: Conférence Internationale Francophone d'Automatique (CIFA'10), June 2010.

[131] P. Lopez, A. S. Nouri, Théorie élémentaire et pratique de la commande par les régimes glissants, Vol. 55. Springer Science & Business Media, 2006.

[132] B. Gao, Y. J. Liu, L. Liu, Adaptive neural fault-tolerant control of a quadrotor UAV via fast terminal sliding mode, Aerospace Science and Technology, Vol. 129, (2022), 107818.

[133] C. C. Lee, Fuzzy logic in control systems: fuzzy logic controller, Part I, In: IEEE Transactions on Systems, Man, and Cybernetics, Vol. 20, No. 2, (March- April 1990), 404-418.

[134] C. C. Lee, Fuzzy logic in control systems: fuzzy logic controller, Part II, In: IEEE Transactions on Systems, Man, and Cybernetics, Vol. 20, No. 2, (March- April 1990), 419-435.

[135] L. A. Zadeh, Making computers think like people [fuzzy set theory], IEEE Spectrum, Vol. 21, No. 8, (1984), 26–32.

[136] C. R. Alavala, Fuzzy logic and neural networks: basic concepts & application, New Age International, 2008.

[137] B. Kosko, Fuzzy systems as universal approximators, IEEE transactions on computers, Vol. 43, No. 11, (1994),1329–1333.

[138] R. Hermann, A. Krener, Nonlinear controllability and observability, IEEE Transactions on automatic control, Vol. 22, No. 5, (1977), 728-740.

[139] Y. Sun, C. Gao, L. Wu, Y. Yang, Fuzzy observer-based command filtered tracking control for uncertain strict-feedback nonlinear systems with sensor faults and event-triggered technology, Nonlinear Dynamics, Vol. 111, No. 9, (2022), 8329-8345.

[140] J. Doyle, G. Stein, Robustness with observers. IEEE transactions on automatic control, Vol. 24, No. 4, (1979), 607-611.

[141] H. K. Khalil, A. Saberi, Adaptive stabilization of a class of nonlinear systems using high-gain feedback, IEEE Transactions on Automatic Control, Vol. 32, No. 11, (1987), 1031–1035.

[142] A. Tornambe, Use of asymptotic observers having high gains in the state and parameter estimation, In: Proceedings of the 28th IEEE Conference on Decision and Control, Austin, Texas, (1989), 1791–1794.

[143] A. Saberi, P. Sannuti, Observer design for loop transfer recovery and for uncertain dynamical systems, IEEE Transactions on Automatic Control, Vol. 35, No. 8, (1990), 878–897.

[144] H. K. Khalil, L. Praly, High-gain observers in nonlinear feedback control, International Journal of Robust and Nonlinear Control, Vol. 24, No. 6, (2013), 993–1015.

[145] H. K. Khalil, High-gain observers in nonlinear feedback control, Society for Industrial and Applied Mathematics (SIAM), Philadelphia, USA, 2017.

[146] Z. Ragoub, M. Lagha, S. Dilmi, Classical and fuzzy sliding mode control for a nonlinear aeroelastic system with unsteady aerodynamic model, International Journal of Computing and Digital Systems, Vol. 9, No. 6, (2020), 1108-1099.

[147] Z. Ragoub, M. Lagha, S. Dilmi, Observer-Based Fuzzy Sliding Mode Control for Nonlinear Aeroelastic Models via Unsteady Aerodynamics, In: Proceedings of the International Conference on Industrial Instrumentation and Control (ICI2C 2021), Springer Nature, Singapore, (February 2022), 277-286.

[148] W. Y. Yang, W. Cao, T. Chung, J. Morris, Applied Numerical Methods Using MATLAB, John Wiley & Sons, 2005.

APPENDIXES

Contents

Appendix A: The Lagrange equations

Introduction

When using Newton's laws in developing a system's equations of motion, all of the forces acting on this system have to be included. In the other hand, when using Lagrange formalism to derive the equations of motion, any force that has no work can be ignored (Like the friction forces and the forces of inextensible connections). In the case of conservative systems (Systems for which the total energy remains constant), the Lagrange method provides an automatic procedure to obtain the equations of motion, by calculating the system's kinetic and potential energies only.

A.1. The degrees of freedom

Before developing the Lagrange equations, the dynamic systems have to be characterized in a systematic way. The most important property here is the number of independent coordinates that should be known to completely specify the position or the configuration of the system. A system has *n* degrees of freedom if exactly the *n* coordinates are used to completely define its configuration.

A.2. The generalized coordinates

Usually, the coordinates are seen as lengths or angles. However, any set of parameters that allows specifying the system's configuration can serve as a coordinate. When the meaning of the expression is generalizes in this way, these new quantities are called generalized coordinates.

The general form of the Lagrange equations for any system (Conservative or non-conservative) is as follows:

$$\frac{d}{dt}\left(\frac{\partial T}{\partial \dot{q}_i}\right) - \frac{\partial T}{\partial q_i} = Q_i \qquad \text{(A.1)}$$

T is the system's kinetic energy and Q_i represents the component of external forces that work according to the degree of freedom q_i

A.3. Lagrange equations for conservative systems

If a system is conservative, the work exerted by the forces can be calculated from the potential energy *U*. The change in the potential energy during a small displacement is defined as the negative of the work done by the forces in the system during the displacement.

$Q_1\delta q_1 + Q_2\delta q_2$ is the work carried out by the forces, so:

$$\delta P = -Q_1\delta q_1 - Q_2\delta q_2 \tag{A.2}$$

q_1 and q_2 are independent and therefore, they can be varied randomly.

If $\delta q_1 = 0$ then $\delta P = -Q_2\delta q_2$ and then:

$$Q_2 = -\frac{\partial P}{\partial q_2} \tag{A.3}$$

It can be found in the same way:

$$Q_1 = -\frac{\partial P}{\partial q_1} \tag{A.4}$$

Replacing Q_2 and Q_1 by their values in the equation, to obtain:

$$\begin{aligned} &\frac{d}{dt}\left(\frac{\partial T}{\partial \dot{q_1}}\right) - \frac{\partial T}{\partial q_1} + \frac{\partial U}{\partial q_1} = 0 \\ &\frac{d}{dt}\left(\frac{\partial T}{\partial \dot{q_2}}\right) - \frac{\partial T}{\partial q_2} + \frac{\partial U}{\partial q_2} = 0 \end{aligned} \tag{A.5}$$

A.4. Lagrange equations for non-conservative systems

For non-conservative systems, the Lagrange function *L* can be defined as follows:

$$L = T - U \tag{A.6}$$

For every generalized coordinate q_j , the expression (A.6) verifies the following equation.

$$\frac{d}{dt}\frac{\partial L}{\partial q_j} + \frac{\partial d}{\partial q_j} - \frac{\partial L}{\partial q_j} = Q_j \tag{A.7}$$

d is the dissipation function of Rayleigh.

Q_j represents the component of external forces that work according to the degree of freedom q_j , it can be obtained by deriving the virtual work W of the external forces.

$$W = \sum_j Q_j U_j \tag{A.8}$$

$$Q_j = \frac{\partial w}{\partial u_j} \tag{A.9}$$

U_j represents the displacement field.

Appendix B: State-space representation for nonlinear systems

Introduction

In automatics, a state representation makes it possible to model a dynamic system in matrix form using state variables in a state space. This representation (That can be linear or non-linear, continuous or discontinuous) should provide the system's state at any future moment having the initial conditions.

B.1. State variables

A system can be fully described using a set of minimal variables. The state variables are continuous, differentiable and independent physical quantities of the system. They are generally gathered in a vector X. Knowing all of the state variables at an instant of time t should make it possible to know all of the system's responses at a time $t + dt$. The same system can be described with different state variables but their number is always the same. This number, designated by the letter n, represents the order of the system. The classical (Most general) state representation for nonlinear systems is as follows (Figure B.1):

$$\dot{x}(t) = f\big(x(t), u(t)\big)$$
$$y(t) = h\big(x(t)\big) \qquad \text{(B.1)}$$

Where : f and h are nonlinear functions.

$x(t)$ is the system's state vector.

$u(t)$ is the control vector.

$y(t)$ is the output vector.

The first equation describes the system's evolution, and the second is the observation equation. The linear state representation is a special case of the form above, obtained when the functions $f(x, u)$ and $h(x)$ are linear.

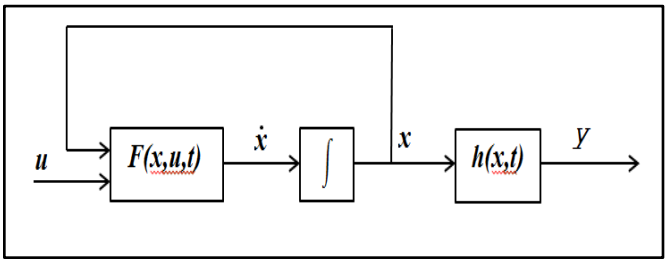

Figure B.1. Diagram of a state-representation for a nonlinear system

B.2. Stability of nonlinear systems

Nonlinear systems' stability is studied using Lyapunov functions. Many types of systems stability can be distinguished (In the sense of Lyapunov, asymptotic, exponential), and it can be local or global, uniform or not, etc.

B.3. Observability of nonlinear systems

Nonlinear systems' observability is totally different from that of linear systems. It depends on the system's input and the initial conditions. In order to give a definition to the nonlinear systems' observability, the notion of indistinguishability has to be defined.

Two initial states $x(t_0) = x_1$ and $x(t_0) = x_2$ of the system described by equations (B.1) are called indistinguishable in the time interval $[t_0, t_1]$ if, for every input $u(t)$, their respective outputs $y_1$and y_2 are identical in this interval.

The system described by equations (B.1) is observable if there is no pair of initial distinct states $\{x(t_0) = x_1 , x(t_0) = x_2 \}$ that is indistinguishable.

It should be also noted that observability depends often on the input. Some inputs do not make it possible to discern any pair of distinct initial states, this is the case of the following example.

$$\dot{x} = ux$$
$$y = x \qquad \text{(B.2)}$$

With $x \in R$

The system (B.1) is observable for any constant non-null input. Therefore, the observer cannot be constructed at or in vicinity of the input 0.

In short, designing an observer requires taking a look at the system's inputs. Considering a nonlinear system, there are generally some so-called singular inputs for which the system is not observable. But finding these inputs for a given system is still a largely open problem in the nonlinear systems theories.